External Scientific Report

APPROVED: 2 July 2024
doi: 10.2903/sp.efsa.2024.EN-8926

EFSA Project on the use of NAMs to explore the immunotoxicity of PFAS

Emanuela Corsini[1], Martina Iulini[1], Valentina Galbiati[1], Ambra Maddalon[1], Francesco Pappalardo[2], Giulia Russo[2], Ron L.A.P. Hoogenboom[3], Karsten Beekmann[3], Aafke W.F. Janssen[3], Jochem Louisse[3], Styliani Fragki[4], Alicia Paini[4]

[1]Università degli Studi di Milano, Italy; [2]Università degli Studi di Catania, Italy
[3]Wageningen Food Safety Research, The Netherlands; [4]ESQlabs GmbH, Germany

Abstract

Perfluorinated substances (PFAS) are a class of synthetic chemicals widely used in industry, to which people and ecosystems are exposed. Epidemiological studies have shown that PFAS can cause immunosuppression, increased risk of infections and decreased response to vaccination, with the underlying mechanism(s) of action still remaining elusive. The aim of this project was to fill some of the data gaps identified in the 2020 EFSA Opinion, using new approach methodologies (NAMs). In particular, we aimed to get information on the mode of action for the immunosuppression effects observed in epidemiological studies (i.e., reduction in the vaccination efficacy and possible increase in the susceptibility to infectious disease), and to address the immunotoxicity of PFAS other than PFOS and PFOA (PFNA and PFHxS), including the assessment of a possible common mode of action and to provide insight into the relative potencies of the tested PFAS. To reach these goals, an integrated testing strategy (ITS) consisting of *in vitro* and *in silico* methods was developed. The effects of PFAS were investigated using target immune human cell-based *in vitro* models, suitable to assess the relevant immunotoxic parameters observed in epidemiological studies (i.e. decreased antibody production). Results obtained fully support the evidence from human epidemiological studies. Furthermore, mathematical fate and distribution models were used to identify nominal concentration of PFAS in the *in vitro* cell system and physiologically based kinetic (PBK) models were used to perform quantitative *in vitro* to *in vivo* extrapolation. The 'Universal Immune System Simulator' was used to complete the ITS and investigate the reduced response to vaccination also on vulnerable populations. The use of these selected NAMs may provide a tool to support, by providing mechanistic information, regulatory risk assessment and to study the immunotoxic potential of other PFAS. The participation of immunotoxicologists, molecular biologists, risk assessors, and computational experts within the Consortium, together with EFSA's engagement, ensured the successful performance of this project and delivery of a NAMs-based strategy that allows generating mechanistic information on PFAS immunotoxicity and support risk assessment.

Key words: New Approach Methodologies; perfluoroalkyl substances; immunotoxicology; antibody response; *in vitro* methods; *in silico* methods.

Question number: EFSA-Q-2024-00135

Correspondence: MESE@efsa.europa.eu

Jochem Louisse was involved in this project until February 2023 and Alicia Paini until December 2023.

Acknowledgements: The Consortium wishes to thank the following for the support provided to this scientific output: the following EFSA Staff for the support provided to this scientific output Maria Chiara Astuto, Irene Cattaneo, Eskes Chantra, Jean Lou CM Dorne, Adriana Scattareggia Marchese, and the expert of the EFSA Working Group (WG) on New Approach Methodologies (NAMs) Tanja Schwerdtle. This study was supported by the European Food Safety Authority (Case Studies NAMS_PFAS Immunotox - OC/EFSA/SCER/2021/13) and by Programma Operativo Nazionale (PON "Ricerca e Innovazione" 2014-2020).

Suggested citation: Corsini E, Iulini M, Galbiati V, Maddalon A, Pappalardo F, Russo G, Hoogenboom R, Beekmann K, Janssen A, Louisse J, Fragki S and Paini A, 2024. EFSA Project on the use of NAMs to explore the immunotoxicity of PFAS. EFSA supporting publication 2024:EN-8926. 146 pp. doi:10.2903/sp.efsa.2024.EN-8926

ISSN: 2397-8325

Summary

This project aimed to fill some of the data gaps in the area of per- and polyfluoroalkyl substance (PFAS) immunotoxicity identified in the EFSA Scientific Opinion "Risk to human health related to the presence of perfluoroalkyl substances in food", published in 2020 by the CONTAM Panel (EFSA CONTAM Panel, 2020) using a New Approach Methodologies (NAMs)-based strategy. Specifically, this work aimed to fill the following data gaps: 1) to get information on the immunosuppression effects mechanisms observed for PFOA and PFOS (i.e. reduction in the vaccination efficacy and possible increase in the susceptibility to infectious disease), which may be useful for the identification of the mode of action, and 2) to address the (*in vitro*) immunotoxicity of PFAS other than perfluorooctane sulfonic acid (PFOS) and perfluooctanoic acid (PFOA), including the assessment of a common mode of action and potency differences.

In this project, the immunotoxic effects of four PFAS were investigated, namely PFOA, PFOS, perfluorononanoic acid (PFNA), and perfluorohexane sulfonic acid (PFHxS), which account for approximately half of the dietary exposure of humans to measured PFAS and contribute most to the levels observed in human serum (EFSA CONTAM Panel, 2020). The project was divided into two work packages (WP): WP-A) development of an integrated approach to testing and assessment (IATA) and conduct NAM-based studies for identifying the mechanisms of PFOS and PFOA-induced immunotoxicity; WP-B) development of the IATA and conduct NAM-based studies for studying the immunotoxic potencies of PFNA, PFHxS.

To reach these goals, an integrated testing strategy (ITS) based on *in vitro* and *in silico* methods to investigate PFAS immunotoxicity was developed. Based on the existing knowledge on PFAS immunotoxicity, availability of in silico and *in vitro* methods, the best experimental approach to characterise the effects of PFAS on antibody production was defined. A battery of *in vitro* assays was used because different components of the immune systems may be targeted by PFAS, resulting in decreased antibody production. To maximize the relevance for humans only human cell-based *in vitro* models were used. The models selected were chosen based on existing evidence on their reliability and relevance. Both primary cells and cell lines were used. Physiologically Based Kinetics (PBK) modelling was used to perform quantitative *in vitro* to *in vivo* extrapolation (QIVIVE) to translate *in vitro* effective concentrations to external doses. Moreover, the PBK model was used to inform the Universal Immune System Simulator (UISS), a mechanistic computational platform able to estimate the immunotoxicity risk (e.g. decreased response to vaccination) posed by PFAS. The UISS is able to simulate the human immune system and offers the possibility to investigate effects on vulnerable populations. It was used to investigate the sensitivity of children and elderly population groups to PFAS, and to predict the threshold dose for immunotoxic effects (e.g., 10% decrease in the response to vaccination).

The different PFAS tested decreased to different extend the parameters investigated, including dendritic cells maturation, T cells proliferation and differentiation, T cell-dependent and T cell–independent antibody production. The two main signal transduction pathways modulated were PPARa and the glucocorticoid receptor (GR). The use of *in silico* models allowed to derive an acceptable daily intake which was found to be within the same range of the actual value established in the 2020 EFSA Opinion and predict the decrease response to

vaccination. This comparison was made through the extrapolation from the tolerable weekly intake (TWI) value present in the 2020 EFSA Opinion (EFSA CONTAM Panel, 2020) to that of the acceptable daily intake (TDI), obtained instead from the QIVIVE data present in this report. Overall, the proposed approach and results allowed to successfully fill some of the existing data gaps, demonstrating the usefulness of NAMs to provide supportive mechanistic information to predict PFAS immunotoxicity without the need of animal studies.

Table of contents

1 Introduction

It is well established from both epidemiological and experimental animal studies that PFAS are immunotoxic (mainly immunosuppressive), affecting both cell-mediated and humoral immunity (EFSA CONTAM Panel, 2020; DeWitt et al., 2019; Corsini et al., 2014). Elevated PFAS blood levels are associated with lower antibody responses to vaccinations in children (Abraham et al., 2020) and in adults (Kielsen et al., 2016). The reduced response to vaccination was selected as critical endpoint by EFSA to establish the tolerable weekly intake (TWI) for the combined exposure to PFOA, PFNA, PFHxS, and PFOS (EFSA CONTAM Panel, 2020). In addition, some studies reported a correlation between PFAS levels in the body and lower resistance to disease or an increased risk of infections (Granum et al., 2013). A relationship between higher PFAS levels and increased risk of asthma as well as increased adolescent food allergies has also been reported (Averina et al., 2019). In experimental animals, reported effects of PFAS include decreased spleen and thymus weights and cellularity, altered cytokine production, reduced specific antibody production, and reduced survival after influenza infection.

In 2020 EFSA made a number of recommendations related to the identified data gaps on PFAS immunotoxicity including the need to conduct studies on the characterisation of the mode of action of PFAS immunotoxicity; the need to conduct of studies on PFAS other than PFOA and PFOS, in particular PFNA and PFHxS on the immune system; and the need to conduct studies that allow derivation of potency factors for PFASs (EFSA CONTAM Panel, 2020).

The goals of this project were to identify models and strategies using NAMs suitable for the identification of the mechanisms underlying the observed immunosuppression of PFAS, being important for the risk assessment. The project evaluated the immunotoxic effects of four PFAS, namely PFOA, PFOS, PFNA, and PFHxS, as they were reported to make up approximately half of the exposure of humans to the measured PFAS and to contribute most to the levels observed in human serum (EFSA CONTAM Panel, 2020). To reach that purpose, an ITS composed of *in vitro* and *in silico* methods able to simulate and reproduce the most important immunological effects observed in the human epidemiological studies, was developed. In accordance with the Next Generation Risk Assessment (NGRA) principles, the Consortium used only NAMs that have the aim to reduce animal testing while increasing robustness, throughput and proving a mechanistic understanding of chemical mode of action.

As mentioned above, EFSA identified the decrease in the antibody response against specific vaccination in children (i.e., diphtheria) as critical endpoint, and set up the TWI for the most common four PFAS based on the effects on the immune system (EFSA CONTAM Panel et al., 2020). Similarly, several US states also used immunological endpoint as the critical effect for their reference dose of PFOS and PFOA (Post, 2021). Starting from that evidence, the Consortium focused the attention on antibody production for the design of an ITS.

The immune system can induce the release of antibodies from B cells in two different ways: through the T cell-dependent (TD) or the T cell-independent (TI) way. In the TD B cell activation three different cell types are involved: DCs, Th cells, and B cells. The antigen is recognized and presented by antigen presenting cells in an MHC class II restricted

mechanism to naive T cells. After the uptake of the antigen, the antigen presenting cells increase MHC class II molecules and expression of co-stimulatory factors such as CD80 and CD86. DCs-activated T cells become able to induce signals to B cell by the interaction of the T cell CD40 ligand (CD40L) with CD40 present on the membrane of B cells and the release of related cytokines. The interaction CD40L-CD40 induces the antibody release characterised by production of specific immunoglobulin (Ig) G, IgA, and IgE antibodies. Signalling through CD40 is essential for the induction of isotype switching which is strongly associated with the development of B cells memory, a critical key event in the success of vaccination (Chaplin, 2010). Nonetheless, the production of antibody can also be induced by TI B cells response. In this case, the antigen is recognised directly by B cells through the binding with the B cell receptor and by the engagement of specific toll-like receptors (TLR) such as TLR-4 and TLR-9. After activation, B cells are transformed into plasma cells that can secrete antibodies (Pone et al., 2015a). TI B-cell response is shorter compared to TD and does not result in the selection of affinity-matured antibodies. However, in specific cases, it has been shown to result in long-lived antibody production (Bortnick et al., 2012).

Starting from these two different mechanisms, an ITS was developed focusing on the different components of the immune response involved in the antibody production and that can be targeted by PFAS. Therefore, the effects of the four selected PFAS on antigen presenting cells, T helper cells, and B cells were investigated. Five different *in vitro* assays were used to investigate the effect of PFAS on the immune system:

- Assessment of leukotoxicity;
- Effects on maturation of dendritic cells (DCs);
- Effects on T helper (Th) cell proliferation and differentiation;
- Effects on T-dependent antibody release (primary antibody response);
- Effects on T-independent antibody release.

To maximize the relevance of the findings for humans, only human cell-based *in vitro* models were used. The models selected were based on evidence of reliability and relevance, and experiences gained in the laboratories involved in the assessment of PFAS immunotoxicity. Both primary cells and cell lines were used, but it should be considered that the latter, while representing in principle an endless source of cells and providing more consistent responses, may be less sensitive compared to primary cells (OECD GD No.360, 2022). For the models based on human purified peripheral blood mononuclear cells (PBMC), 5 donors for each gender were used. While for models based on the use of cell lines, three independent experiments were conducted.

The project also took advantage of the progress made in *in silico* models, both for the quantification of cellular exposure, the *in vitro* to *in vivo* dose extrapolation, the simulation of the immune response and relative potency estimation. An *in silico* fate and distribution model, known as Armitage (Armitage et al., 2014) was used to estimate the free concentration of the chemical available for cellular exposure. Physiologically Based Kinetic (PBK) models that enable the QIVIVE of the *in vitro* immunotoxicity data were employed here in order to estimate corresponding external (oral) toxic dose levels. Nowadays, the use of *in vitro* methods and computer simulations provide the opportunity to establish new knowledge, and approaches that support the protection of human health from e.g., PFAS.

1.1 Background and terms of reference as provided by the requestor

This contract was awarded by EFSA to: Università degli Studi di Milano (UNIMI)

Contractor: University of Catania (UNICT); Wageningen Food Safety Research (WFSR); esqLABS GmbH (ESQ). UMIL acted as joint tender leader.

Contract title: Case study on use of NAMs to address PFAS immunotoxicity.

Contract number: OC/EFSA/SCER/2021/13[1]

1.2 Additional information (if appropriate)

The objectives of the contract resulting from this procurement procedure were grouped in two Workpackages:

Workpackage A: Developing the IATA (Integrated Approach to Testing and Assessment) and design the NAM-based studies for identifying the mode of action of PFOS and PFOA.

Workpackage B: Developing the IATA (Integrated Approach to Testing and Assessment) and design the NAM-based studies for studying the immunotoxicity potency of different PFAS.

In the table below (Table 1), the Workplan summary of the project is reported.

Table 1: Workplan summary of the project

WORKPACKAGE	OBJECTIVE	TASK	DELIVERABLE
Workpackage A: Developing the IATA (Integrated Approach to Testing and Assessment) and design the NAM-based studies for identifying the mode of action of PFOS and PFOA	A-1	Preparation of a proposal for the battery of studies to be conducted for identifying the mode of action of PFOS and PFOA (Objective A-1), discuss the proposal with EFSA and experts in the field, and finalise the test design	D-1: Interim report 1, containing the proposed battery of studies and the study protocols
	A-2	Conduct the studies for assessing the mode of action (Objective A-2) according to the agreed test designs and protocols	D-2: Interim report 2, containing the study results
	A-3	Analyse the results and propose an AOP-like approach for the immunotoxicity mode of action of PFOS and PFOA	D-3: Interim report 3, containing a structured proposal on the possible mode(s) of action of PFOS and PFOA
Workpackage B: Developing the IATA (Integrated Approach to Testing and Assessment) and design the NAM-based studies for studying the immunotoxicity potency of different PFAS	B-1	Prepare a proposal of relevant studies for analysing the potency of different PFAS in vitro and the approach for the QIVIVE (Objective B-1), discuss the proposal with EFSA and experts in the field, and finalise the test design	D-4: Interim report 4, containing the proposed studies for addressing immunosuppression potency and the study protocols
	B-2	Conduct the studies for assessing the immunosuppression potency (Objective B-2) according to the agreed test designs and protocols	D-5: Interim report 5, containing the study results
	B-3	Analyse the results, conduct the QIVIVE and propose (relative) potency values for immunotoxicity for the studied PFAS (Objective B-3)	D-6: Draft Final Report compiling the results of both Workpackages
Workshop and Final Report	-	Organise an expert workshop, involving EFSA and international experts in the field, and produce the Final Report	D-7: Final Report, containing the key conclusions, summary of all published data and details for all unpublished experimental results and analyses. The Final Report will be submitted to EFSA for approval and to be published in the EFSA Journal as External Publication

While the project was divided in two work packages, to allow a better presentation and discussion of the results obtained, the report is divided into three parts: the in vitro

[1] https://etendering.ted.europa.eu/cft/cft-display.html?cftId=9110

functional tests (conducted by UMIL), the whole genome gene expression profiling (conducted by WFSR), and the *in silico* part (conducted by UNICT, ESQ and UMIL). In each of the three parts, materials and methods, results and discussion are reported. The four PFAS studied are presented together to easily compare them.

2 *In vitro* methods

2.1 Introduction

In order to investigate PFAS immunotoxicity a strategy was used whereby the antibody response was dissected and effects on the different immune cells involved in antibody production were investigated together with antibody production toward TD and TI antigens. In particular, the effect on DC maturation DCs, Th cells proliferation and differentiation and antibody production were assessed.

2.2 Materials and methods

Chemicals: PFOA (Perfluorooctanoic acid; CAS #335-67-1), PFNA (Perfluorononanoic acid, CAS #375-95-1), PFHxS (Tridecafluorohexane-1-sulfonic acid potassium salt. CAS #3871-99-6), PFOS (Heptadecafluorooctanesulfonic acid solution ~40% in H_2O; CAS #1763-23-1), Cyclosporin A (CAS #59865-13-3), Dexamethasone (DEX, 9α-fluoro-16 α-methylprednisolone, CAS #50-02-2) and Rapamycin (CAS # 53123-88-9) were purchased from Sigma-Aldrich at the highest purity available (St Louis, MO, United States). All the chemicals were diluted in dimethyl sulfoxide (DMSO, CAS #67-68-5), to obtain 10 mg/mL stock solutions for PFOA, PFNA, PFHxS and PFOS, 1.2 mg/mL stock solution for Cyclosporin A, 150 mg/mL stock solution for DEX, while 1 mg/mL stock solutions for Rapamycin and subsequently diluted before each experiment. The final concentration of DMSO in cell culture was ≤ 0.1%.

Cells: two different types of cells were used. For the analysis of the effect of PFAS on DCs maturation, THP-1 cells (Elabscience Biotechnology Inc. - Houston, Texas, USA) were used. While for all the other protocols only human PBMC isolated from the buffy coats were used. For more details about the PBMC isolation see Annex A - List of Standard Operating Procedures (SOPs) section A.1. SOP for Purification of peripheral blood mononuclear cells (PBMC) from buffy coat.

Both cells were treated with increasing concentrations of the four selected PFAS, Cyclosporin A/DEX/Rapamycin as a positive control or DMSO as vehicle control (negative control).

2.2.1 Leukotoxicity

Cells treatment

For experiments, PBMC ($1x10^5$ cells/mL) were treated in complete medium composed by RPMI 1640 without phenol red containing 2 mM L-glutamine, 100 IU/mL penicillin, 0.1 mg/mL streptomycin, 10 µg/mL gentamycin, 50 µM 2-mercaptoethanol, supplemented with 5% of human serum. Cells were treated in 96 well plate with increasing concentrations

of four selected PFAS and DMSO as vehicle control and incubated at 37 °C in 5% CO_2 for 24 and 96h, 6 and 12 days.

Determination of the LDH release

For the determination of the leukotoxicity, the CyQUANT™ LDH Cytotoxicity Assay Kit was used (Invitrogen™ Corporation, Massachusetts, US) and the manufacturers procedures followed. To determinate LDH activity, the 680-nm absorbance value (background) from the 490-nm absorbance was subtracted before calculation of % cytotoxicity. The equation used was:

$$LDH\ leakage\ \% = \frac{compound\ treatd\ LDH\ activity}{vehicle\ treated\ LDH\ activity} x\ 100$$

LDH activity data were analysed with SoftMax Pro software. For more details about the protocol see Annex A - List of Standard Operating Procedures (SOPs) section A.2. SOP for assessment of leukotoxicity (LDH leakage).

2.2.2 Effects on dendritic cell maturation

Cell differentiation and treatment

THP-1 cells ($1x10^5$ cells/mL) were treated for 5 days with rhIL-4 (1500 UI/mL — ImmunoTools GmbH, Friesoythe, Germany) and rhGM-CSF (1500 UI/mL — ImmunoTools GmbH) to acquire the properties of immature DCs (iDCs) as described by Berges et al. (2005). RPMI 1640 containing 2 mM glutamine, 0.1 mg/mL streptomycin, 100 UI/mL penicillin, 50 µM 2-mercaptoethanol, supplemented with 10% heated-inactivated fetal bovine serum (FBS) was used as a medium and cells were cultured at 37 °C in 5% CO_2. At day 5, the cells ($1x10^6$ cells/mL) were exposed to the four selected PFAS, DEX as positive control and DMSO as vehicle control for 24h in RPMI 1640 without phenol red containing 2 mM L-glutamine, 0.1 mg/mL streptomycin, 100 UI/mL penicillin, 50 µM 2-mercaptoethanol, supplemented with 5% heated-inactivated delipidated fetal bovine serum. After 24h of treatment, the maturation cocktail composed of rhIL-4 (3000 UI/mL), rhGM-CSF (1500 UI/mL), rhTNF-α (2000 UI/mL — Sigma Aldrich) and ionomycin (200 ng/mL — Sigma Aldrich) were added to obtain mature DCs (mDCs). After an additional 24 and 72h, specific cell surface markers, namely CD83, CD86 and HLA-DR, were assessed to evaluate the maturation process of the cells and to estimate the potential of PFAS to interfere with this process.

Cell surface markers expression

Cell surface markers were evaluated by flow cytometry analysis. Cells stained with specific FITC/PE-conjugated antibodies against CD40, CD80, CD83, CD86 and HLA-DR (BD Pharmingen™, Milan, Italy and ImmunoTools GmbH) or with isotype control antibodies at 4°C following supplier's instructions. The intensity of fluorescence was analysed using Novocyte3000 flow cytometer, and data were quantified using NovoCyte software (NovoCyte). Changes in surface marker expression are expressed as Stimulation Index (SI) calculated on the Mean Fluorescence Intensity (MFI) values (treated cells/control cells - mDCs). For more details about the protocol see Annex A - List of Standard Operating

Procedures (SOPs) section A.3. SOP for dendritic cells differentiation and maturation starting from THP-1 cell line.

2.2.3 Effects on T cells proliferation and differentiation

Cell staining and treatment

For the experiments, PBMC ($2x10^6$ cells/mL) obtained from human buffy coats, were treated in complete medium composed by RPMI 1640 without phenol red containing 2 mM L-glutamine, 100 IU/mL penicillin, 0.1 mg/mL streptomycin, 10 µg/mL gentamycin, 50 µM 2-mercaptoethanol, supplemented with 5% of human serum. Before the incubation with the PFAS and the activation of T cells, PBMC need to be stained to assess cell proliferation. This step was performed only for the assessment of the proliferation (not for the assessment of T helper cells differentiation). To do this, PBMC were stained with 5 µM CellTrace CFSE (Cell Proliferation Kit for flow cytometry, Invitrogen™ Corporation) in PBS and incubated for 20 min at 37°C and 5% CO_2, protected from the light. After the incubation timing the cells were resting for 5 min at room temperature in complete medium and then centrifuge and incubated for 10 min in new complete medium at 37°C and 5% CO_2, to allow CellTrace reagent to undergo acetate hydrolysis. After that, both of the cells (the one for study the proliferation and the one for study the differentiation) were treated in 48 well plate with increasing concentrations of the four selected PFAS, Cyclosporin A as a positive control and DMSO as vehicle control and incubated at 37°C in 5% CO_2 for 24h. Then the cells were stimulated with antiCD3 plus antiCD28 (T Cell TransAct, Miltenyi Biotec) for 4 days to induce Th cells maturation and differentiation.

Assessment of cell proliferation

To assess cell proliferation, cells stained with CFSE were transferred into flow cytometer tubes, centrifuged at 1500 rpm for 5 min and resuspended in 1 mL of PBS. Data were acquired using flow cytometer (Novocyte 3000). T cells proliferation results were analysed studying the discrete peaks in the histogram plots, representing successive generations of proliferating cells, comparing to unstained cells.

T helper/Treg differentiation assessment

The Human Th1/Th2/Th17 Phenotyping Kit (BD Pharmingen™) was used for the assessment of Th differentiation, while the Treg Phenotyping Kit, anti-human, REAfinity™ (Miltenyi Biotec) was used for the assessment of Treg differentiation. Before the staining, GolgiStop Protein Transport Inhibitor (BD Pharmingen™– contained in the kit) was add to the well without the CFSE staining, and the plate incubate for 5h at 37°C in 5% CO_2. After 5h of incubation, the cells were transferred in flow cytometric tubes, counted, and centrifuged at 1500 rpm for 10 min. The supernatants were collected and stored at -20°C for the analysis of cytokines release. The cells were resuspended in 1 mL of stain buffer (PBS + 0.5% FBS) and the content divided in two flow cytometric tubes, in a way that each tube contains approximately 1 x 10^6 cells. One tube was dedicated for the assessment of Th1/Th2/Th17, while the other one for the assessment of Treg.

For the assessment of Th1, Th2 and Th17, the Human Th1/Th2/Th17 Phenotyping Kit was used, and the manufacturer's instructions were followed. The cells were stained with the antibody cocktail containing human CD4 PerCP-Cy5.5 (clone: SK3), human IL-17A PE

(clone: N49-653), human IFN-γ FITC (clone: B27) and human IL-4 APC (clone: MP4-25D2) and the data acquired using flow cytometer (Novocyte 3000).

For the assessment of Treg, the Treg Detection Kit was used, and the manufacturer's instructions were followed. The cells were stained with the antibodies CD45-VioBlue, CD4-VioGreen, CD25-VioBright 515, and CD127-PE and anti-FoxP3-Vio667 and the data acquired using flow cytometer.

Th1/Th2/Th17 Phenotyping was represented by % of cells positive to the selected antibody. Autofluorescence cell debris were excluded in P1. From P1 gate, only CD4+ positive cells were analysed (gate P2). From P2 gate, Th1, 2 and 17 cells were analysed based on the comparison between IFN-γ, IL-4 and IL-17A. Also, Treg Phenotyping was represented by % of positive cells. CD45+ cells were gated (P1), from P1 gate, only single cells were analysed (P2). From P2 CD4+ cells were gated (P3) and from P3 gate, Treg cells can be analysed based on the comparison between CD25, CD127 and FoxP3 expression. Flow cytometer data were analysed using the software NovoExpress.

Cytokine release

Cytokine release was assessed on cell-free supernatants obtained from the treatment without CFSE staining, using commercially available ELISA, following manufacturer's instructions. IL-4, IL-10, and IFN-γ were purchased from ImmunoTools GmbH, whereas IL-17A and TGF-β were purchased from R&D Systems (Minneapolis, Minnesota, US). The optical density was acquired with a spectrophotometer (MolecularDevice SpectraMax ABS) at a wavelength of 595 nm and the results are expressed as fold-change of chemicals treated cells versus vehicle treated. Cytokines release data were analysed with SoftMax Pro software.

For more details about the protocol see Annex A - List of Standard Operating Procedures (SOPs) section A.4. SOP T helper cells proliferation and differentiation from human PBMC.

2.2.4 T cell-dependent antibody production

Cell treatment

For experiments, PBMC ($2.5x10^6$ cells/mL) were treated in complete medium composed by RPMI 1640 without phenol red containing 2 mM L-glutamine, 100 IU/mL penicillin, 0.1 mg/mL streptomycin, 10 µg/mL gentamycin, 50 µM 2-mercaptoethanol, supplemented with 5% of human serum. Cells were treated in 24 well plate with increasing concentrations of the four selected PFAS, rapamycin and DMSO as vehicle control and incubated at 37°C in 5% CO_2 for 24h. Then stimulated or not with 25 µg/mL of KLH (Keyhole limpet hemocyanin; CAS# 9013-72-3, Sigma-Aldrich) and 30 µg/mL of SAC (*Staphylococcus aureus* Cowan I; PANSORBIN® Cells, Sigma-Aldrich) for other 5 days. After a total of 6 days, the medium was changed: the cells were washed twice with PBS and then resuspended in new fresh complete medium. After that the cells were again treated with PFOA, PFNA, PFHxS, PFOS, rapamycin and DMSO as at day 1 and it was also added in all the condition 60 IU/mL of rhIL-2 (Miltenyi Biotec, Bergisch Gladbach, Germany) as a booster. The cells were incubated at for another 5 days at 37°C in 5% CO_2.

Antibody release

To determinate the release of antibody against KLH, after a total of 11 days, PBMC were centrifuged for 5 min at 25°C at 2000 rpm. Supernatants were collected and stored at -20°C until measurement. The release of human IgM anti-KLH was assessed using commercially available ELISA kit (Cusabio, Houston, TX, United States; CSB E16534h). Assays were performed following manufacturer's instructions. If the ODsample was ≥ 2.1x ODnegative control the release of IgM antiKLH was deemed adequate according to the kit. To determine optical densities, Molecular Devices SpectraMax ABS was used. Data was collected and analysed by integrated software. Results are expressed as fold-change of chemicals treated cells versus vehicle treated.

For more details about the protocol see Annex A section A.5. SOP for *in vitro* primary antibody response.

2.2.5 T cell-independent antibody production

Cell treatment

For experiments, PBMC ($1.26x10^6$ cells/mL) were treated in complete medium composed by RPMI 1640 without phenol red containing 2 mM L-glutamine, 100 IU/mL penicillin, 0.1 mg/mL streptomycin, 10 µg/mL gentamycin, 50 µM 2-mercaptoethanol, supplemented with 5% of human serum. Cells were treated in 48 well plate with increasing concentrations of four selected PFAS, rapamycin and DMSO as vehicle control and incubated at 37°C in 5% CO_2 for 24h. After that PBMC was stimulated or not with 1 µg/mL of ODN2006 (ODN 7909, InvivoGen, San Diego, CA, USA) and 100 IU/mL of rhIL-2 for other 5 days.

Immunoglobulin release

To determinate the release of total IgG and IgM, after a total of 6 days, PBMC were centrifuged for 5 min at 25°C at 2000 rpm. Supernatants were collected and stored at -20°C until measurement. The release of immunoglobulins IgG and IgM was performed following the procedure reported in the Annex A section A.6. SOP for activation of primary human B cells. The optical densities were determinate using the Molecular Devices SpectraMax ABS, and data were collected and analysed by integrated software. Results are expressed as fold-change of chemicals treated cells versus vehicle treated.

2.2.6 RNA extraction and quantification

Ad hoc experiments were also performed to carry out transcriptomic analyses. The whole genome gene expression profiling was focused on studying the effect of PFOA and PFOS and positive controls in different cell types. More in detail, iDCs and PBMCs were exposed to PFOA (10 µg/10^6 cells), PFOS (10 µg/ 10^6 cells), DEX (150 µg/ 10^6 cells) and GW7647 (1 µM, Sigma Aldrich) for 24h, whereas mDCs where exposed to PFOA and PFOS only for 48 and 96h. In addition, effects of similar compounds were also investigated in T cells. Lastly, the effect of PFOA, PFOS and rapamycin (2 ng/10^6 cells) was studied on B cells. For RNA extraction, the RNeasy Mini Kit was used (Qiagen, Hilden, Germany), following the manufacturer's instructions. In brief, the cells were lysed with RTL buffer/β-mercapthoethanol (1:100) the lysate was vortexed for 1 min at maximum speed and the supernatant was transferred to a new RNase-free tube, followed by a mixture of the same volume of 70% ethanol. RNA was bound to the RNeasy spin column by transferring the

sample to the column and centrifuging at 9500g for 30 sec. In order to remove the residual buffer, 350 µL Buffer RW1 was added and centrifuged at 9500g for 30 sec and the flow-through was discarded. For on-column DNase digestion, 80 µL of DNase mixture (10 µL DNase stock solution mix with 70 µL Buffer RDD) was added to the membrane and incubated for 15 min at room temperature. For the RNA wash step, 350 µL of Buffer RW1 was added to the column and flow-through was discarded after centrifuging at 9500g for 30 sec. Then 500 µL of Buffer RPE was added for a second wash, followed by 30 sec of centrifugation. This process was repeated with 2 min of centrifugation. After that, the column was subjected to additional centrifugation for 1 min at maximum speed to dry the membrane. For the RNA elution step, the column was inserted to a new 1.5 mL RNase-free microtube, in which 30 µL of RNase-free water was added and RNA was harvested after 1 min of centrifugation at 9500g. Then, the obtained RNA was stored at − 80°C.

RNA purity and concentration were assessed by determination of RNA absorbance in RNase-free water at 230, 260, and 280 nm using a NanoReady F-3100 spectrophotometer (Life Real, Zhejiang, China). The optical density (OD) A260/A280 and A260/A230 ratio was used to evaluate RNA purity.

2.2.7 Statistical analysis

Data obtained are expressed as mean ± standard error of mean (SEM) of 3 independent experiment for THP-1 cells, while 5 male and 5 female donors for the experiments in which human PBMC were used. Statistical analysis was performed using GraphPad Prism version 9.4.0 (GraphPad Software, La Jolla, CA, United States). Significant differences were determined using paired or unpaired T-test, or analysis of variance (ANOVA), followed, when significant, by an appropriate post hoc test, as indicated in the Figure legends. Effects were designated as significant if the P value was ≤ 0.05.

2.3 Results and discussion

2.3.1 Leukotoxicity

Initial experiments were performed using human PBMC purified from buffy coats obtained from healthy male and female donors to identify the non-cytotoxic concentrations of the four selected PFAS. A broad range of concentrations were used to cover low levels (ng/mL) relevant for the general population and higher levels (µg/mL) relevant for highly exposed workers. Concentration and time dependent experiments were conducted, and the leakage of intracellular LDH was used to define cytotoxicity (CyQUANT™ LDH Cytotoxicity Assay Kit). The following range of nominal concentrations were tested: 0.001, 0.01, 0.1, 1 and 10 µg/mL. LDH leakage was investigated after 24 and 96h, 6 and 12 days of treatment. The LDH assay is a colorimetric assay that provides a simple and reliable method for determining cellular cytotoxicity. The amount of colour produced is measured at 490 nm by standard spectroscopy and is proportional to the number of damaged cells in the culture. Thanks to the inherent linearity of this LDH cytotoxicity assay, it can be effortlessly employed to precisely ascertain the percentage of damaged or compromised cells in a given sample.

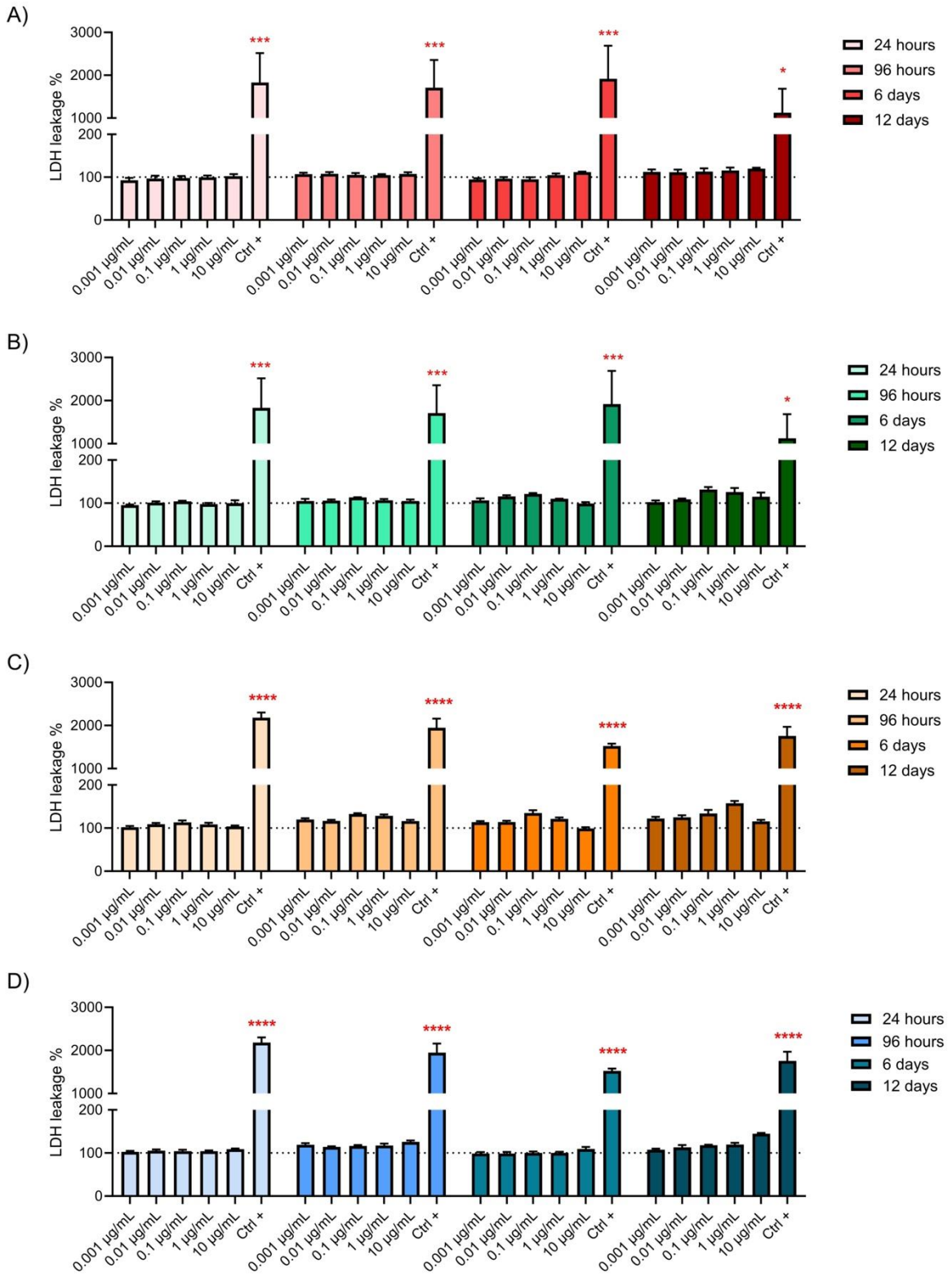

Figure 1: Effects of PFOA, PFNA, PFHxS and PFOS on cell viability. PBMCs (1x10^5 cells/ml) were treated for 24 and 96h, 6 and 12 days with increasing concentrations of PFOA (A), PFNA (B), PFHxS (C) and PFOS (D). The concentrations of PFAS and vehicle control were

corrected for the effectively cell density of the treatment under examination by comparing the ug administered to $1x10^6$ of cells

The Ctrl + is the LDH positive control present in the CyQUANT™ LDH Cytotoxicity Assay Kit. Results are expressed as percentage (%) of cytotoxicity. Each value represents the mean ± standard error of the mean (SEM), with n = 2 male and 2 female donors pooled together. Statistical analysis was performed using two-way ANOVA, followed by Dunnett's test. Results were considered significant if $p \leq 0.05$, with * $p \leq 0.05$ and ** $p \leq 0.001$ vs DMSO (represented by the dot line set at 100 %).

As shown in Figure 1, all concentrations of the four PFAS tested were not significantly cytotoxic after 24, 96h and 6 days of exposure compared to vehicle control treated cells (DMSO). A slight increase, not statistically significant, in LDH leakage was observed for all tested PFAS at the higher concentrations after 12 days of treatment. An increase in LDH leakage at 12 days is expected, as culture medium was not changed. In addition, to the preliminary dose range findings experiments, cell viability was also evaluated in all experiments conducted SOPsto ensure that effects observed were not due to cytotoxicity. . In these cases, cell viability was assessed using propidium iodide (PI) staining. PI staining is a viability dye flow cytometry method used to assess cell viability. Taking all data into account, we can conclude that all concentrations that will be used in the different functional tests are not cytotoxic.

2.3.2 Effects on dendritic cell maturation

Antigen recognition and processing by antigen presenting cells is central to the activation of specific immune responses. DCs are the main cells involved in this type of response. While it is possible to work with primary DCs, obtaining them is laborious and results are variable. Thus, it was agreed to use differentiated THP-1 cells. The protocol developed by Berges et al. (2005) represents a reproducible and robust method to assess DC differentiation and maturation. THP-1-derived DCs display the morphologic, phenotypic, molecular, and functional properties of DCs generated from human donor-derived monocytes or CD34+ hematopoietic progenitor cells (Berges et al., 2005). THP-1 cells were first differentiated into iDCs, with the use of rhIL-4 and rhGM-CSF and then exposed to the four selected PFAS for 24h. After 24h of treatment, the maturation cocktail (rhIL-4, rhGM-CSF, rhTNF-α and ionomycin) was added to obtain mDCs. After an additional 24 and 72h, specific cell surface markers, namely CD83, CD86 and HLA-DR, were assessed to evaluate the maturation process of the cells and to estimate the potential of PFAS to interfere with this process.

CD83 was selected as it is an activation marker present on the surface of immune cells, present on the surface of mDCs. It is also able to induce the upregulation of MHC II and CD86 required for T cell activation (Li et al., 2019). As mentioned, CD86 provides co-stimulatory signals essential for the adhesion and activation of T lymphocytes. This molecule is expressed by the cell only following the recognition of an antigen and cells activation and maturation. The binding between CD86 and CD28 present on T cells promotes the production of cytokines important for the T cells proliferation and differentiation. HLA-DR is a cell surface receptor belonging to MHC II able to interact with the T cells receptor. The main function off MHC II, including HLA-DR, is to present antigens to Th cells, eliciting or suppressing T cell responses with the consequence of promoting the production of antibodies toward T cell cell dependent antigens (Kaiko et al., 2008).

To induce the differentiation of THP-1 cells to iDCs, cells were treated in complete RPMI-1640 medium supplemented with the growth factors rhIL-4 and rhGM-CSF. After 5 days, the differentiation was verified by evaluating the expression of the surface markers CD40, CD80 and CD86 (Figure 2). The intensity of fluorescence or the percentage of positive cells were analysed using Novocyte3000 flow cytometer, and data quantified using NovoExpress software (NovoCyte). The isotype values were subtracted to markers expression. Changes in surface marker expression were expressed as SI calculated on the Geo Mean values (treated cells/control cells).

Figure 2 shows that the expression of the three differentiation markers (CD40, CD80, CD86) increased in iDCs compared to naïve THP-1, confirming the cell differentiation to iDCs.

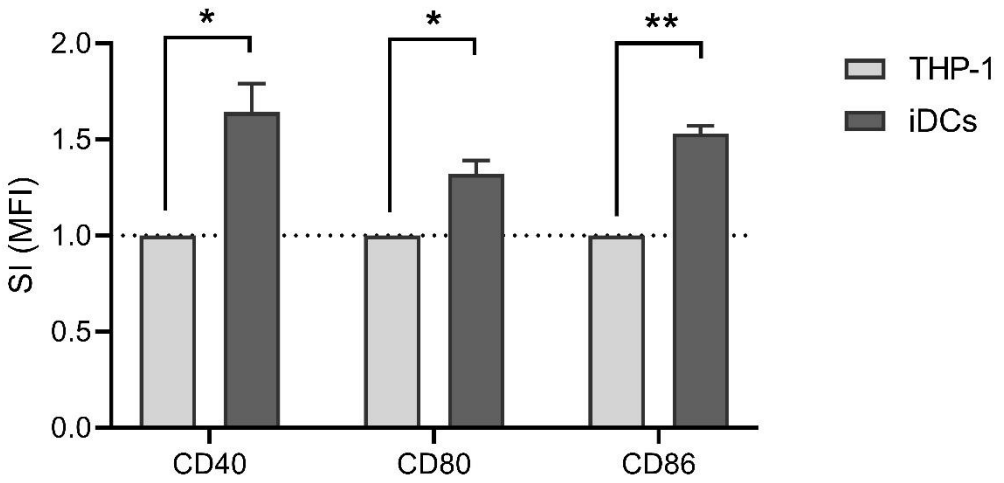

Figure 2: Differentiation of naïve THP-1 cells to iDCs. THP-1 cells were treated for 5 days with rhIL-4 (1500 IU/mL) and rhGM-CSF (1500 IU/mL), acquiring the properties of iDCs, represented in dark grey. Surface markers CD40, CD80 and CD86 were evaluated by FACS analysis. Results are expressed in SI with respect to vehicle-treated cells. The dashed line is set to 1, in relation to the control value (undifferentiated THP-1). Results are reported as mean ± SEM, with n = 3 independent experiments. Statistical analysis was evaluated by one-way ANOVA, followed by Dunnett's test. The results were considered significant if $p \leq 0.05$, with * $p \leq 0.05$ and ** $p \leq 0.01$ vs naïve THP-1

The effects of the four selected PFAS on DCs maturation was then tested. iDCs were treated with increasing concentrations of PFOA, PFNA, PFHxS, PFOS or DEX, as a positive control, for 24h. Subsequently, maturation cocktail (composed by rhIL-4 (3000 IU/mL), rhGM-CSF (1500 IU/mL), rhTNF-α (2000 IU/mL) and ionomycin (200 ng/mL)) was added to each condition to obtain mDCs. Cells were investigated after 24 and 72h from the addition of the maturation cocktail, and the surface markers CD83, CD86 and HLA-DR were evaluated by FACS analysis. The obtained results are reported in Figure 3.

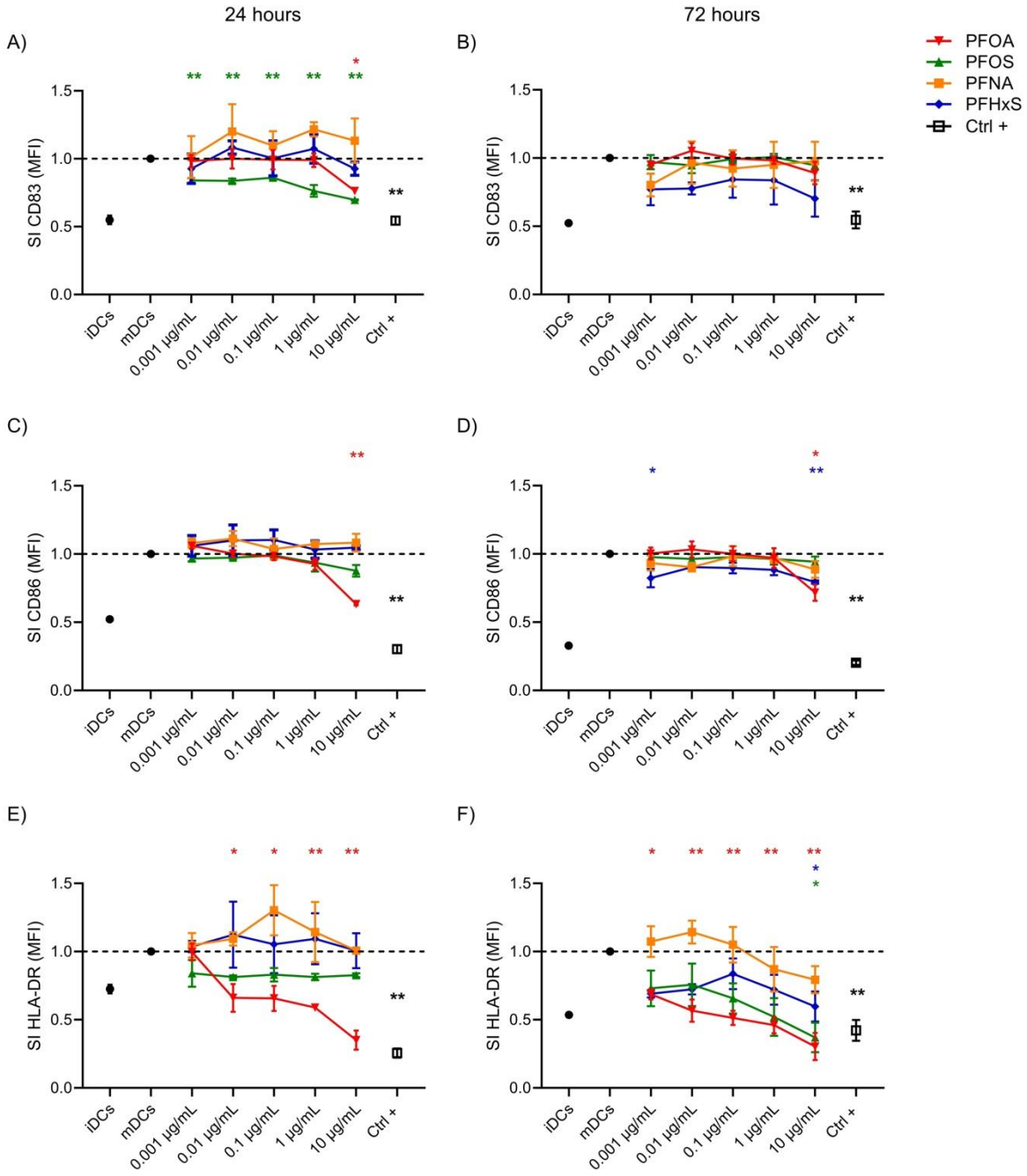

Figure 3: Effect of PFOA, PFNA, PFHxS and PFOS on surface marker expression associated with DC maturation. Analysis of the expressions of CD83 (A, B), CD86 (C, D) and HLA-DR (E, F) were reported. iDCs (1x10^6 cells/mL) were treated with increasing concentration of the four selected PFAS or the positive control DEX (150 µg/mL, Ctrl +) for 24h. Then, the maturation cocktail composed of rhIL-4 (3000 IU/mL), rhGM-CSF (1500 IU/mL), rhTNF-α (2000 IU/mL) and ionomycin (200 ng/mL) was added for additional 24 and 72h to acquire the properties of mDCs. After 24 and 72h, surface markers were evaluated. The dashed line was set to 1, in relation to the control cells (mDCs). The results of the maturation are reported and expressed as SI of MFI. Any value shown in the graph represents the mean ± SEM, with n = 3 independent experiments. Statistical analysis was carried out using one-

way ANOVA, followed by Dunnett's test for PFAS vs mDCs, while unpaired t-test for DEX vs mDCs. Results were considered significant if $p \leq 0.05$, with * $p \leq 0.05$ and ** $p \leq 0.01$ vs mDCs. The color of the asterisks matches the color used to indicate different compounds

Figure 3 shows that the four tested PFAS induced different effects on the markers associated with DCs maturation. The different markers have a different kinetic and optimal time of expression: 24h for CD83 and CD86, 72h for HLA-DR, which is also reflected in their modulation by PFAS.

CD83 is a marker present only on mDCs, and it is important for the stabilization of MHC II on cell membrane. The expression of CD83 was statistically significantly reduced at 24h by PFOS at all concentration tested and by PFOA at 10 µg/mL (Figure 3A). PFNA and PFHxS showed no effect on CD83 expression.

CD86 is a protein constitutively expressed on antigen presenting cells and along with CD80, CD86 provides costimulatory signals necessary for T cell activation and survival. This marker was only marginally modulated by PFAS, without any clear dose response. A statistically significantly reduction was observed at 24 and 72h by PFOA at the highest concentration tested (Figure 3C and 3D) and by PFHxS only at 72h at the concentrations 0.001 and 10 µg/mL (Figure 3D).

The last marker analysed was HLA-DR, a class II MHC cell surface receptor, and its main role is to present antigens to Th cells. PFOA was able to down-regulate the expression of HLA-DR already after 24h of treatment (Figure 3E) and that suppression was also present after 72h at all concentration tested (Figure 3F). The same marker was also downregulated in a statistically significantly way by PFHxS and PFOS at the higher concentration (10 µg/mL). It is interesting to note that, for the HLA-DR marker, the immunosuppressive response is comparable to the positive control DEX, a known immunosuppressant drug, indicative of a marked immunosuppressive effect of PFOA, PFOS and PFHxS. PFNA did not significantly alter the expression of HLA-DR, only a modest reduction of HLA-DR expression at the higher concentration tested (10 µg/mL) after 72h of treatment could be observed (Figure 3F), which was not statistically significant.

Under the experimental conditions used, the marker more consistently affected by PFAS was HLA-DR. In term of potency, regarding the effects on DC maturation, PFAS can be ranked as follow: PFOA>PFOS>PFHxS>>>PFNA. Considering the role of HLA class II in Th cell activation, the decrease observed can contribute to a defective Th lymphocyte activation.

2.3.3 Effects on T cell proliferation and Th cell differentiation

Th cells are the primary orchestrators of the adaptive immune response, mediating subsequent cellular and humoral responses. They can differentiate into Th1, Th2, Th9, Th17, Th22, Tfh, Treg cells, depending on the pathogen and types of cytokines present in the cellular microenvironment, with each Th cell subsets characterized by unique functions. Th cells are responsible for responding to both intracellular and extracellular pathogens and they are also involved in various diseases, like autoimmunity and allergy. Th1 cells secrete pro-inflammatory cytokines such as interferon-gamma (IFN-γ), tumor necrosis factor-alpha (TNF-α), interleukin-2 (IL-2), IL-8, and IL-12p70, that can activate

macrophages and cell-mediated immune reactions that play critical roles in resistance to infection by intracellular pathogens, in cytotoxic and rejection reactions. Th2 cells secrete IL-4, IL-6, IL-10, and IL-13, which induce antibody production and are associated with strong humoral immunity. IL-17 and IL-22 are the main Th17 effector cytokines, which are related to protective immunity against extracellular microbes, and several autoimmune diseases and neutrophilic asthma. Transforming growth factor-β (TGF-β) is secreted by regulatory T (Treg) cells and has anti-inflammatory functions.

To mimic this event, PBMC obtained from human buffy coats, were treated with increasing concentration of the four selected PFAS for 24h and then stimulated with antiCD3 plus antiCD28 for 4 days to induce Th cells maturation and differentiation. At the end of the treatment, T cells proliferation (using CFSE staining), Th cells differentiation (Th1, Th2, Th17, Treg) and cytokine production (IL-4, IL-10, IL-17A, IFN-γ and TGF-β) were assessed by flow cytometer analysis and ELISA, respectively.

To assess cell proliferation, CFSE staining was used. The technique depends on CFSE's capacity to covalently bind to long-lived intracellular molecules using the intensely fluorescent carboxyfluorescein dye. After each cellular division, the even distribution of these fluorescent molecules among the progeny cells leads to a halving of the fluorescence in the daughter cells, a phenomenon that is observed in the histograms. CFSE staining was able to detect up to 8 cellular divisions. Figure 4 reports examples of histogram provided by the Novo Express software after PFOA treatment in female donors.

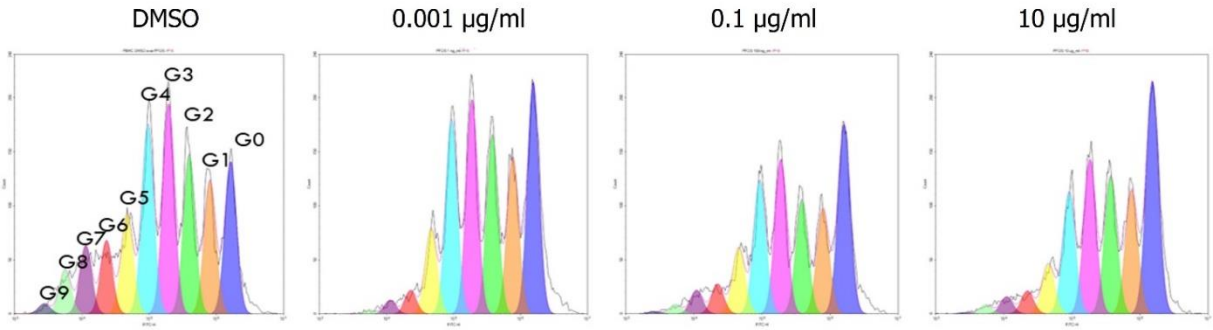

Figure 4: Representative CFSE histograms following of PFOA exposure in female PBMC. Cells (2x106 cells/mL) were then treated for 24h with increasing concentration of PFOA (0.001, 0.1 and 10 µg/mL), and then stimulated with antiCD3 and anti CD28 (1:100 titer) for 4 days. At the end, proliferation was evaluated by flow cytometer analysis and representative histograms showed. The concentrations of PFAS and vehicle control were corrected for the effectively cell density of the treatment under examination by comparing the ug administered to 1x106 of cells

Tables 2 to 5 report the results obtained for male donors, while tables 6 to 9 report the results obtained for female donors. Results are expressed as the mean percentage of cells present in each duplication population ± SEM. The G0 population represents the initial undivided cell population. As can be seen, as the concentration of the four selected PFAS increases, there is a statistically significant increase in the percentage of cells in G0 with respect to the control, and a consequent reduction of the percentage of cells in the latter dividing populations (G5-G7), which indicates that PFOA, PFNA, PFHxS and PFOS were able to inhibit Th cell clonal expansion. More in detail, the statistically significant increase can

be observed for PFNA and PFHxS (10 µg/mL) in male donors, and for PFOA, PFOS and PFNA (10 µg/mL) in female one.

Table 2: Effect of PFOA on T cell proliferation in male donors

		PFOA		
	Ctrl	**0.001 µg/mL**	**0.1 µg/mL**	**10 µg/mL**
G0	10.96 ± 3.50	22.73 ± 4.80	14.59 ± 4.68	25.16 ± 6.27
G1	7.63 ± 2.51	8.79 ± 2.63	8.03 ± 2.89	6.82 ± 2.77
G2	13.03 ± 4.35	14.78 ± 6.16	13.31 ± 4.44	11.93 ± 2.49
G3	19.66 ± 4.56	17.88 ± 4.51	19.30 ± 5.28	16.40 ± 2.41
G4	18.94 ± 4.36	14.55 ± 4.37	17.89 ± 3.70	17.71 ± 2.18
G5	11.04 ± 4.21	10.98 ± 4.66	11.48 ± 4.87	9.49 ± 4.20
G6	6.64 ± 2.99	3.86 ± 1.87	5.41 ± 2.89	4.41 ± 2.541
G7	7.72 ± 3.15	3.91 ± 1.84	6.13 ± 3.41	5.28 ± 2.83
G8	3.98 ± 1.41	2.41 ± 1.33	3.47 ± 1.91	2.64 ± 1.48
G9	0.42 ± 0.20	0.12 ± 0.05	0.40 ± 0.24	0.18 ± 0.15

Before the incubation with PFOA and T cell activation, PBMC ($2x10^6$ cells/mL) were stained with CFSE. Cells were then treated for 24h with increasing concentration of PFOA (0.001, 0.1 and 10 µg/mL), and then stimulated with antiCD3 and anti CD28 (1:100 titer) for 4 days. The concentrations of PFAS and vehicle control were corrected for the effectively cell density of the treatment under examination by comparing the ug administered to $1x10^6$ of cells. At the end, proliferation was evaluated by flow cytometer analysis. Each value represents the mean ± SEM, with n= 5 male donors. Statistical analysis was carried out using one-way ANOVA, followed by Dunnett's test. The results were considered significant if $p \leq 0.05$. No statistical significant results were detected.

Table 3: Effect of PFOS on T cell proliferation in male donors

		PFOS		
	Ctrl	**0.001 µg/mL**	**0.1 µg/mL**	**10 µg/mL**
G0	10.96 ± 3.50	13.35 ± 3.75	13.81 ± 4.43	28.27 ± 10.05
G1	7.63 ± 2.51	8.02 ± 2.84	7.71 ± 2.58	8.10 ± 2.36
G2	13.03 ± 4.35	13.28 ± 4.43	12.63 ± 4.42	11.53 ± 2.66
G3	19.66 ± 4.56	20.30 ± 5.56	19.63 ± 5.07	17.83 ± 5.13
G4	18.94 ± 4.36	17.80 ± 3.71	17.54 ± 3.68	15.96 ± 2.99
G5	11.04 ± 4.21	10.72 ± 4.23	10.96 ± 4.45	7.49 ± 3.18
G6	6.64 ± 2.99	4.89 ± 2.58	5.37 ± 2.57	4.39 ± 2.50
G7	7.72 ± 3.15	6.58 ± 3.68	6.42 ± 3.22	4.11 ± 2.95
G8	3.98 ± 1.41	4.63 ± 2.59	4.55 ± 2.33	2.02 ± 1.53

Before the incubation with PFOS and the activation of T cells, PBMC ($2x10^6$ cells/mL) were stained with CFSE. Cells were then treated for 24h with increasing concentration of PFOS (0.001, 0.1 and 10 µg/mL), and then stimulated with antiCD3 and anti CD28 (1:100 titer) for 4 days. The concentrations of PFAS and vehicle control were corrected for the effectively cell density of the treatment under examination by comparing the ug administered to $1x10^6$ of cells. At the end, proliferation was evaluated by flow cytometer analysis. Each value represents the mean ± SEM, with n = 5 male donors. Statistical analysis was carried out using one-way ANOVA, followed by Dunnett's test. The results were considered significant if $p \leq 0.05$. No statistical significant results were detected.

Table 4: Effect of PFNA on T cell proliferation in male donors

		PFNA		
	Ctrl	**0.001 µg/mL**	**0.1 µg/mL**	**10 µg/mL**
G0	19.01 ± 5.16	18.29 ± 5.27	15.96 ± 1.47	33.07 ± 8.41 *
G1	6.61 ± 0.83	6.67 ± 0.91	7.13 ± 0.95	7.07 ± 0.80
G2	10.07 ± 1.00	10.25 ± 1.00	10.45 ± 1.20	10.51 ± 1.15
G3	16.14 ± 2.14	15.69 ± 1.79	16.26 ± 1.88	15.16 ± 2.39
G4	22.23 ± 2.68	22.58 ± 2.85	22.56 ± 2.09	18.20 ± 3.73
G5	17.58 ± 3.36	17.20 ± 3.12	16.67 ± 2.51	11.39 ± 2.65
G6	4.12 ± 1.43	4.56 ± 1.46	4.73 ± 1.79	2.76 ± 0.78
G7	4.23 ± 2.21	4.76 ± 1.97	6.23 ± 3.53	1.85 ± 0.71

Before the incubation with PFNA and the activation of T cells, PBMC ($2x10^6$ cells/mL) were stained with CFSE. Cells were then treated for 24h with increasing concentration of PFNA (0.001, 0.1 and 10 µg/mL), and then stimulated with antiCD3 and anti CD28 (1:100 titer) for 4 days. The concentrations of PFAS and vehicle control were corrected for the effectively cell density of the treatment under examination by comparing the ug administered to $1x10^6$ of cells. At the end, proliferation was evaluated by flow cytometer analysis. Each value represents the mean ± SEM, with n = 5 male donors. Statistical analysis was carried out using one-way ANOVA, followed by Dunnett's test. The results were considered significant if $p \leq 0.05$, with * $p \leq 0.05$ vs Ctrl.

Table 5: Effect of PFHxS on T cell proliferation in male donors

		PFHxS		
	Ctrl	**0.001 µg/mL**	**0.1 µg/mL**	**10 µg/mL**
G0	19.01 ± 5.16	16.30 ± 2.68	17.10 ± 2.84	28.36 ± 6.82 *
G1	6.61 ± 0.83	6.98 ± 0.76	7.40 ± 0.67	7.85 ± 0.59
G2	10.07 ± 1.00	10.52 ± 1.09	10.93 ± 0.98	11.19 ± 0.94
G3	16.14 ± 2.14	16.87 ± 1.78	17.43 ± 1.88	16.65 ± 2.07
G4	22.23 ± 2.68	23.88 ± 1.70	24.03 ± 1.87	20.38 ± 3.40
G5	17.58 ± 3.36	17.06 ± 2.84	16.07 ± 2.38	11.20 ± 1.80 *
G6	4.12 ± 1.43	4.08 ± 1.21	3.45 ± 1.10	2.62 ± 0.87
G7	4.23 ± 2.21	4.31 ± 2.14	3.79 ± 2.05	1.75 ± 0.60

Before the incubation with PFHxS and the activation of T cells, PBMC ($2x10^6$ cells/mL) were stained with CFSE. Cells were then treated for 24h with increasing concentration of PFHxS (0.001, 0.1 and 10 µg/mL), and then stimulated with antiCD3 and anti CD28 (1:100 titer) for 4 days. The concentrations of PFAS and vehicle control were corrected for the effectively cell density of the treatment under examination by comparing the ug administered to $1x10^6$ of cells. At the end, proliferation was evaluated by flow cytometer analysis. Each value represents the mean ± SEM, with n = 5 male donors. Statistical analysis was carried out using one-way ANOVA, followed by Dunnett's test. The results were considered significant if $p \leq 0.05$, with * $p \leq 0.05$ vs Ctrl.

Table 6: Effect of PFOA on T cell proliferation in female donors

		PFOA		
	Ctrl	**0.001 µg/mL**	**0.1 µg/mL**	**10 µg/mL**
G0	31.23 ± 5.34	49.12 ± 8.33	46.91 ± 8.59	68.54 ± 7.86 **
G1	6.28 ± 1.33	7.06 ± 1.23	6.96 ± 0.86	6.64 ± 1.38
G2	9.83 ± 0.83	9.47 ± 1.23	8.77 ± 1.08	7.66 ± 1.66
G3	14.26 ± 0.92	12.38 ± 1.39	11.92 ± 1.32	7.47 ± 1.37 **
G4	18.12 ± 1.51	11.41 ± 1.79 *	11.90 ± 2.17	4.30 ± 1.55 **
G5	12.42 ± 3.44	4.40 ± 1.86	5.77 ± 1.81	2.30 ± 1.04 **
G6	2.59 ± 1.44	2.67 ± 1.64	3.23 ± 1.62	1.43 ± 0.88
G7	2.61 ± 1.53	2.03 ± 1.58	2.54 ± 1.25	1.40 ± 0.84
G8	1.95 ± 1.68	1.25 ± 1.16	1.85 ± 0.91	0.24 ± 0.16
G9	0.71 ± 0.69	0.22 ± 0.20	0.14 ± 0.09	0.02 ± 0.02

Before the incubation with PFOA and the activation of T cells, PBMC ($2x10^6$ cells/mL) were stained with CFSE. Cells were then treated for 24h with increasing concentration of PFOA (0.001, 0.1 and 10 µg/mL), and then stimulated with antiCD3 and anti CD28 (1:100 titer) for 4 days. The concentrations of PFAS and vehicle control were corrected for the effectively cell density of the treatment under examination by comparing the ug administered to $1x10^6$ of cells. At the end, proliferation was evaluated by flow cytometer analysis. Each value represents the mean ± SEM, with n = 5 male donors. Statistical analysis was carried out using one-way ANOVA, followed by Dunnett's test. The results were considered significant if $p \leq 0.05$, with * $p \leq 0.05$ and ** $p \leq 0.01$ vs Ctrl.

Table 7: Effect of PFOS on T cell proliferation in female donors

		PFOS		
	Ctrl	**0.001 µg/mL**	**0.1 µg/mL**	**10 µg/mL**
G0	31.23 ± 5.34	56.13 ± 10.89	49.08 ± 9.34	73.12 ± 10.10 **
G1	6.28 ± 1.33	6.29 ± 0.72	6.07 ± 1.8	6.64 ± 1.27
G2	9.83 ± 0.83	8.12 ± 1.09	8.30 ± 1.68	6.62 ± 2.43
G3	14.26 ± 0.92	9.78 ± 2.16	10.11 ± 1.71	5.59 ± 2.64 **
G4	18.12 ± 1.51	8.96 ± 2.54 *	10.76 ± 1.66	4.79 ± 2.23 **
G5	12.42 ± 3.44	4.15± 2.16	7.00 ± 2.70	1.52 ± 1.00 *
G6	2.59 ± 1.44	3.19 ± 2.29	4.03 ± 2.04	1.28 ± 0.96
G7	2.61 ± 1.53	2.28 ± 2.08	2.32 ± 2.02	0.24 ± 0.17
G8	1.95 ± 1.68	0.87 ± 0.79	2.20 ± 1.33	0.18 ± 0.17

Before the incubation with PFOS and the activation of T cells, PBMC ($2x10^6$ cells/mL) were stained with CFSE. Cells were then treated for 24h with increasing concentration of PFOS (0.001, 0.1 and 10 µg/mL), and then stimulated with antiCD3 and anti CD28 (1:100 titer) for 4 days. The concentrations of PFAS and vehicle control were corrected for the effectively cell density of the treatment under examination by comparing the ug administered to $1x10^6$ of cells. At the end, proliferation was evaluated by flow cytometer analysis. Each value represents the mean ± SEM, with n = 5 male donors. Statistical analysis was carried out using one-way ANOVA, followed by Dunnett's test. The results were considered significant if $p \leq 0.05$, with * $p \leq 0.05$ and ** $p \leq 0.01$ vs Ctrl.

Table 8: Effect of PFNA on T cell proliferation in female donors

		PFNA		
	Ctrl	**0.001 µg/mL**	**0.1 µg/mL**	**10 µg/mL**
G0	47.58 ± 13.22	38.11 ± 9.41	43.35 ± 11.77	60.58 ± 14.58 *
G1	6.47 ± 1.08	5.15 ± 0.98	6.90 ± 1.22	5.07 ± 0.81
G2	8.69 ± 1.30	9.53 ± 1.09	9.72 ± 1.64	6.89 ± 1.84
G3	12.41 ± 2.97	15.16 ± 2.17	14.28 ± 2.78	8.84 ± 3.69 *
G4	13.10 ± 5.04	17.27 ± 3.43	14.28 ± 2.78	10.90 ± 5.18
G5	8.79 ± 4.17	9.99 ± 3.47	8.45 ± 3.99	6.10 ± 3.41
G6	2.12 ± 1.12	2.83 ± 1.04	2.04 ± 0.82	1.09 ± 0.57
G7	0.62 ± 0.15	1.55 ± 0.53	0.79 ± 0.24	0.36 ± 0.20

Before the incubation with PFNA and the activation of T cells, PBMC ($2x10^6$ cells/mL) were stained with CFSE. Cells were then treated for 24h with increasing concentration of PFNA (0.001, 0.1 and 10 µg/mL), and then stimulated with antiCD3 and anti CD28 (1:100 titer) for 4 days. The concentrations of PFAS and vehicle control were corrected for the effectively cell density of the treatment under examination by comparing the ug administered to $1x10^6$ of cells. At the end, proliferation was evaluated by flow cytometer analysis. Each value represents the mean ± SEM, with n = 5 male donors. Statistical analysis was carried out using one-way ANOVA, followed by Dunnett's test. The results were considered significant if $p \leq 0.05$, with * $p \leq 0.05$ vs Ctrl.

Table 9: Effect of PFHxS on T cell proliferation in female donors

		PFHxS		
	Ctrl	**0.001 µg/mL**	**0.1 µg/mL**	**10 µg/mL**
G0	47.58 ± 13.22	41.99 ± 9.61	41.85 ± 10.74	56.39 ± 13.49
G1	6.47 ± 1.08	6.98 ± 1.45	7.81 ± 1.20	6.06 ± 0.92
G2	8.69 ± 1.30	10.56 ± 1.43	10.69 ± 1.86	7.44 ± 1.41
G3	12.41 ± 2.97	15.24 ± 2.11	15.31 ± 2.62	10.46 ± 3.23
G4	13.10 ± 5.04	14.94 ± 3.83	14.35 ± 4.47	11.06 ± 5.02
G5	8.79 ± 4.17	8.10 ± 3.60	7.98 ± 3.76	6.05 ± 2.89
G6	2.12 ± 1.12	1.57 ± 0.91	1.37 ± 0.79	1.29 ± 0.47
G7	0.62 ± 0.15	0.40 ± 0.18	0.41 ± 0.21	0.54 ± 0.33

Before the incubation with PFHxS and the activation of T cells, PBMC ($2x10^6$ cells/mL) were stained with CFSE. Cells were then treated for 24h with increasing concentration of PFHxS (0.001, 0.1 and 10 µg/mL), and then stimulated with antiCD3 and anti CD28 (1:100 titer) for 4 days. The concentrations of PFAS and vehicle control were corrected for the effectively cell density of the treatment under examination by comparing the ug administered to $1x10^6$ of cells. At the end, proliferation was evaluated by flow cytometer analysis. Each value represents the mean ± SEM, with n = 5 male donors. Statistical analysis was carried out using one-way ANOVA, followed by Dunnett test. The results were considered significant if $p \leq 0.05$. No statistical significant results were detected.

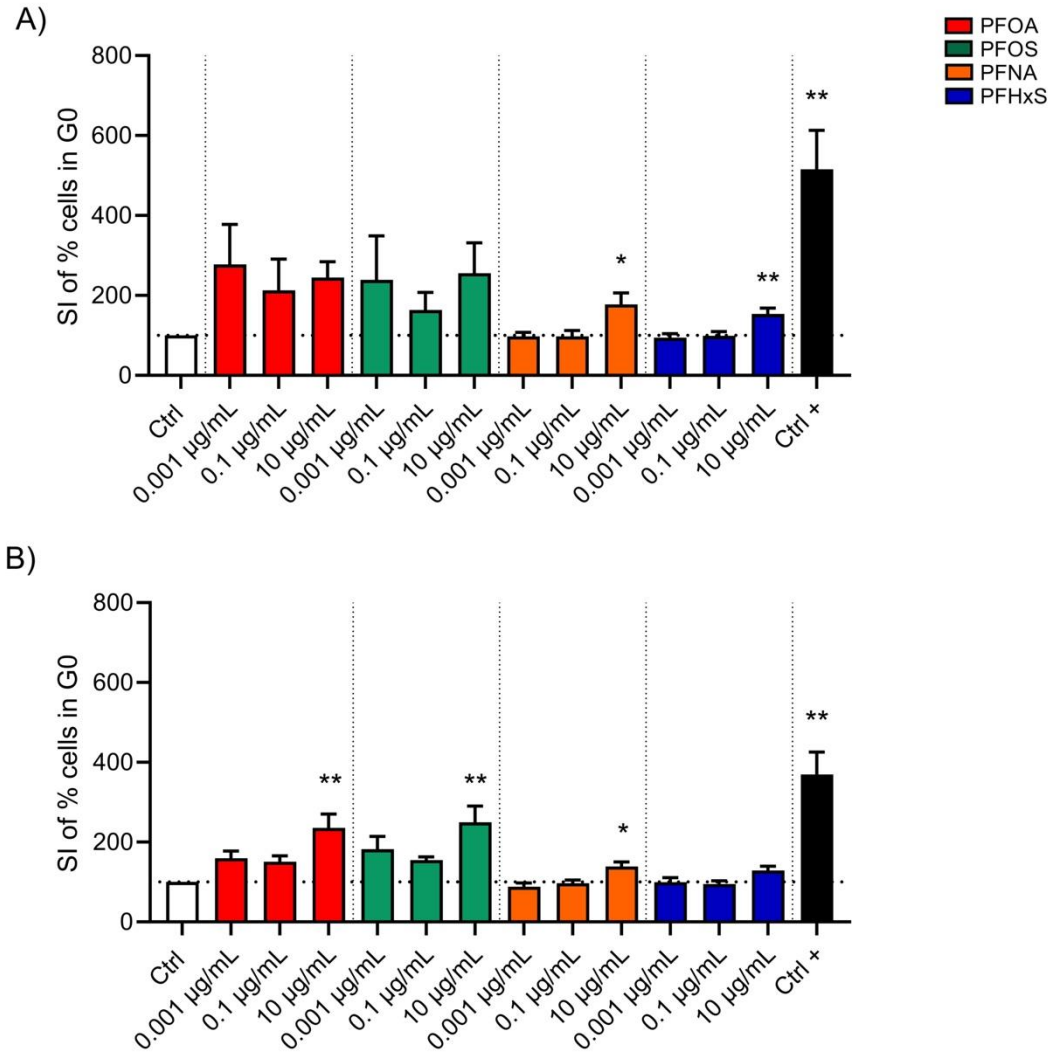

Figure 5: Effect of PFHxS, PFNA, PFOA and PFOS on G0 of T cell proliferation in male (A) and female (B) donors. Before the incubation with the selected chemicals and the activation of T cells, PBMC ($2x10^6$ cells/mL) were stained with CFSE. Cells were then treated for 24h with increasing concentration of PFHxS, PFNA, PFOA and PFOS (0.001, 0.1 and 10 µg/mL) and positive control Cyclosporin A (1.2 µg/mL, Ctrl +) and then stimulated with antiCD3 and anti CD28 (1:100 titer) for 4 days. The concentrations of PFAS, DMSO and Ctrl + were corrected for the effectively cell density of the treatment under examination by comparing the ug administered to $1x10^6$ of cells. At the end, proliferation was evaluated by flow cytometer analysis. Each value represents the mean ± SEM, with n = 5 male and n = 5 female donors. Statistical analysis was carried out using one-way ANOVA, followed by Dunnett's test for PFAS vs Ctrl (represented by the dot line at 1), while unpaired Welch's t-test for Cyclosporin A (Ctrl +) vs Ctrl. Results were considered significant if $p \leq 0.05$, with * $p \leq 0.05$ and ** $p \leq 0.01$ vs Ctrl

Overall, the results of T cell proliferation indicate a reduction in the number of duplication cycles following exposure to PFAS, as evidenced by a higher percentage of cells in G0 (Figure 5). These findings indicate the ability of PFAS to contrast clonal expansion, which is the initial step in all acquired immune responses. The process of clonal expansion not only increases the quantity of specialized lymphocytes to establish a strong protective response against the pathogen but also leads to the selection and differentiation of these responding lymphocytes, producing a variety of cell destinies necessary to protect us against different pathogens (Adams et al., 2020). By compromising T cell proliferation, all TD immune responses will be affected. To further support the consequences of the inhibition of T cell proliferation, an AOP linking the inhibition of calcineurin activity (i.e., target of cyclosporin A), pivotal in T cell proliferation, with impaired TDAR has been recently published (Komatsu et al., 2021). In term of potency, overall, the data indicate also in relation to dose and gender a higher percentage of cells in G0 following exposure to PFOA=PFOS>PFNA>PFHxS.

Subsequently, the effects of the selected PFAS on Th cells differentiation and cytokines productions were investigated. Cyclosporin A (Ctrl +) was used as positive control. To perform these analyses, after 4 days of treatment, Golgi stop was added to block intracellular protein transport processes. After 5h, intracellular proteins were analyses by flow cytometer, and released cytokines were assessed by ELISA. Results are shown in Figures 6 to 8.

Figure 6 shows the results relative to Th1, Th2 and Th17 (and related cytokine release) in male donors; the same results for female donors are reported in Figure 7. Results relative to Treg are reported in Figure 9. For the assessment of Th1, Th2 and Th17, commercially Human Th1/Th2/Th17 Phenotyping Kit (BDbioscences) was used.

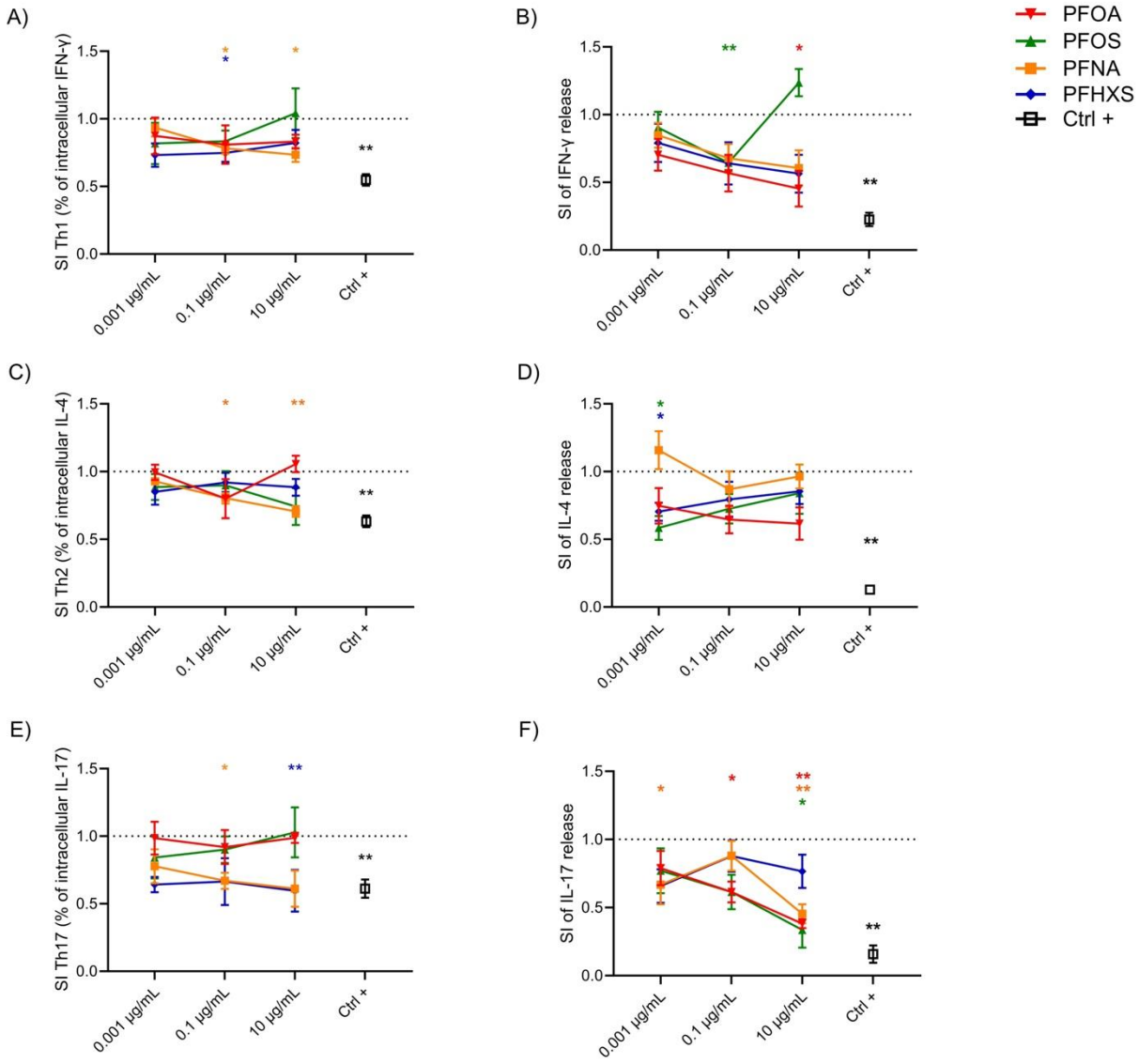

Figure 6: Effect of the PFOA, PFNA, PFHxS and PFOS on Th1, Th2 and Th17 differentiation in male donors. Analysis of the Th1/Th2/Th17 subsets after PFAS treatment in male human donors. Human PBMC ($2x10^6$ cells/mL) were treated for 24h with increasing concentration of PFOA, PFNA, PFHxS and PFOS (0.001, 0.1 and 10 µg/mL) or Cyclosporin A (Ctrl +, 1.2 µg/mL) and then, cells were stimulated with antiCD3 plus antiCD28 (1:100 titer) to induce the T cell differentiation. After 4 days, Golgi stop was added for 5h, and intracellular protein (6A, 6C, 6E) analysed using flow cytometer, while the release of cytokines (6B, 6D, 6F) was analysed by ELISA. The concentrations of PFASwwre normalised to $1x10^6$ of cells, in order that in all experiments the cells will receive the same amount of PFAS. At the end, proliferation was evaluated by flow cytometer analysis. The results are expressed as SI relative to vehicle treated cells. Each value represents the mean ± SEM, with n = 5 different male donors. Statistical analysis was carried out using one-way ANOVA, followed by Dunnett's test for PFAS vs Ctrl (represented by the dot line at 1), while unpaired Welch's t-test for Cyclosporin A (Ctrl +) vs Ctrl. Results were considered significant if $p \leq 0.05$, with * $p \leq 0.05$ and ** $p \leq 0.01$ vs Ctrl. The colour of the asterisks matches the colour used to indicate different compounds

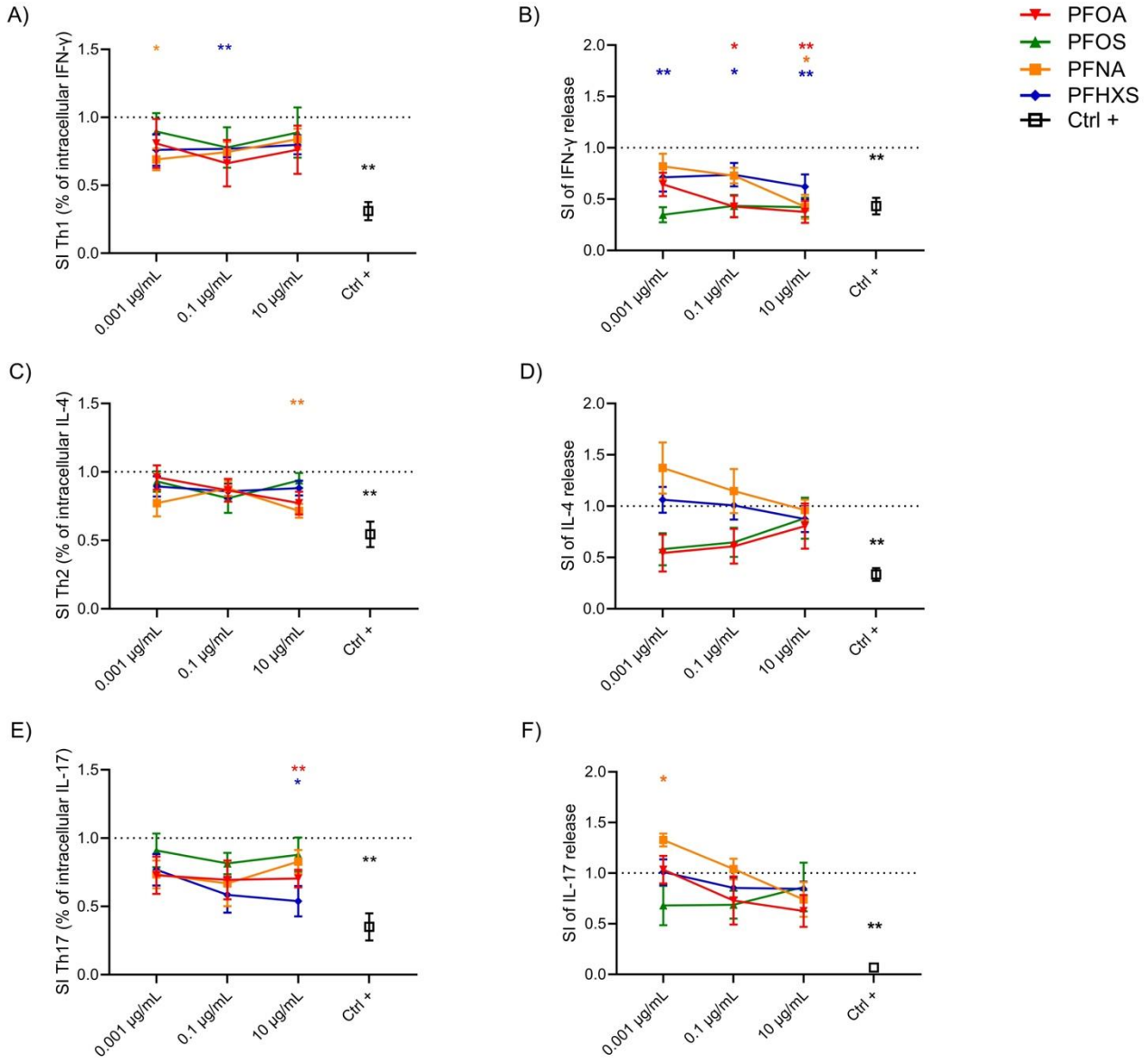

Figure 7: Effect of the PFOA, PFNA, PFHxS and PFOS on Th1, Th2 and Th17 differentiation in female donors. Analysis of the Th1/Th2/Th17 subsets after PFAS treatment in female human donors. Human PBMC ($2x10^6$ cells/mL) were treated for 24h with increasing concentration of PFOA, PFNA, PFHxS and PFOS (0.001, 0.1 and 10 µg/mL) or Cyclosporin A (Ctrl +, 1.2 µg/mL) and then, cells were stimulated with antiCD3 plus antiCD28 (1:100 titer) to induce the T cell differentiation. After 4 days, Golgi stop was added for 5h, and intracellular protein (7A, 7C, 7E) analysed using flow cytometer, while the release of cytokines (7B, 7D, 7F) was analysed by ELISA. The concentrations of PFAS, DMSO and Ctrl + were corrected for the effectively cell density of the treatment under examination by comparing the µg administered to $1x10^6$ of cells. At the end, proliferation was evaluated by flow cytometer analysis. The results are expressed as SI relative to vehicle treated cells. Each value represents the mean ± SEM, with n = 5 different female donors. Statistical analysis was carried out using one-way ANOVA, followed by Dunnett's test for PFAS vs Ctrl (represented by the dot line at 1), while unpaired Welch's t-test for Cyclosporin A (Ctrl +)

vs Ctrl. Results were considered significant if $p \leq 0.05$, with * $p \leq 0.05$ and ** $p \leq 0.01$ vs Ctrl. The colour of the asterisks matches the colour used to indicate different compounds

As shown in Figure 6 and Figure 7, all PFAS tested were able to affect to a different extent T cell differentiation both in male and female donors. In most of the cases, results did not show clear dose responses. The release of IFN-γ seems to be the parameters more affected in both of the gender in which is possible appreciated a general trend of reduction in the release for all the four PFAS tested compared to the control with some significant statistical results for PFOS ad PFOA in male donors, and for PFOA, PFNA and PFHxS in female one. More in detail, following PFHxS exposure in females, the release of IFN-γ was equally statistically significantly decreased at all concentration tested, suggesting a receptor mediated effect already saturated at the lower concentration. Moreover, in male donors it is possible appreciate a statistically significant reduction of the IL-17 release following PFOA, PFNA and PFOS exposure. Overall, the results relating to Th cell differentiation indicate modest effects, the direction of which suggests a reduction in differentiation, consistent with the observed inhibitory effect on proliferation. Th1 cells appear to be more affected compared to Th2, which can support the *in vivo* observation of reduced resistance to infection in children (Dalsager et al., 2016; Granum et al., 2013).

In Figure 8, results obtained in male and female donors are compared to appreciate possible gender effects. In some instances, it is possible to observe sporadic differences in response on the differentiation of Th correlated to the sex of the donors. PFOA at 10 µg/mL was able to suppress more Th2 and Th17 cells in female compare male donors (Figure 8A and 8B). At the contrary, PFNA was able to alter the Th17 phenotyping more in male that female donors at the concentration of 0.001 µg/mL (Figure 8C and 8D). The release of IL-4 was more suppressed in male donors after PFHxS treatment, and it was possible to observe also that the ratio of the release IFN-γ/IL-4 is more balance on Th2 phenotyping in female donors compare to male (Figure 8E and 8F). Lastly, the release of IFN-γ was more suppressed in female donors compare to the male and it is possible to see that the ratio of IFN-γ/IL-4 is more balanced on Th1 phenotyping for male donors, while is more Th2 phenotyping for female one (Figure 8G e 8H).

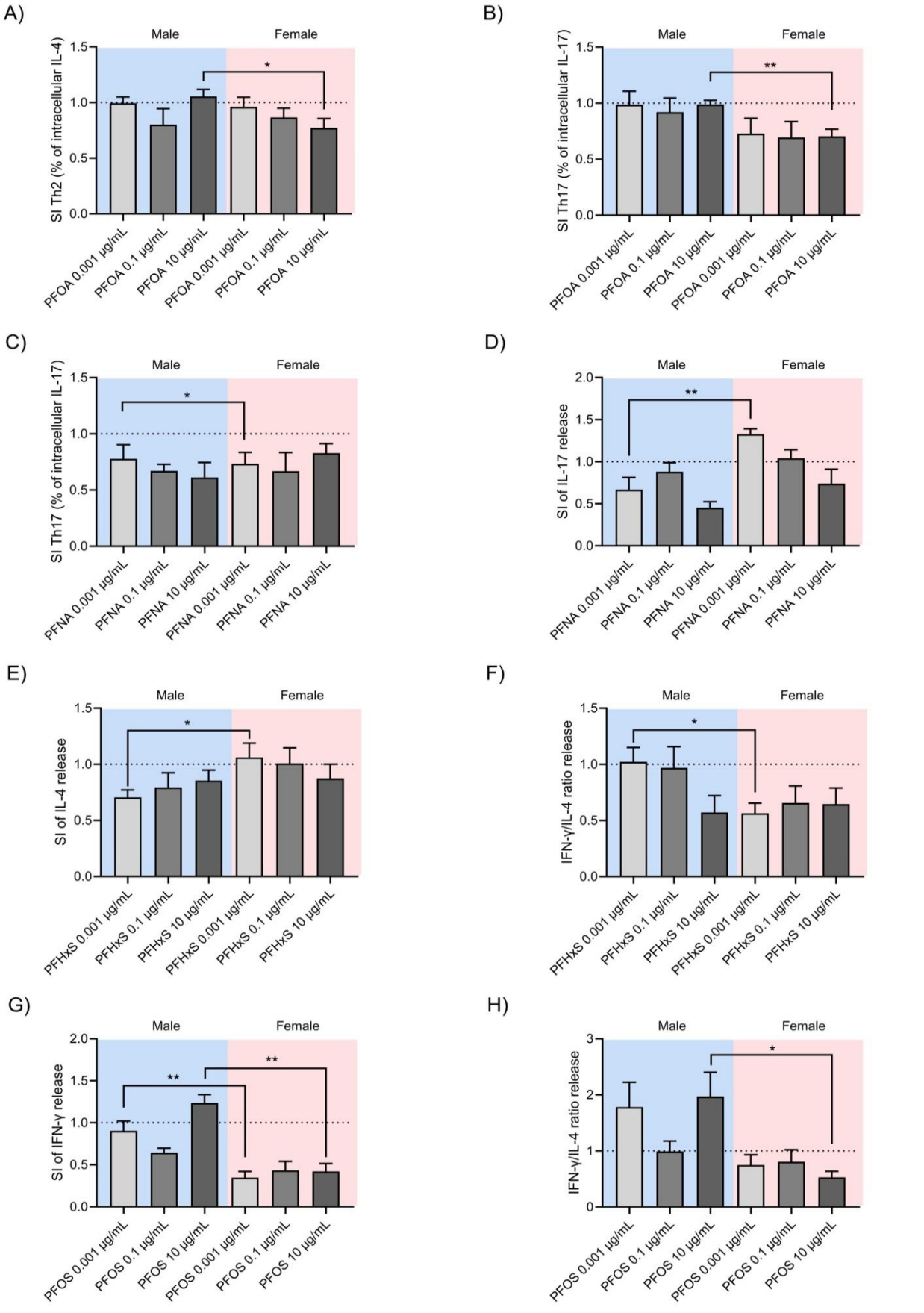

Figure 8: Comparison of the effects of PFOA, PFNA, PFHxS and PFOS on Th1, Th2 and Th17 differentiation in male and female donors. Analysis of the Th1/Th2/Th17 phenotypes in male and female donors following exposure to PFAS to assess possible gender difference. Human PBMC ($2x10^6$ cells/ml) were treated for 24h with increasing concentration of PFOA, PFNA, PFHxS and PFOS (0.001, 0.1 and 10 µg/mL) and then, cells were stimulated with antiCD3 plus antiCD28 to induce the T cell differentiation. After 4 days, Golgi stop was added for 5h and in the end the intracellular protein (8A, 8B and 8C) were analysed using flow cytometer, while the release of cytokines (8D, 8E, 8F, 8G and 8) was analysed thought ELISA. The concentrations of PFAS, DMSO and Ctrl + were corrected for the effectively cell density of the treatment under examination by comparing the µg administered to $1x10^6$ of cells. At the end, proliferation was evaluated by flow cytometer analysis. The results are expressed as SI respect to vehicle treated cells. Each value represents the mean ± SEM, with n = 5 different male donors. Statistical analysis was carried out using unpaired Welch's t-test for male vs female. Results were considered significant if $p \leq 0.05$, with * $p \leq 0.05$ and ** $p \leq 0.01$ male vs female

For the assessment of Treg cells, the Treg Detection Kit was used (Milteny biotec). As shown in Figure 9 in both male (Figure 9A) and female (Figure 9B) donors, all the four PFAS were able to downregulate the Tregs (CD25+FoxP3+CD127-). The related cytokines TGF-β was not altered (Figure 9E, 9F), while the release of IL-10 was slightly suppressed at the higher concentration of PFOA, PFHxS and PFOS in male donors (Figure 9C) and at the higher concentration of PFOA, PFNA and PFHxS in female donors (Figure 9D), consistent with the decrease in the % of Treg.

The reduction in Treg following PFAS exposure suggests a generalized inhibition of Th maturation, differentiation, and activation. The Treg phenotype in male was statistically significant suppressed by all the four chemicals at the higher concentration (10 µg/mL) and it is possible to notice that PFOS was able to suppress that phenotype already at the lower concentration of 0.001 µg/mL. In female donors the Treg phenotype was statistically significant suppressed by PFOA at al concentration tested and by PFNA at the higher concentration (10 µg/mL), suggesting difference correlated to the sex. Furthermore, the release of IL-10 was statistically significant suppressed in both in male (by PFHxS, PFOA and PFOS) and female donors (by PFNA, PFOA and PFHxS) and that suppression is comparable with the positive control Cyclosporin A (1.2 µg/mL). As a negative regulator, IL-10 plays an important role during immune responses (Zheng et al., 2011). IL-10 is a potent anti-inflammatory cytokine such as IFN-γ and TNF-α by Th1 (Fiorentino et al., 1989). IL-10 also promotes B cell differentiation, proliferation, survival, and antibody production (Saxena et al., 2015) and this evidence can be associated with the results obtained in which there is a correlation between the reduction of IL-10 and a reduction in the release of immunoglobulins (Igs) IgG and IgM antibodies mediated by B cells (for the result about this part see section 2.3.4 below). It was also possible to observe a difference in response correlated to the sex of the donors, with TGF-β more affected in female compare male donors after PFOA (Figure 10A), PFNA (Figure 10D) and PFHxS (Figure 10B) treatments. In contrast, the total Treg expression appear statistically significant affect more in male donors compare female one after PFNA exposure (Figure 10C).

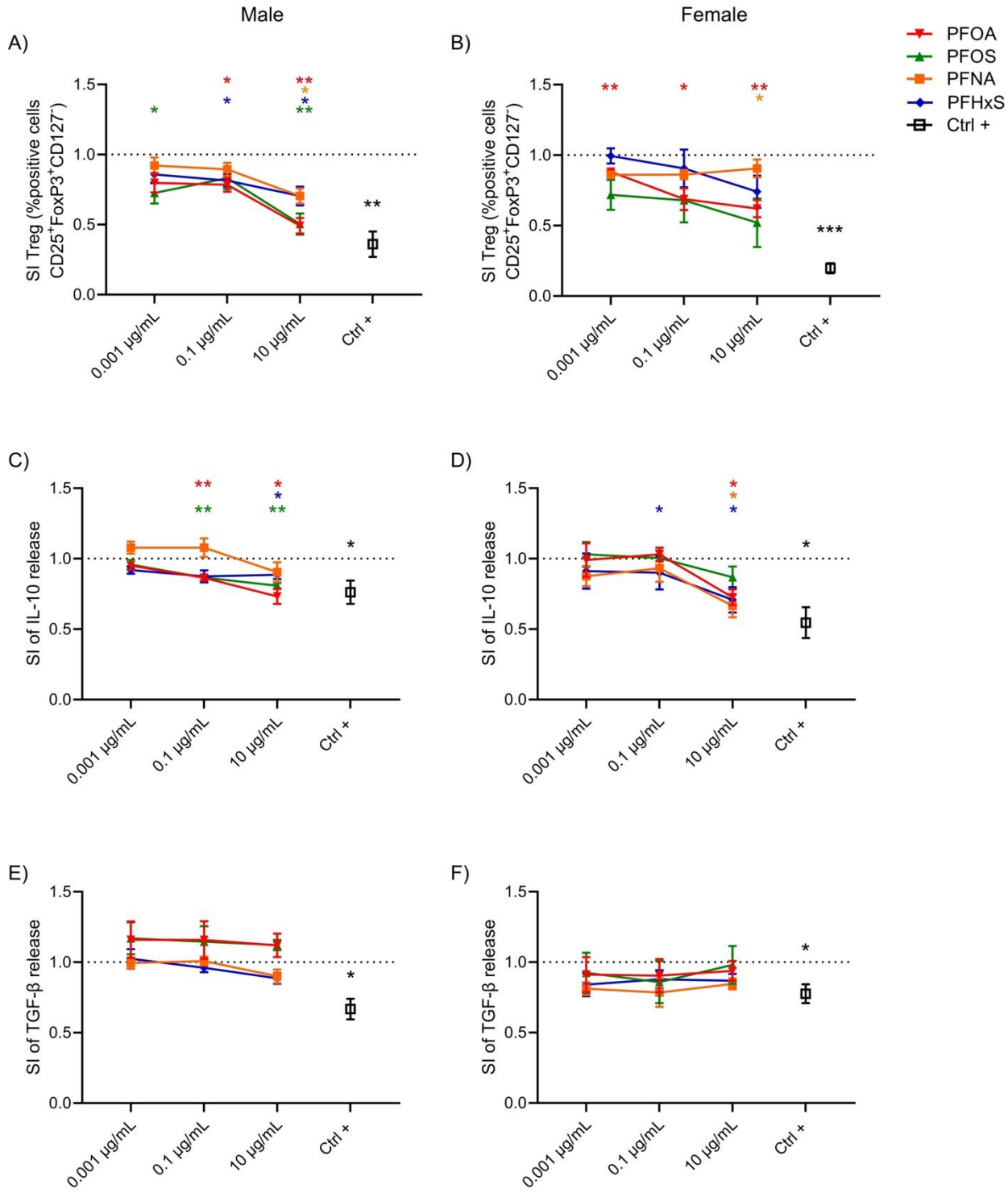

Figure 9: Effect of the PFOA, PFNA, PFHxS and PFOS on Treg differentiation in male and female donors. Analysis of the Treg Phenotyping after four PFAS selected treatment in male (9A, 9C, 9E) and female (9B, 9D, 9F) human donors. Human PBMC ($2x10^6$ cells/mL) were treated for 24h with increasing concentration of the selected PFAS (0.001, 0.1 and 10 µg/mL) or Cyclosporin A (Ctrl +, 1.2 µg/mL) and then, cells were stimulated with antiCD3

plus antiCD28 (1:100 titer) to induce the T cell differentiation. After 4 days, Golgi stop was added for 5h and in the end the CD25, CD127 and FoxP3 (9A and 9B) were analysed using flow cytometer, while the release of cytokines (9C, 9D, 9E and 9F) was analysed thought ELISA. The concentrations of PFAS, DMSO and Ctrl + were corrected for the effectively cell density of the treatment under examination by comparing the µg administered to $1x10^6$ of cells. At the end, proliferation was evaluated by flow cytometer analysis. The results are expressed as SI respect to vehicle treated cells. Each value represents the mean ± SEM, with n = 5 different male and 5 different female donors. Statistical analysis was carried out using one-way ANOVA, followed by Dunnett's test for PFAS vs Ctrl (represented by the dot line at 1), while unpaired Welch's t test for Cyclosporin A (Ctrl +) vs Ctrl. Results were considered significant if $p \leq 0.05$, with * $p \leq 0.05$ and ** $p \leq 0.01$ vs Ctrl. The colour of the asterisks matches the colour used to indicate different compounds

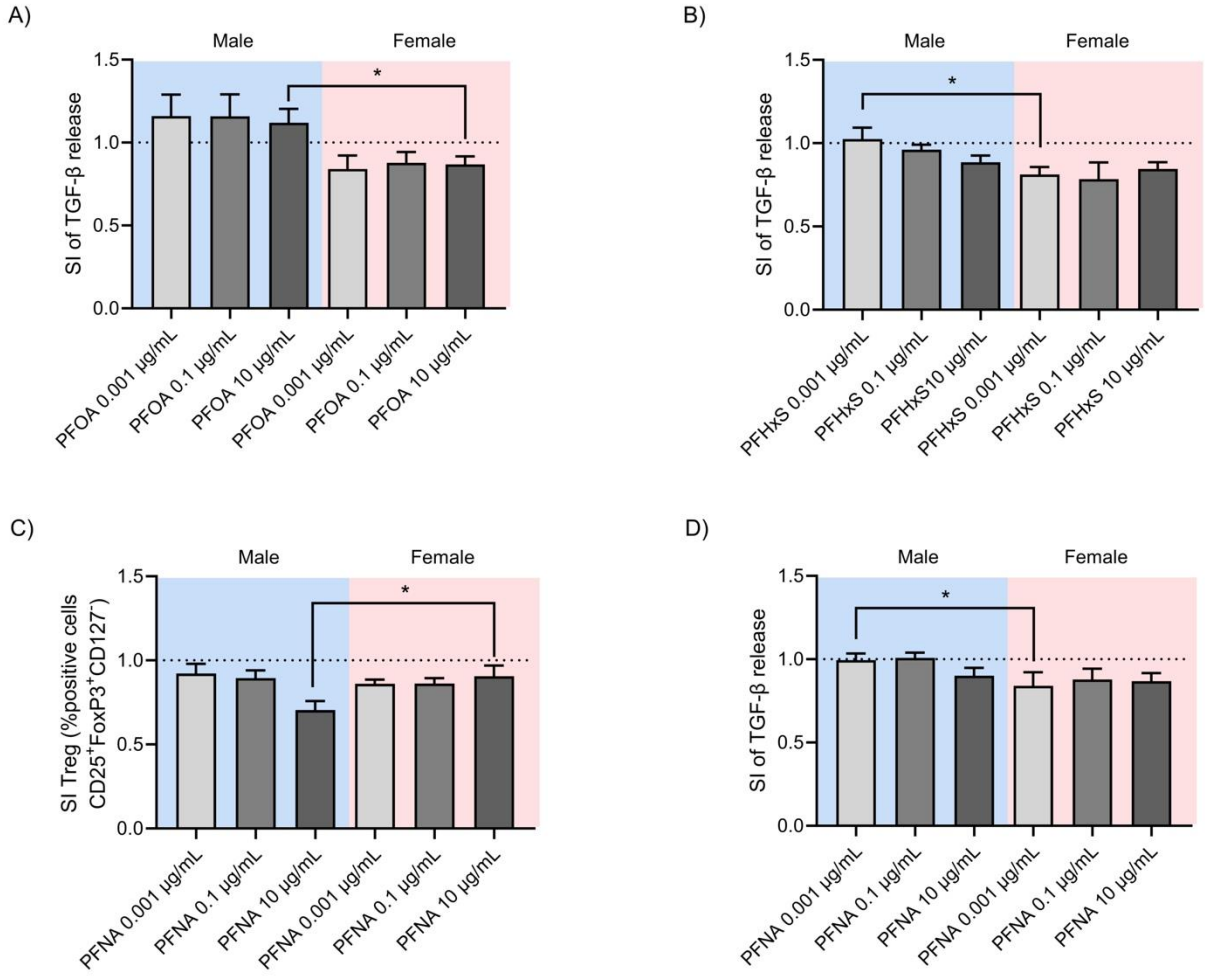

Figure 10: Effect of the PFOA, PFNA and PFHxS on Treg differentiation in male and female donors. Analysis of the Treg Phenotyping after PFOA, PFNA and PFHxS selected treatment in male and female human donors to assess possible gender difference. Human PBMC ($2x10^6$ cells/mL) were treated for 24h with increasing concentration of the selected PFAS (0.001, 0.1 and 10 µg/mL) and then, cells were stimulated with antiCD3 plus antiCD28 (1:100 titer) to induce the T cell differentiation. After 4 days, Golgi stop was added for 5h and in the end the CD25, CD127 and FoxP3 were analysed using flow cytometer, while the release of cytokines was analysed thought ELISA. The concentrations of PFAS, DMSO and Ctrl + were corrected for the effectively cell density of the treatment under examination by comparing the µg administered to $1x10^6$ of cells. At the end, proliferation was evaluated by flow cytometer analysis. The results are expressed as SI respect to vehicle treated cells. Each value represents the mean ± SEM, with n = 5 different male and 5 different female donors. Statistical analysis was carried out using unpaired Welch's t test for male vs female. Results were considered significant if $p \leq 0.05$, with * $p \leq 0.05$ male vs female

Taken together results suggest that gender may matter in PFAS-induced immunotoxicity. In term of potency, the different parameters are modulated to a different extend by all

PFAS tested, with no clear difference emerging between the four, making impossible a ranking based on Th cells differentiation.

2.3.4 T-dependent antibody production

The most critical effect reported from epidemiological studies on PFAS is the reduced response to vaccination (EFSA CONTAM Panel, 2020). The most relevant endpoint to measure the immunosuppressive potential of chemicals is the TDAR, which is considered the gold standard in animal studies. One of the aims of this project was the development of NAMs able to investigate the immunotoxicity of PFAS, and in particular, the decreased antibody response. Therefore, we developed an *in vitro* approach to investigate such effect. In our approach, both TD and TI antibody production were investigated. Knowing the difficulties to obtain a primary antibody response using *in vitro* human PBMC, due to the low frequency of naïve T and B cells, the method developed by Komatsu et al. (1986) was adapted. Komatsu et al. (1986) used an *in vitro* antigen-specific antibody production against 4-Hydroxy-3-iodo-5-nitrophenylacetyl (NIP) hapten conjugated with KLH in non-adherent cells derived from human PBMC. Starting from their method in our protocol PBMCs were treated for 24h with PFAS at increasing concentrations (0.001-10 mg/mL) or with the positive control Rapamycin (100 ng/mL). Afterwards, cells were cultured with 25 µg/mL of KLH in the presence of SAC at a concentration of 0.003% (30 mg/mL) for 5 days. Cells were then washed and further incubated in the presence of a booster of rhIL-2 (60 IU/mL) (Kennel et al., 2014), PFAS and positive control for an additional 5 days. SAC was used as a potent B cells polyclonal activator, TLR2 ligand, able to promote the B cell proliferation but without a significant increase of Ig secretion. At the end, a specific anti-KLH IgM antibody ELISA kit was used to measure the primary antibody response.

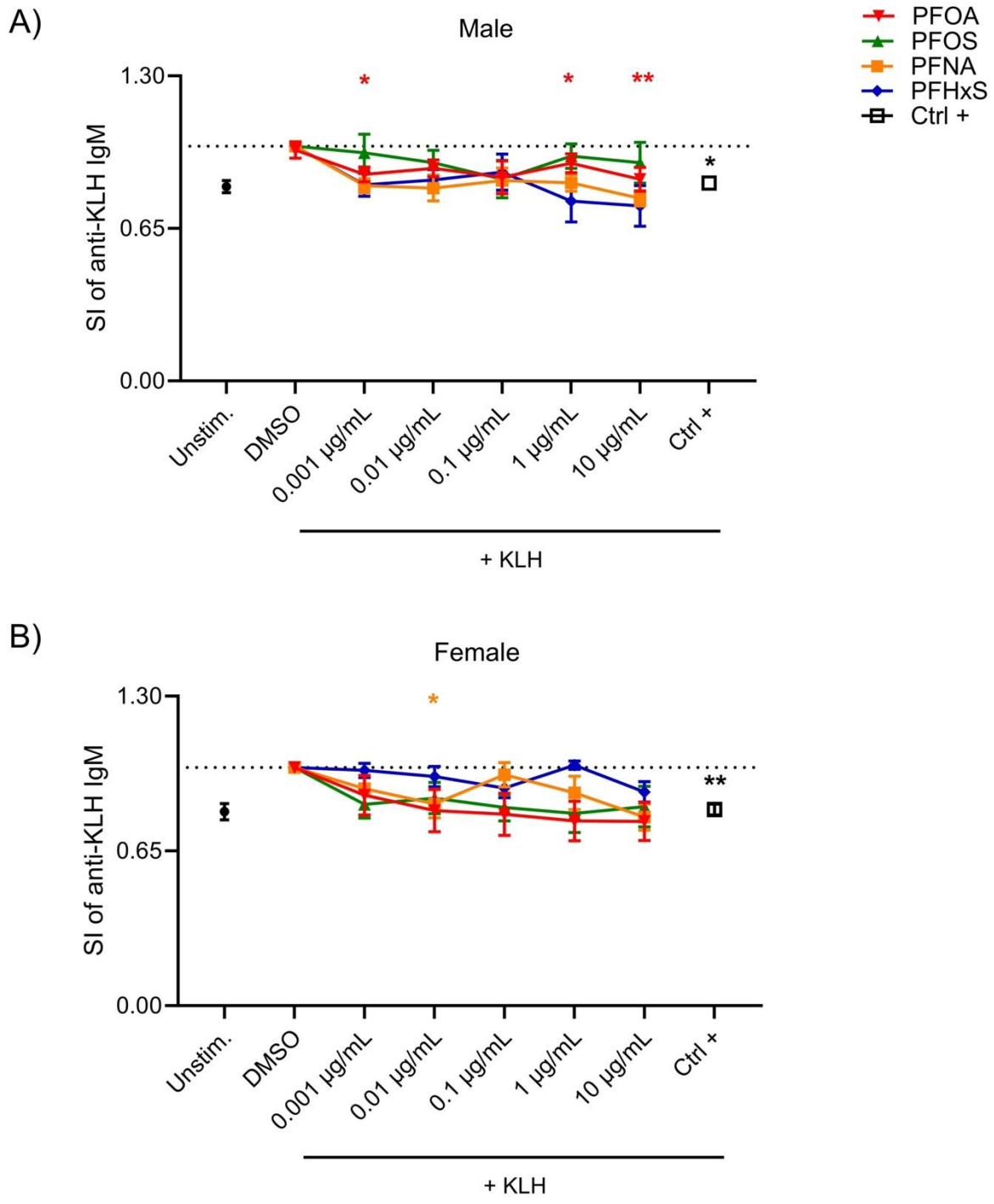

Figure 11: Effect of PFOA, PFNA, PFHxS and PFOS on the production of antiKLH IgM. Analysis of the release of specific antiKLH IgM after PFOA, PFNA, PFHxS and PFOS treatment in male (11A) and female (11B) human donors. PBMC ($2.5x10^6$ cells/mL) were treated for 24h with increasing concentration of the selected PFAS (0.001, 0.01, 0.1, 1 and 10 µg/mL) or with the positive control Rapamycin (Ctrl+, 100 ng/mL). Cells were then stimulated with KLH and SAC. After 5 days the medium was change and cells incubated in presence of chemicals and a booster of rhIL-2 for another 5 days. At the end, the release

of specific antiKLH IgM was analysed. The concentrations of PFAS, DMSO and Ctrl + were corrected for the effectively cell density of the treatment under examination by comparing the µg administered to $1x10^6$ of cells. At the end, proliferation was evaluated by flow cytometer analysis. The results are expressed as SI of IgM antiKLH. Each value represents the mean ± SEM, with n = 5 males and n = 5 females. Statistical analysis was carried out using one-way ANOVA, followed by Dunnett's test for PFNA vs Ctrl, while unpaired t test for Ctrl + (Rapamycin 100 ng/mL) vs DMSO. Results were considered significant if p p ≤ 0.05, with * p ≤ 0.05 and ** p ≤ 0.01 vs DMSO. The colour of the asterisks matches the colour used to indicate different compounds

In Figure 11 report the effects of PFOA, PFNA, PFHxS and PFOS on primary antibody response to KHL. The results show that female donors have a greater antibody response compared to male donors, which allows to better appreciate the immunomodulatory effects of PFOA and PFOS, although not statistically significant the response clearly indicates a dose related decrease. In males, all concentrations of PFOA prevented the antibody response to KLH in a statistically significantly way. The inhibitory effect of PFNA and PFHxS on antiKHL IgM is more pronounced in males compared to females. The decrease in antibody production reached statistical significance in female donors treated with PFNA only at the concentration of 1 ng/mL. A modest, but statistically significant, immunosuppressive effect with the control positive rapamycin was also observed.

Overall, we were able to confirm the possibility of measuring the primary antibody response *in vitro*. In addition, a reduction in the antibody response following PFAS exposure was observed, confirming the *in vivo* findings and reaching one of the objectives of the project. The method, however, could be improved, to obtain a higher response by considering current knowledge on the factors involved in the antibody response. Its optimization requires further investment in terms of funding and time, which was not feasible within the present project. In term of potency, overall, the data indicate also in relation to dose and gender similar trends in decreased antibody production between the four PFAS tested with a statistically significant suppression after PFOA exposure in male donors (Figure 11A).

2.3.5 T-independent antibody production

The main actors in antibody production are B cells. The effects of PFAS were investigated in an *in vitro* B-cell differentiation culture system based on PBMCs obtained from human buffy coats, as developed by Tuijnenburg et al. (2020). This assay was developed to investigate therapeutic targets for B-cell differentiation aiming to identify drugs that may be of value in B-cell-depleting treatment regimens in autoimmune disorders (Tuijnenburg et al., 2020). PBMCs were cultured for 24h with increasing concentrations of PFAS (0.001, 0.1, 10 µg/mL) and then stimulated with 1 µg/mL ODN2006 and with 100 iU/mL IL-2 for 6 days to induce IgM and IgG production. ODN2006, a TLR9 agonist, is particularly efficient in inducing naive B cell proliferation and survival. Rapamycin (mTORC1 inhibitor, 2 ng/mL) was used as positive control. As read out, total IgM and IgG were quantified using specific ELISAs.

Figure 12 shows the results on release of IgG and IgM after PFAS treatments in male (12A) and female (12B) donors. All four tested PFAS were able to reduce the release of total Ig. The reduction was statistically significant and comparable with the one induced by the positive control rapamycin. More in detail, it is possible to observe that all four tested PFAS

were able to induce a concentration-dependent reduction of Ig release in both male and female donors. PFOA in female donors (Figure 12B) significantly decreased IgG and IgM release at the lowest concentration tested (0.001 µg/mL). PFNA induced a dose-dependent reduction of release, affecting more female compared to male donors (Figure 12A and 12B). In addition, females seem to be slightly more susceptible compared to male donor as reported in Figure 13 in which the statistically significantly deviations were reported.

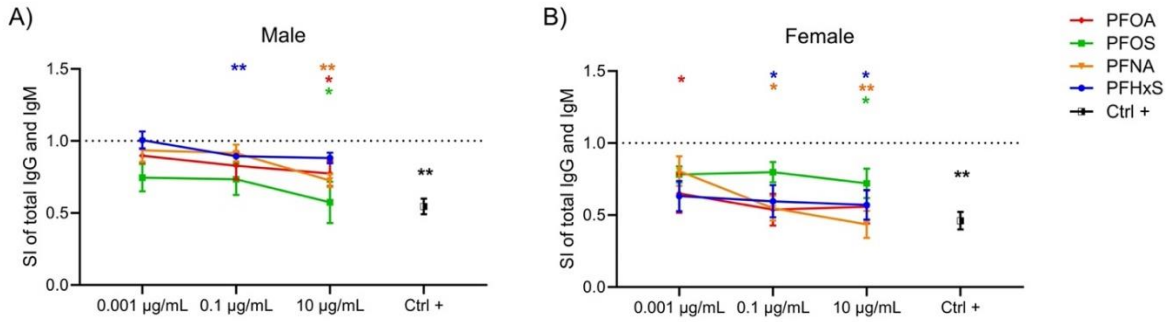

Figure 12: Effect of the PFOA, PFNA, PFHxS and PFOS on total IgG and IgM release. Analysis of the release of total IgM and IgG after PFAS treatment in male (12A) and female (12B) human donors. Human PBMC ($1.26x10^6$ cells/mL) were treated for 24h with increasing concentration of PFOA, PFNA, PFHxS and PFOS (0.0001, 0.1 and 10 µg/mL) or with the positive control Rapamycin (Ctrl +, 2 ng/mL). Then, cells were stimulated with 1 µg/mL of ODN2006 and 100 IU/mL of IL-2 to induce the B cell differentiation. After 6 days, the release of total IgG and IgM was analysed. The concentrations of PFAS, DMSO and Ctrl + were corrected for the effectively cell density of the treatment under examination by comparing the µg administered to $1x10^6$ of cells. At the end, proliferation was evaluated by flow cytometer analysis. Results are expressed as SI of total IgG and IgM respect to vehicle treated cells. Each value represents the mean ± SEM, with n = 5 different male and 5 different female donors. Statistical analysis was carried out using one-way ANOVA, followed by Dunnett's test for PFAS vs Ctrl (represented by the dot line at 1), while unpaired t-test for Rapamycin (positive control) vs Ctrl. Results were considered significant if $p \leq 0.05$, with * $p \leq 0.05$ and ** $p \leq 0.01$ vs Ctrl

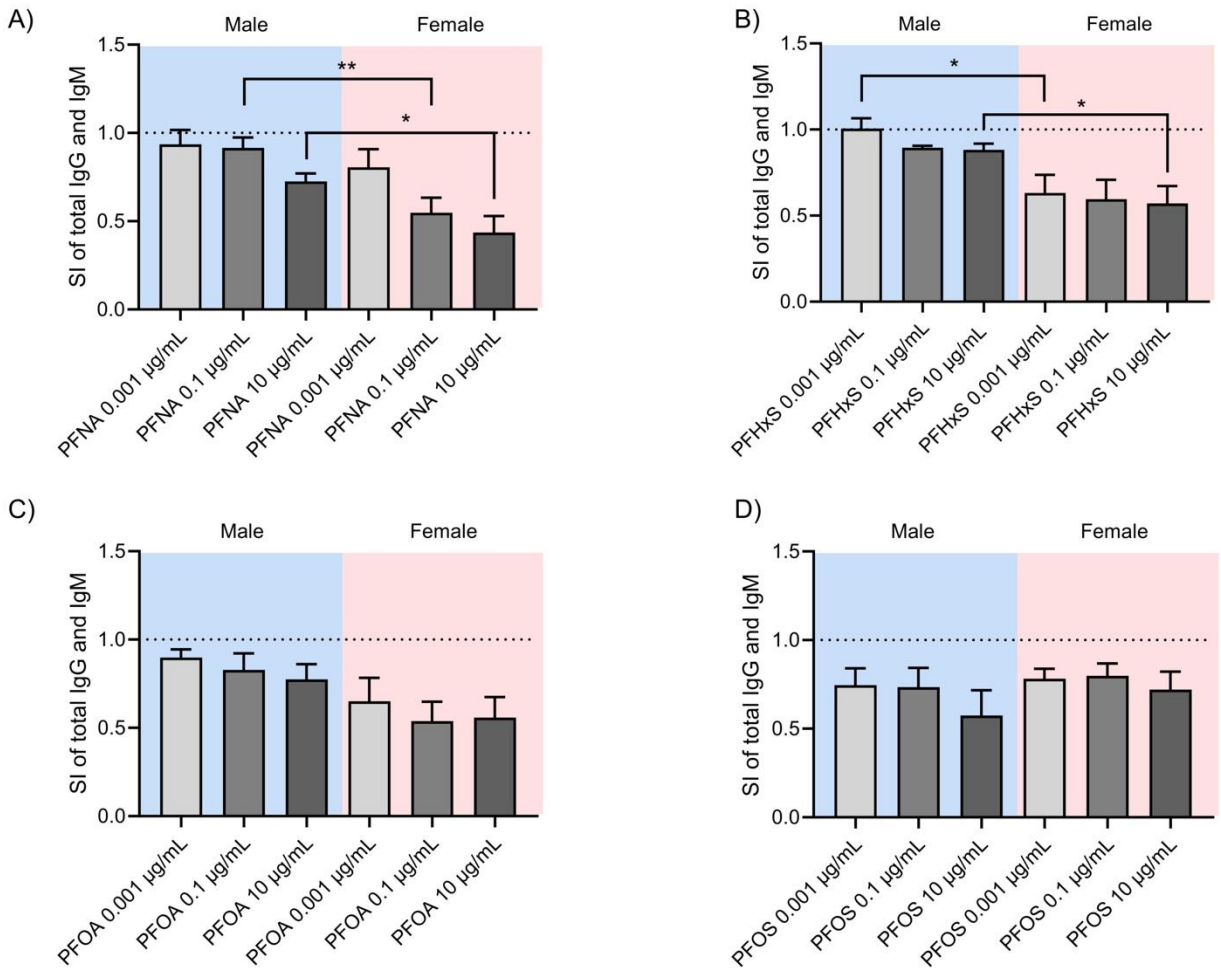

Figure 13: Effect of the four selected PFAS on total IgG and IgM release. Analysis of the release of total IgM and IgG after PFNA (13A), PFHxS (13B), PFOA (13C) and PFOS (13D) treatment in male and female human donors to assess possible gender difference. Human PBMC ($1.26x10^6$ cells/mL) were treated for 24hwith increasing concentration of the four PFAS (0.0001, 0.1 and 10 µg/mL). Then, cells were stimulated with 1 µg/mL of ODN2006 and 100 IU/mL of IL-2 to induce the B cell differentiation. After 6 days, the release of total IgG and IgM was analysed. The concentrations of PFAS, DMSO and Ctrl + were corrected for the effectively cell density of the treatment under examination by comparing the µg administered to $1x10^6$ of cells. At the end, proliferation was evaluated by flow cytometer analysis. The results are expressed as SI of total IgG and IgM respect to vehicle treated cells. Each value represents the mean ± SEM, with n = 5 different male and 5 different female donors. Statistical analysis was carried out using unpaired Welch's t-test male vs female. Results were considered significant if $p \leq 0.05$, with * $p \leq 0.05$ and ** $p \leq 0.01$ male vs female

Overall, these results support the observations from epidemiological human studies and *in vivo* animal studies, and indicate the ability of PFAS to inhibit the production of T-independent antibodies, directly affecting B cell activation. It should be underlined that this effect was observed even at very low concentrations (0.001 µg/mL) more relevant for the

general population. In term of potency, overall, the data indicate also in relation to dose and gender similar trends in decreased antibody production. Together with the decrease observed in th KLH antibody production, the results show the ability of PFAS to inhibit antibody production and confirm the success of the proposed *in vitro* approach in studying the immunotoxicity of this important class of environmental contaminants.

2.4 Conclusions of *in vitro* methods

Results obtained allow to fill some of the gaps identified in the EFSA opinion, namely the mode of action for the observed immunosuppressive effects (i.e., reduction in the vaccination efficacy and possible increase in the susceptibility to infectious disease), and to address the immunotoxicity of PFAS other than PFOS and PFOA (PFNA and PFHxS).

In the *in vitro* studies, a broad range of concentrations (0.001-10 µg/mL) were tested to cover the levels observed in the general population and in highly exposed individuals. This allowed to identify effects, their relevance to humans, and to highlight differences among the four PFAS tested.

Among the parameters investigated of relevance are the dose-related inhibition of HLA-DR expression at 72h in DCs, which indicated a compromise of the antigen presentation, central for the Th cell activation. Moreover, it is necessary highlight the inhibition of immunoglobulin production, which can be directly related to the decrease antibody production observed in several epidemiological human studies. The TI immunoglobulin production was suppressed in a dose dependent manner at all tested concentrations of PFAS in both genders, indicating that even the lowest concentration tested (0.001 µg/mL) is sufficient to suppress the immune system. Interestingly, a gender difference could be observed where the total IgG and IgM responses in female donors were found to be more suppressed compared to males. Also TD antibody production was suppressed, indicating the possibility to obtain *in vitro* a primary antibody response. However, this assay require further optimization to improve the response. TD antibody production is considered the gold standard in animal immunotoxicology investigation due to its high predictive capacity as a standalone assay (Luster at al., 1992). The *in vitro* TDAR is notoriously a challenge due to low frequency of specific naive T cells. Nevertheless, we were able to reproduce an old protocol (Komatsu et al., 1986), indicating that the in vitro TDAR is feasible. The increase in anti-KLH antibody production was not optimal, as the induction of anti-KLH IgM was overall modest especially in male human donors. The protocol requires further optimization, but it is certainly a protocol that has high potential. Considering the relevance of the endpoint, efforts should be devoted to the optimization of the test.

The four tested PFAS affected, to different extent, all immune cells involved in the antibody production both in male and female donors: from antigen presenting cells (decrease HLA-DR expression) to T helper cells to B cells. Some effects, e.g. Ig release for PFOA and PFOS or HLA-DR for PFOS, or Treg for PFOA, were observed at very low concentration (0.001 µg/mL), relevant to humans. Overall, immunoglobulin release data indicate a dose response effect for all four PFAS, reaching statistical significance in some groups, with females being more sensitive.

Regarding the potency, taking into account all parameters investigated and ranking the four PFAS based on the most potent (statistical significance at the lowest concentration),

PFOA and PFOS were similarly potent and more potent compared to PFNA and PFHxS, which were similar to each other.

3 Whole-genome gene expression profiling

For RNA sequencing, the concentration of 10 µg/mL for both PFOA and PFOS was chosen, i.e. the highest concentrations tested, as this concentration demonstrated the most substantial effects on the tested parameters in the *in vitro* assays in all immune cells. Below, the methods used, and the results obtained are reported.

3.1 Methods of RNA sequencing and analysis

For selected conditions of the *in vitro* studies described above, RNA was collected for transcriptomics analysis. These include samples from the studies on the effects of PFOA and PFOS on antigen presenting cells (iDCs and mDCs; see Section 3.2) and adaptive immune cells (PBMC, T cells and B cells; see Section 3.3). The samples and conditions chosen, and the results of the analyses are described in the following sections.

RNA was collected and RNA concentrations were determined using a NanoDrop spectrophotometer before samples were sent to WFSR. Upon arrival in Wageningen, the integrity of the RNA in the samples were analysed using a Bioanalyzer (Agilent) to determine the RIN (RNA integrity number) values, RNA concentrations, and 28S/18S ratios. All with the exception of one sample met the criteria for quantity and quality. The obtained RIN values and RNA concentrations (quantified with NanoDrop) are summarized in Annex C.

Library preparation and sequencing were tendered, and performed by BGI Genomics Co., Ltd and Azenta Life Sciences. The results of the sample quality and quantity analysis are summarised in the Annex D1 for the RNA samples send to BGI Genomics Co., Ltd and in Annex D2 for the RNA samples that were send to Azenta Life Sciences. At the sequencing facility, poly(A) selection and library preparation (NEBNext Ultra (II)) was performed, and samples were sequenced using Illumina sequencing with paired end reads (2 x 150 bp length), generating at least 12Gb per sample. At WFSR, the resulting RNAseq reads were used to quantify transcript abundances. To this end the tool Cutadapt (version 1.16) was used to trim adapters from the reads and HISAT2 (version 2.2.1) was used to map the reads to the GRCh38.p13 human genome assembly-based transcriptome sequences as annotated by the GENCODE consortium. HISAT2 output was converted and sorted by chromosomal position using Samtools (version 1.9). HTSeq (version 0.11.2) was used to count reads in transcripts using gene-level quantification. Differences in library size were adjusted by the trimmed mean of M-values normalization method, implemented in the package edgeR (version 3.36.0). DESeq2 (version 3.16) and limma (version 3.50.3) were used to calculate differential gene expression and prepare output for subsequent analysis in Qiagen Ingenuity Pathway Analysis (IPA) (V84978992) and Gene Set Enrichment analysis (GSEA version 4.3.2).

3.2 Effects of PFOA and PFOS on antigen presenting cells

To obtain insight into the cellular and molecular effects of PFOA and PFOS on antigen presenting cells, specifically DCs, in relation to the observed effects on cell surface expression of CD83, CD86 and HLA-DR as described in Section 2.3.2., whole genome gene expression analysis was performed. Initially, transcriptomics analysis was performed on iDCs exposed to PFOA or PFOS for 24h prior to the addition of maturation factors for either 24 or 72h resulting in a total PFAS exposure duration of 48 or 96h. In order to be able to capture initiating events of the observed effects in DCs, in a second study, iDCs were exposed to PFOA or PFOS for 24h and subjected to transcriptomics analysis.

In iDCs exposed to PFOA and PFOS for 48 and 96h, PFAS seemed to activate PPARα as well as the GR. Therefore, in the second analysis, iDCs were also exposed to the GR agonist DEX and the PPARα agonist GW7647 to be able to compare the transcriptomics profile of PFOA and PFOS with these model substances.

Considering that shorter exposure durations (i.e., 24h instead of 48 or 96h) primarily capture the earlier, and potentially initiating events of PFAS on DCs, than the longer durations, first the effect of 24h exposure to PFOA and PFOS on whole genome gene expression in iDCs is addressed. Subsequently, effects of 48 and 96h exposure of PFOA and PFOS on DCs are described.

3.2.1 Gene expression profiling of iDCs exposed to PFOA or PFOS for 24 hours

To assess the effects of PFASs in iDCs and compared to the activity of known PPARα and GR agonists, iDCs were exposed for 24h to the following substances (15 samples in total):

- Solvent control (3 samples)
- 10 µg/mL PFOA (3 samples)
- 10 µg/mL PFOS (3 samples)
- 1 µM GW7647 (3 samples)
- 150 µg/mL DEX (3 samples)

Raw files showing differentially expressed genes (log2 fold changes and p-values) can be found in Annex E.

Using a cutoff of $p<0.01$, under the tested conditions PFOA altered the expression of 155 genes, and PFOS of 128 genes; using a cutoff of $p<0.05$, PFOA altered the expression of 671 genes, and PFOS of 704 genes.

To compare genes modulated by PFOA and PFOS exposure to genes modulated by exposure to GW7647 and DEX, two heatmaps were prepared (see Annex F - Figure F1). For GW7647, a list of all genes that were significantly ($p<0.05$) regulated by GW7647 was compiled (1,666 genes). The differential expression (compared to solvent control) of these genes was compared to the differential gene expression induced by PFOA and PFOS and visualized in a heatmap (Annex F – Figure F1A). PFOA and PFOS appear to cause a similar pattern of differential gene expression as GW7647 in iCs, albeit GW7647 appeared to have a higher efficacy or potency (as seen by larger fold changes under the conditions tested). For DEX, a list of all genes that were significantly ($p<0.05$) differentially expressed (DE) with a log2 fold change between -1 and 1 was compiled (6,971 genes). The differential expression of

these genes was compared to genes differentially expressed upon treatment with PFOA and PFOS (Annex F - Figure F1B). The gene expression profile of PFOA and PFOS in iDCs did not appear to be similar to that of DEX, suggesting a lesser or no role of GR in PFOA and PFOS exposure in iDCs within 24h of exposure.

Lists of the 10 most significantly regulated genes, the 10 most highly upregulated genes, and the 10 most highly downregulated genes by PFOA and PFOS are shown in Annex F (Table F1). In these lists also several PPARα target genes can be identified. Interestingly, the three most significantly upregulated genes by PFOA are all PPARα target genes (i.e. *PLIN2*, *PDK4* and *CPT1A*). Also in the top 10 most significantly upregulated genes by PFOS *PLIN2* can be identified.

To obtain further insight in the possible mode of action of PFAS on iDCs, IPA was performed using the transcriptomics data. Gene lists containing gene identifiers (Ensembl Gene ID), and corresponding log2 fold changes and p-values were used for the analysis. Input criteria for the analysis were a p-value below 0.05. Using the 'upstream regulator analysis' module in IPA, upstream regulators that are known to lead to comparable changes in gene expression can be identified, serving to better understand processes upstream to the observed gene expression changes. The top 50 suggested upstream regulators based on the lowest p-value of overlap in iDCs exposed to GW7647 were identified and the activation status of these upstream regulators were compared to the activation status of the upstream regulators in iDCs exposed to PFOA and PFOS (Annex F – Table F2). The activation status of the suggested upstream regulators of iDCs exposed to PFOA was very similar to the activation status of the upstream regulators suggested for iDCs exposed to GW7647. There were only 6 upstream regulators not suggested for iDCs exposed to PFOA and the majority of the other upstream regulators had similar activation status as compared to the activation status of the iDCs exposed to GW7647, albeit sometimes with a lower of higher z-score. The activation status of the upstream regulators of the iDCs exposed to PFOS were less similar to the activation status of the upstream regulators of the iDCs exposed to GW7647, but overall still quite similar to those of PFOA. A total of 16 of the suggested upstream regulators in iDCs exposed to GW7647 were not suggested in iDCs exposed to PFOS. Taken together, transcriptomics analysis points towards activation of PPARα in immature DCs with PFOA being more potent or efficacious in inducing expression of PPARα-target genes than PFOS. Interesting to note, the second most significant suggested upstream regulator in the iDCs exposed to GW7647 is DEX, suggesting that PPARα and GR have a certain overlap in their activities. While it seems very apparent that PFAS can activate PPARα, that does not necessarily entail that this is also their mode of action behind the observed immunotoxic effects. Yet, the potential overlap in activity between PPARα and GR would make an actual involvement of PPARα in the observed effects more likely.

In the canonical pathway analysis module in IPA, which identifies the activation status of well-characterised metabolic and signalling pathways based on the expression of the genes in the data set, four pathways related to cholesterol biosynthesis were most significantly changed in iDCs exposed to GW7647. These four pathways were also very high ranked in the canonical pathway analysis of iDCs exposed to PFOA. This is of interest to note, as previously, effects on cholesterol biosynthesis were used as critical effect for the PFAS risk assessment. Surprisingly, the pathway PPARα/RXRα activation was ranked relatively lowly

on its p-value (position 56) in iDCs exposed to GW7647, despite GW7647 being known for its potent and efficacious PPARα activation.

Next, GSEA was performed to identify induced or suppressed gene sets. Gene sets were derived from Biocarta, KEGG and WikiPathway databases and ranked based on the Normalized Enrichments Score (NES) (cut-off nominal p-value <0.05 and FDR q-value <0.25). Only gene sets comprising more than 15 and fewer than 500 genes were considered. Statistical significance of GSEA results was determined using 1000 permutations. Strikingly, there were no gene sets significantly altered in iDCs exposed to 10 µg/mL PFOA or PFOS for 24h.

3.2.2 Gene expression profiling of mDCs exposed to PFOA or PFOS for 48 or 96h

To obtain insight into the cellular and molecular effects of 48 and 96h exposure of PFOA and PFOS on the mDCs, in relation to the observed effects on cell surface expression of CD83, CD86 and HLA-DR as described in Section 2.3.2., transcriptomics analysis was performed for the following conditions (18 in total):

- 48h exposure: solvent control (3 samples), 10 µg/mL PFOA (3 samples), 10 µg/mL PFOS (3 samples);
- 96h exposure: solvent control (3 samples), 10 µg/mL PFOA (3 samples), 10 µg/mL PFOS (3 samples).

The concentrations of PFOA and PFOS were chosen as they demonstrated the most significant impact on tested parameters (e.g., HLA-DR), as detailed in section 2.3.2. Raw files showing differentially expressed genes (log2 fold changes and p-values) can be found in Annex G for both 48h and 96h exposure studies.

Using a statistical cutoff of $p<0.01$, 48h exposure to PFOA altered the expression of 1,764 genes and 48h exposure to PFOS 244 genes. In the 96h exposure to PFOA and PFOS, 2,636 genes and 478 genes were significantly differentially expressed, respectively. Moreover, the significantly altered genes after 96h exposure to PFOA and PFOS showed a higher fold change than after 48h exposure.

To evaluate the effects of PFOA and PFOS on the maturation of DCs, a list of marker genes for immature and mature DCs was compiled (Annex H - Table H1). 48h exposure to PFOA and PFOS decreased the expression of the iDCs markers CD1A, AQP3 and CD209, while there was no effect after 96h exposure to PFOA and PFOS (Annex H – Table H1). One of the mDCs markers is HLA-DR, a class II MHC cell surface receptor. HLA-DR is composed of α and β chain, which are encoded by several genes. The α chain is encoded by the HLA-DRA locus and the β chain is encoded by 4 loci (HLA-DRB1, HLA-DRB3, HLA-DRB4 and HLA-DRB5). Only genes HLA-DRA, HLA-DRB1 and HLA-DRB5 were found to be differentially expressed in the THP-1-derived DCs under the conditions applied. At protein level, HLA-DR was found to be reduced by 10 µg/mL PFOA after 48 and 96h exposure and by 10 µg/mL PFOS after 96h exposure. However, at gene expression level only at 48h exposure to PFOA there was a significantly reduced expression of HLA-DRA, HLA-DRB1 and HLA-DRB5 (Annex H Table H1). In addition, 48h exposure to PFOA also reduced the expression

of the mDCs markers CD40, CCR7 and CD54 (Annex H - Table H1). These results suggest that PFOA and to a lesser extent also PFOS affect the maturation of DC.

To obtain better insight in the possible mode of action of PFASs on DCs, IPA was performed on the transcriptomics data. Gene lists containing gene identifiers (Ensembl Gene ID), and corresponding log2 fold changes and p-values were uploaded. Input criteria for analysis were -0.5 < log2 fold change of > 0.5 for 48h exposure studies and -1 < log2 fold change of > 1 for 96h exposure studies, and a p-value below 0.05. Using the 'upstream regulator analysis' tool in IPA, upstream regulators that are known to lead to comparable changes in gene expression were identified. Also after prolonged exposure (i.e. 48 and 96h exposure) PPARα remains very important suggested upstream regulator, as in the iDCs exposed for 24h. One of the important upstream regulators identified in the dataset of the DCs exposed to PFOA for 48 and 96h was PPARα and related PPARα agonists (Annex H – Table H2). Indeed, several PPARα-target genes were found to be induced by PFOA after 48 and 96h (Annex H – Table H3A and H3B. 96h exposure to PFOA and PFOS led to higher fold induction of PPARα-target genes as compared to 48h exposure. Interestingly, PDK4, ANGPTL4 and FABP4 are also listed in the top 10 most highly induced genes by PFOA after 48h (Annex H - Table H3A and H6), and PDK4 and ANGPTL4 in the top 10 most highly induced genes by PFOA after 96h (Annex H - Table H3A and H7).

In literature there is evidence that PFAS may activate PPARα. Using reporter gene systems several studies showed that PFAS bind and activate gene expression via the nuclear receptor PPARα and that activation of other nuclear receptors, including CAR, FXR, LXRα, PPARδ, PPARγ, PXR, RARα and RXRα, was limited (Behr et al., 2018, 2020). In addition, PFAS carboxylates were found to be more potent in activating PPARα than PFAS sulfonates (Behr et al., 2020; Evans et al., 2022), which is in accordance with our data with PFOA being apparently more potent in inducing the expression of PPARα-target genes than PFOS (Annex H - Table H3A and H3B).

Next, GSEA was performed to identify induced or suppressed gene sets. Gene sets were derived from Biocarta, KEGG and WikiPathway databases and ranked based on the NES (cut-off nominal p-value <0.05 and FDR q-value <0.25). Only gene sets comprising more than 15 and fewer than 500 genes were taken into account. Statistical significance of GSEA results was determined using 1,000 permutations. Table H4A and H4B (Annex H) shows all gene sets that were induced or suppressed by PFOA. There we no gene sets significantly altered by PFOS. Gene sets related to PPAR signaling ('PPAR signaling' and 'peroxisome') and fatty acid oxidation ('mitochondrial long chain fatty acid beta oxidation', 'fatty acid beta oxidation', 'fatty acid transporters' and 'fatty acid metabolism') featured prominently among the gene sets induced by PFOA after 96h exposure. PPARα is the major regulator of lipid metabolism and is activated during conditions of energy deprivation by fatty acids. Upon activation, PPARα regulates numerous genes involved in fatty acid transport, fatty acid binding and activation, and fatty acid β oxidation. In addition, several gene sets related to 'DNA replication' and 'Pyrimidine metabolism' were induced by PFOA after 96 h exposure. Taken together, gene set enrichment analysis also points towards activation of PPARα upon exposure of DCs to PFOA.

Next to PPARα related activities, also several glucocorticoids were suggested as possible upstream regulator (Annex H - Table H5). The 10 most significantly regulated genes, 10 most highly upregulated genes and 10 most highly downregulated genes by PFOA and PFOS are shown in Table H6 (Annex H) for 48h exposure and in Table H7 (Annex H) for 96h exposure. In these lists several PPARα-target genes can be identified (e.g. PDK4, ANGPTL4, FABP4, MMP12) as well as several GR-target genes (e.g. TSC22D3, KLF9, CCL13, C1QA, C1QB, PDK4, ANGPTL4, CCR7, FKBP5 and ADORA3). Together, these data suggest that, in addition to PPARα, PFOA and PFOS may also influence glucocorticoid signalling in DCs, unless, again, there is an overlap in the activities of both pathways. For iDCs (see Section 3.2.1) it appeared that there is a limited or no role of GR in PFOA and PFOS exposure in iDCs within 24h of exposure based on the comparison with the gene expression profile of iDCs exposed to DEX. However, when iDCs were exposed to PFOA and PFOS for 24h, DEX also emerged as potential upstream regulator (Annex F – Table F2), similar to the scenario observed during prolonged exposure of DCs, especially to PFOA. The discrepancy between overall gene expression profiles (based on the heatmaps in Annex F – Figure F1) between DEX and PFOA/PFOS in comparison with the suggested upstream regulators could be due to, among others, the high concentration of DEX (in comparison to PFOA and PFOS) that is used, or other, additional effect of DEX.

In summary, the mode of action of PFOA and PFOS in DCs may be primarily mediated though PPARa, with the potential involvement, albeit to a lesser extent, of glucocorticoid-receptor signalling. How these receptors are involved in the observed effects remains to be further elucidated. A hypothesis for the PFAS-mediated effects on immunotoxicity via PPARα and/or GR signalling will be elaborated below in section 3.5.

3.3 Effects of PFOA and PFOS on adaptive immune cells

To obtain insight into the cellular and molecular effects of PFOA and PFOS on adaptive immune cells (i.e. T and B cells), in relation to the observed effects as described in Section 2.3.3 and 2.3.5, transcriptomic analysis was performed. Initially, analyses were only performed using PBMC exposed to either PFOA or PFOS for 24h and subsequently stimulated using CD3/CD28 for 4 days to activate T cells or to IL-2/ODN2006 for 6 days to induce B cell differentiation and antibody production. To capture potential initiating events of PFASs on T and B cells, in a second study PBMC were exposed to PFOA or PFOS for 24h and subjected to transcriptomic analysis. Given that both T and B cell activation protocols involve pre-exposure of PBMC to PFOA or PFOS for 24h, data obtained in this second RNAseq study is relevant for the interpretation of the total of RNAseq data obtained with T and B cells.

In the T and B cells exposed to PFOA or PFOS, PFAS seemed to activate the GR, and to a lesser or limited extent PPARα (see data further below). Therefore, in the second study, PBMC were also exposed to the GR agonist DEX and the PPARα agonist GW7647 to be able to compare the transcriptomics profile of PFOA and PFOS to these model substances.

Considering that shorter exposure durations (e.g., 24h instead of 5 days for the T cells or 7 days for the B cells) are more likely to capture earlier, and potentially initiating events of PFAS on PBMC, first the effect of 24h exposure to PFOA and PFOS on whole genome gene

expression in PBMC is addressed. Subsequently, effects of prolonged exposure to PFOA and PFOS on T and B cells are described.

3.3.1 Gene expression profiling of PBMC exposed to PFOA or PFOS for 24h

To study the mode of action of PFOA and PFOS in PBMC in relation to PPARα and GR signalling, the following conditions were studied (41 samples in total):

- Male donors (5 donors): solvent control (5 samples), 10 µg/mL PFOA (5 samples), 10 µg/mL PFOS (5 samples), 1 µM GW7647 (3 samples), 150 µg/mL DEX (3 samples).
- Female donors (5 donors): solvent control (4 samples), 10 µg/mL PFOA (5 samples), 10 µg/mL PFOS (5 samples), 1 µM GW7647 (3 samples), 150 µg/mL DEX (3 samples).

Raw files showing differentially expressed genes (log2 fold changes and p-values) can be found in Annex I for male and female donors.

Using a statistical cutoff of $p<0.01$, exposure to PFOA altered the expression of 58 genes and PFOS 1,251 genes in PBMC from male donors. In PBMC from female donors, less genes were affected with PFOA altering 43 genes and PFOS 688 genes. Using a statistical cutoff of $p<0.05$, exposure to PFOA altered the expression of 320 genes and PFOS 2,737 genes in PBMC from male donors, whereas in PBMC from female donors PFOA altered the expression of 305 genes and PFOS of 2,268 genes. Overall, in both sexes PFOS altered the expression of more genes than PFOA.

To compare gene expression profiles following exposure to PFOA and PFOS to gene expression profiles following exposure to GW7647 and DEX, two heatmaps were prepared for each sex. For GW7647, a list of all genes that were significantly ($p<0.05$) regulated by GW7647 was compiled. GW7647 significantly altered the expression of 3,705 genes in PBMC from male donors and 1,675 genes in PBMC from female donors. Subsequently, the differential expression of these genes was compared to the differential expression of these genes induced by exposure to PFOA and PFOS and visualized in a heatmap (Annex J – Figure J1). Gene expression changes induced by PFOS were highly similar to the changes induced by GW7647. In contrast, PFOA did not cause comparable changes in differential gene expression. The gene expression profile of the PBMC exposed to PFOA clustered close to the gene expression profile of the PMBC exposed to the solvent control of the same donor. For DEX, also a list of all genes that were significantly ($p<0.05$) regulated by DEX was compiled, being 6,159 genes for PBMCs obtained from male donors and 4,683 genes for the PMBC obtained from female donors. The relative expression of these genes was compared between PBMC exposed to PFOA, PFOS and DEX and visualized in a heatmap (Annex J – Figure J2). The gene expression profile of the PBMC obtained from male donors exposed to PFOS clustered together and displayed similar gene expression changes as the PBMC obtained from male donors exposed to DEX. For the PBMC obtained from female donors, there is some overlap between the gene expression profile of the PBMC exposed to PFOS and DEX, but to a lesser extent than in the male donors. Also here, for PBMC obtained from both male and female donors, the gene expression profile of the PBMC exposed to PFOA clustered close to the gene expression profile of the PBMC exposed to the solvent control of the same donor.

In the heatmaps of Annex J - Figure J1 and J2, only the genes that were significantly affected by either GW7647 or DEX were included, while there were also genes affected only by the other treatments. Of the 2,737 significantly affected genes by PFOS in samples from male donors, 2,081 overlapped with GW7647 and 2,029 with DEX. Of the 2,268 genes significantly affected by PFOS in samples from female donors, 996 overlapped with GW7647, and 1,081 with DEX. Overall, PFOA affected far less genes than the other test substances. Of the 320 significantly differentially expressed genes in samples from male donors treated with PFOA, about 50% were also significantly affected by both GW7647 and DEX. Of the 305 significantly affected genes in samples from female samples, around 30% overlapped with GW7647, and 40% with DEX. PFOA and PFOS shared 189 and 172 significantly affected genes in samples from male and female donors, respectively.

Lists of the 10 most significantly regulated genes, 10 most highly upregulated genes, and 10 most highly downregulated genes by PFOA and PFOS in PBMC are shown in Tables J1, J2 and J3 (Annex J), respectively. In these lists, several typical glucocorticoid-related target genes can be identified (e.g. FKBP5, TSC22D3 and ADORA3), especially in the PBMC that were exposed to PFOS. Taken together, above results suggest that in these cells, both PPARα (as shown above in the profiles) and GR, or at least their typical gene expression pathways, are activated by PFOS, but not by PFOA. To which extent the activities of these receptors might interact remains to be further investigated.

To obtain further insight in the possible mode of action of specifically PFOS in PBMC, IPA was performed using the transcriptomics data. Gene lists containing gene identifiers (Ensembl Gene ID), and corresponding log2 fold changes and p-values were used for this analysis. Input criteria for analysis were a p-value below 0.05 for exposure studies with PMBC from female donors and -0.5 < log2 fold change of > 0.5 and a p-value below 0.05 for exposure studies with PBMC from male donors. Using the 'upstream regulator analysis' module in IPA, upstream regulators that are known to lead to comparable changes in gene expression were identified. Comparison of the top 25 potential upstream regulators, based on the lowest p-value of overlap, showed high similarity between the upstream regulators suggested for PBMC exposed to PFOS, DEX and GW7647, with a higher similarity for PBMC obtained from male donors (Annex J – Table J4) than of female donors (Annex J – Table J5). For example, in PBMC obtained from male donors and exposed to PFOS, GW7647 and DEX, six similar upstream regulators (lipopolysaccharide, TNF, DEX, immunoglobulin, beta-estradiol and IL-4) appeared among the top 10, exhibiting all the same direction of z-score. In PBMC obtained from male donors exposed to PFOA, also lipopolysaccharide and TNF are listed in the top 10 of upstream regulators, albeit a lower negative z-score. Strikingly, just as in the iDCs, in PBMC obtained from both male and female donors exposed to GW7647, DEX was the third most significant upstream regulator, suggesting potential overlap or synergy in their activities, or unspecific activity of GW7647 besides PPARα activation. Taken together, considering the overlap in suggested upstream regulators between PFOS, GW7647 and DEX, also based on these results, it can be concluded that in PBMC (particularly those obtained from male donors), PFOS activates both PPARα and GR, whereas this activation is either absent or limited by PFOA.

Next, GSEA was performed to identify induced or suppressed gene sets. Gene sets were derived from Biocarta, KEGG and WikiPathway databases and ranked based on the NES (cut-

off nominal p-value <0.05 and FDR q-value <0.25). Only gene sets comprising more than 15 and fewer than 500 genes were taken into account. Statistical significance of GSEA results was determined using 1000 permutations. The top 10 most strongly induced or repressed gene sets upon PFOA or PFOS treatment in PBMC obtained from male donors presented in Table J6A and J6B (Annex J) and from female donors in Table J7A and J7B (Annex J). In PBMC obtained from male donors there were no gene sets induced by PFOA, but several gene sets were repressed. These repressed gene sets were mostly related to immune responses to the coronavirus SARS-CoV-2 (Annex J – Table J6A). The induced gene sets upon exposure to PFOS were mostly related to cholesterol biosynthesis and metabolism, whereas gene sets repressed by PFOS were related to proteasome and also immune responses to the coronavirus SARS-CoV-2 (Annex J – Table J6B). In PBMC obtained from female donors, the gene set containing the highest normalized enrichment score upon both PFOA and PFOS exposure was related to lysosome (Annex J – Table J7A and J7B). Interestingly, PFOS also induced several gene sets related to cholesterol metabolism, including 'cholesterol metabolism' and 'cholesterol synthesis disorders', and to farnesoid X receptor pathway. Of the repressed gene sets upon exposure of PBMC to PFOA obtained from female donors, gene sets related to the ribosome featured prominently, but also several gene sets related to immune signalling, including 'cytokine and inflammatory response', 'overview of proinflammatory and profibrotic mediators' and 'immune infiltration in pancreatic cancer' (Annex J – Table J7A).

3.3.2 Gene expression profiling of PBMCs exposed to PFOA and PFOS for 24h followed by T cell stimulation for 4 days

To obtain insight into the cellular and molecular effects of PFOA and PFOS on T cells in relation to the observed effects on T cell proliferation and differentiation as described in Section 2.3.3, transcriptomic analysis was performed on samples from the following exposure conditions:

- Male donors (5 donors): solvent control (5 samples), 10 µg/mL PFOA (5 samples), 10 µg/mL PFOS (5 samples);
- Female donors (5 donors): solvent control (5 samples), 10 µg/mL PFOA (5 samples), 10 µg/mL PFOS (5 samples).

Raw files showing differentially expressed genes (log2 fold changes and p-values) can be found in Annex K for male and female donors.Using a statistical cutoff of $p<0.01$, exposure to PFOA altered the expression of 1,438 genes and PFOS 338 genes in T cells from male donors. In T cells from female donors, less genes were affected with PFOA altering 457 genes and PFOS 104 genes. In addition, in both sexes PFOA altered the expression of more genes than PFOS.

To obtain more insight in the effects of PFAS on T cells, IPA was performed. Gene lists containing gene identifiers (Ensembl Gene ID), and corresponding log2 fold changes and p-values were uploaded. Input criteria were -0.5 < log2 fold change of > 0.5 and a p-value < 0.05. Using the 'upstream regulator analysis' tool, upstream regulators that are known to lead to comparable changes in gene expression can be identified. Also after prolonged exposure (i.e. 5 days) GR remains a very important suggested upstream regulator, as in the PBMC exposed to PFOS for 24h. Interestingly, in T cells obtained from female donors exposed to PFOA, the suggested upstream regulator with the lowest p-value was the GR agonist DEX

(Annex L – Table L1). In PBMC, however, the effects of PFOS instead of PFOA, appeared to be mediated by GR (Annex J – Figure J2). In addition to DEX, also other glucocorticoids have been suggested as possible upstream regulator for the observed changes in gene expression in female T cells exposed to PFOA, but also in male T cells exposed to PFOA and female T cells exposed to PFOS (Annex L – Table L1).

Lists of the 10 most significantly regulated genes, the 10 most highly upregulated genes, and the 10 most highly downregulated genes by PFOA and PFOS in T cells are shown in Tables L2, L3 and L4 (Annex L), respectively. Interestingly, in T cells obtained from both male and female donors, the most significantly upregulated gene by PFOA was the GR-target gene *FKBP5* with a p-value of $3.0x10^{-7}$ and $8.9x10^{-8}$, respectively (Annex L - Tables L2A and L2C). Although *FKBP5* is not among the 10 most significantly altered or most highly upregulated genes by PFOS (Annex L - Tables L2B, L2D, L3B and L3D), PFOS also significantly induced *FKBP5* gene expression. A hypothesis for the PFAS-mediated effects on immunotoxicity via GR signalling and its target gene FKBP5 will be elaborated below in Section 3.5. Next to *FKBP5*, in the top 10 most significantly regulated genes by PFOA, also *MYH6* and *TLR2* were identified as GR-target genes (Annex L - Tables L2A and L2C). Also several GR-target genes are listed in the most highly upregulated genes upon exposure to PFOA, including *C1QC*, *C1QA*, *MYH6* and *C1QB* in T cells obtained from male donors (Annex L - Table L3A), and *CD163*, *MYH6* and *LPL* in T cells obtained from female donors (Annex L - Table L3C). In T cells exposed to PFOA or PFAS, PPARα and related PPARα agonists were also suggested as possible upstream regulators (Annex L – Table L5), though with lower z-scores and p-values of overlap than for glucocorticoids (Annex L – Table L1). Consequently, no PPARα-target genes were noted in the top lists of genes modified by PFOA or PFOS.

GSEA was performed to identify induced or suppressed gene sets. Gene sets were derived from Biocarta, KEGG and WikiPathway databases and ranked based on the NES (cut-off nominal p-value <0.05 and FDR q-value <0.25). Only gene sets comprising more than 15 and fewer than 500 genes were taken into account. Statistical significance of GSEA results was determined using 1000 permutations. The 10 most strongly induced or repressed gene sets upon PFOA or PFOS treatment in T cells from male donors are presented in Table L6A and L6B (Annex L) and for T cells from female donors in Table L7A and L7B (Annex L). In T cells obtained from male donors exposed to PFOS, several gene sets related to nuclear receptors, including the androstane receptor, pregnane X receptor and PPARα, as well as drug metabolism were induced (Annex L – Table L6B). Although there were no gene sets induced upon exposure to PFOA in T cells from male donors, several gene sets were repressed. These gene sets were mostly related to DNA replication, RNA degradation and protein translation (Annex L – Table L6A). In T cells from female donors, PFOA induced several gene sets related to the complement system (Annex L – Table L7A). Gene sets related to the adaptive immune system, including 'modulators of TCR signalling and T cell activation', 'antigen processing and presentation', 'T cell receptor signalling pathway', featured prominently among the gene sets that were repressed upon exposure to PFOA (Annex L – Table L7A). Interestingly, the gene set 'modulators of TCR signalling and T cell activation' was also repressed upon PFOS exposure (Annex L – Table L7B).

Taken together, gene expression profiling of T cells exposed to PFOA and PFOS points towards the activation of glucocorticoid signalling. A hypothesis for the PFAS-mediated effects on

immunotoxicity via GR signalling will be elaborated below in Section 3.5. Since it is not clear which genes are specifically modulated by the GR in T cells, in a second transcriptomics analysis, the effect of the GR-agonist DEX was studied. The following conditions were chosen (12 samples in total):

- Male donors (3 donors): solvent control (3 samples), 150 µg/mL DEX (3 samples);
- Female donors (3 donors): solvent control (3 samples), 150 µg/mL DEX (3 samples).

In order to compare the study of T cells exposed to DEX with the previous study of T cells exposed to PFOA and PFOS, data from both experiments were analysed in the same analysis run, thus normalizing data together. Raw files showing differentially expressed genes (log2 fold changes and p-values) can be found in Annex M for male and female donors.

To evaluate whether the differentially expressed genes upon exposure to PFOA and PFOS are similar to the differently expressed genes upon exposure to DEX, two heatmaps were prepared for each sex. A list of all genes that were significantly ($p<0.05$) regulated with a log2 fold change between -1 and 1 by DEX was compiled, being 3,504 genes for cells obtained from male donors and 4,236 genes for the cells obtained from female donors. The differential expression was compared to the differential expression upon exposure to PFOA and PFOS and visualized in a heatmap (Annex N – Figure N1). The changes induced by PFOS and PFOA did not appear similar to gene expression changes induced by DEX. Exposure of T cells to PFOA and PFOS modulated several GR-target genes though, and IPA also suggested several GR agonists as upstream regulator. However, comparing gene expression profile of T cells exposed to PFOA or PFOS to the profiles of cells exposed to DEX suggests no similarities in the overall profiles. This is possibly due, among others, to the long exposure duration of 5 days, the high concentration of DEX (in comparison to the test substances) that is used, or other, additional effects of DEX.

3.3.3 Gene expression profiling of PBMCs exposed to PFOA and PFOS for 24h followed by B cell stimulation for 6 days

In addition to the effects of PFASs on DCs and T cells, the effects of PFOA and PFOS on 'B cell differentiation and antibody production' were also studied. Here, PFOA and PFOS lowered the release of IgM and IgG at concentrations that are likely to be physiologically relevant, which may indicate this to be a sensitive endpoint (see section 2.3.5). To explore the mechanisms underlying the effects of PFASs on antibody production in PBMC-derived B cells, RNAseq analysis were also performed on samples from this study.

The following conditions were chosen (30 samples in total):

- Male donors (5 donors): solvent control (5 samples), 10 µg/mL PFOA (5 samples), 10 µg/mL PFOS (5 samples);
- Female donors (5 donors): solvent control (5 samples), 10 µg/mL PFOA (5 samples), 10 µg/mL PFOS (5 samples).

Raw files showing differentially expressed genes (log2 fold changes and p-values) can be found in Annex O for male and female donors. Using a statistical cutoff of $p<0.01$, exposure to PFOA altered the expression of 200 genes and PFOS 414 genes in B cells from male donors.

In B cells from female donors, less genes were affected with PFOA altering 100 genes and PFOS 179 genes. Overall, in both sexes PFOS altered the expression of more genes than PFOA.

To obtain further insight in the possible mode of action of PFASs on B cells, IPA was performed on the generated transcriptomics data. Gene lists containing gene identifiers (Ensembl Gene ID), and corresponding log2 fold changes and p-values were used for the analysis. Input criteria for analysis were a p-value below 0.05 for exposure studies with B cells from female donors and a -0.5 < log2 fold change of > 0.5 and a p-value below 0.05 for exposure studies with B cells from male donors. The 'upstream regulator analysis' module in IPA reported DEX as the top upstream regulator with the highest z-score in B cells obtained from female donors exposed to PFOA. In B cells obtained from male donors exposed to PFOA 'glucocorticoid' emerged as the third highest upstream regulator with the highest z-score. Additionally, also several other glucocorticoids were suggested as upstream regulator in B cells exposed to PFOA and PFOS (Annex P – Table P1). Together, these data suggests that effects on B cells by PFOA and PFOS may be mediated via GR related signalling.

Surprisingly, only in B cells obtained from female donors exposed to PFOA PPARα was suggested as a potential upstream regulator, though with a modest z-score of 0.334 (p-value 0.04). Conversely, in B cells from female donors exposed to PFOS, as well as in B cells from male donors exposed to PFOA or PFOS, PPARα did not surface as a likely upstream regulator. Furthermore, there were no PPARα-target genes noted in the top lists of genes modified by PFOA or PFOS (Annex P – Table P2, P3 and P4).

Lists of the top 10 most significantly regulated genes are shown in Table P2 (Annex P). Interestingly, as was also observed in T cells exposed to PFAS, the GR-target gene FKBP5 is also significantly upregulated in B cells exposed to PFASs. In B cells from female donors, the second most significantly regulated gene by PFOA and PFOS is FKBP5 showing a p-value of $6.2x10^{-6}$ and $4.5x10^{-7}$, respectively. Although FKBP5 is not listed in the top 10 most significantly altered genes in B cells obtained from male donors (Annex P -Tables P2A and PB), PFOA significantly induced FKBP5 with a fold change of 2.0 and PFOS with a fold change of 2.3. A hypothesis for the PFAS-mediated effects on immunotoxicity via GR signalling and the target gene FKBP5 will be elaborated below in Section 3.5.

In Tables P3 and P4 (Annex P) the 10 most highly upregulated and downregulated genes by PFOA and PFOS are highlighted. Also here the expression of several GR-target genes were upregulated upon exposure to PFOS, including CD163 and C1QC in B cells obtained from male donors (Annex P - Table P3B). Among the 10 most highly upregulated genes by PFOA and PFOS in B cells obtained from female donors are the GR-target genes CD163, C1QC and C1QB (Annex P - Tables P3C and P3D).

Taken together, above results indicate that in B cells, PFOS changes gene expression more potently or efficaciously than PFOA. While PFOS increases expression of GR-target genes in B cells obtained from both male and female donors, PFOA increased expression of GR-target genes in B cells obtained from female donors.

GSEA was performed to identify induced or suppressed gene sets. Gene sets were derived from Biocarta, KEGG and WikiPathway databases and ranked based on the NES (cut-off nominal p-value <0.05 and FDR q-value <0.25). Only gene sets comprising more than 15 and fewer than 500 genes were taken into account. Statistical significance of GSEA results was determined using 1000 permutations. The 10 most strongly induced or repressed gene sets upon PFOA or PFOS treatment in B cells obtained from male donors are presented in Table P5A and P5B (Annex P) and for B cells obtained from female donors in Table P6A and P6B (Annex P). In B cells obtained from male donors, several gene sets associated to the proteasome, ribosome and oxidative phosphorylation were induced in response to both PFOA and PFOS. Furthermore, PFOA specifically triggered the induction of gene sets related to the 'complement system' and 'complement activation' in B cells from male donors (Annex P – Table P5A). Notably, PFOA did not significantly repress any gene sets, while PFOS repressed only one gene set, namely 'Natural killer cell mediated cytotoxicity' (Annex P – Table P5B). Similar to the B cells from male donors, B cells obtained from female donors exhibited the induction of gene sets related to the ribosome, including 'ribosome' and 'cytoplasmic ribosomal proteins' in response to both PFOA and PFOS (Annex P – Table P6A and P6B). Interestingly, PFOA induced the gene set 'steroid hormones biosynthesis'. Given that glucocorticoids are steroid hormones, this observation may suggest induction of pathways associated with glucocorticoid synthesis. In contrast, PFOS induced the gene set 'fatty acid omega oxidation', possibly indicating a connection to PPARα signalling (Annex P – Table P6B). Among the gene sets that were repressed by PFOA and PFOS in B cells from female donors, those related to cholesterol metabolism were notably affected, including 'cholesterol metabolism with bloch and kandutsch russel pathways', 'cholesterol synthesis disorders', 'cholesterol biosynthesis pathway in hepatocytes' and 'cholesterol biosynthesis pathway'. Of interest, PFOA and PFOS both repressed the 'B cell receptor signalling pathway' in B cells obtained from female donors (Annex P – Table P6A and P6B). Taken together, gene set enrichment analysis points towards inhibition of cholesterol metabolism and B cell receptor signalling in B cells exposed to PFOA and PFOS, in particular in those obtained from female donors.

3.4 Concluding remark RNA sequencing

In Table 10 an overview is presented regarding the most pronounced affected signalling pathways in each immune cell system that was exposed to PFOA or PFOS. The mode of action of PFOA and PFOS in DCs, T cells and B cells is suggested to be primarily mediated by PPARα and GR-related signalling (Table 9). In these studies, iDCs were exposed to PFOA and PFOS for 48 and 96h, T cells for 5 days and B cells for 7 days. These relatively long exposure durations will not only capture initiating events, but very likely also secondary effects and differential gene expression related to potential shifts in cellular composition. In order to capture initiating events of the observed effects in DCs, T cells and B cells, immature DCs and PBMC were exposed to PFOA, PFOS, and model substances for 24h. In these short-term studies, effects on gene expression of PFOA and PFOS were most similar to the effects of the PPARα agonist GW7647, suggesting that effects of PFOA and PFOS are potentially mediated by PPARα signalling.

In mDCs, T cells and B cells, differential gene expression induced by PFOA and PFOS appeared to be related to GR signalling. Though, the studies presented in this report also showed that the overall gene expression profiles (based on the presented heatmaps, see Annexes) differed between DEX and the test substances. This is possibly due, among others, to the long exposure duration of 5 days (in T cells), the high concentration of DEX (in comparison to the test substances) that is used, or other, additional effects of DEX.

Taken together, transcriptomics analysis revealed that exposure to PFOA and PFOS caused gene expression changes that appear to involve PPARα and GR. It is important to note that it appears difficult to draw a line between the activities of the two receptors, and that their activities might overlap or be synergistic. How these receptors are involved in the observed effects, and how their activities interact remains to be further elucidated. These presented pathways support the observed decreased antibody responses. A hypothesis for the PFAS-mediated effects on immunotoxicity via PPARα or GR signalling will be elaborated below in Section 3.5.1 and 3.5.2, respectively.

Table 10: Overview of observed findings in immune cells exposed to PFOA and PFOS based on whole genome gene expression data

		Most pronounced:		
	Cell system	**Signalling pathway**	**PFAS (PFOA or PFOS)**	**Sex**
In vitro	**iDCs**	PPARα	PFOA	N.a.
	mDCs	PPARα and glucocorticoid	PFOA	N.a.
Ex vivo	**PBMC**	PPARα	PFOS	Male
	T Cells	Glucocorticoid	PFOA	Female
	B cells	Glucocorticoid	PFOA	Female

N.a.: not applicable for *in vitro* cell lines

3.5 Possible modes of action and conclusions *in vitro* experimentation

Results obtained clearly indicate that PFAS can act at different levels, being able to a different extend to directly affect DC activation, T cell proliferation and differentiation, B cell activation and antibody production. The use of the RNASeq allowed to get inside on the possible mode(s)

of action, identifying PPARα and GR as the main pathways affected; these hypotheses are described in more detail in the following sections.

3.5.1 PFAS-mediated effects through PPARα signalling

In several immune cell systems, including DCs and PBMC, exposure to PFOA and PFOS caused gene expression changes that appear to involve PPARα. The endogenous agonists of PPARα are fatty acids. The chemical structure of PFAS carboxylates is highly similar to fatty acids (e.g. octanoic acid) as they are both composed of a carbon chain with an attached carboxylic acid group (Figure 14). This could explain why PFAS carboxylates are also able to activate PPARα. The only difference is that fatty acids have hydrogen atoms attached to the carbon chain, while PFAS have fluor atoms attached. As compared to PFAS carboxylates, PFAS sulfonates have a sulfonate group attached to the carbon chain, possibly explaining why PFAS sulfonates (e.g. PFOS) are less potent in activating PPARα. Surprisingly though, in PBMC the gene expression profile of GW7647 was more similar to PFOS than to PFOA; it should be added that even though GW7647 is a very potent PPARα agonist, it does not share the same structural features as endogenous ligands for the receptor.

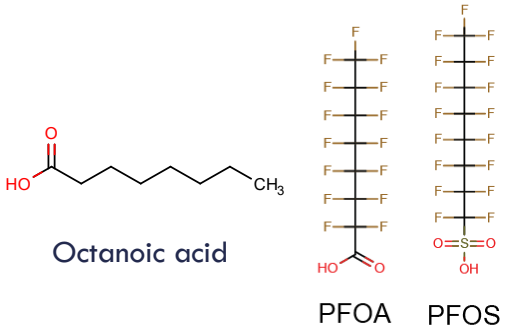

Figure 14: Chemical structure of the endogenous PPARα agonist octanoic acid, PFOA and PFOS

Since PPARα is the major regulator of lipid metabolism, activation of PPARα by PFAS instead of fatty acids might affect energy homeostasis. Activation of PPARα causes a shift from carbohydrate oxidation towards fatty acid oxidation. If glycolysis is shut down, which may occur via upregulation of PDK4 (as in DCs exposed to PFOA/PFOS for 48 or 96h), and not sufficient fatty acids are available for fatty acid oxidation (in a scenario where e.g. PFOA activates the receptor instead of an abundance of fatty acids) this may lead to a disturbance in energy metabolism. In addition to the function of fatty acids as an energy source, the localization and organization of fatty acids also directly influences proteins involved in immune cell activation (e.g., T cell responses and antigen presentation) (Wculek et al., 2019; Yaqoob et al., 2007; Zhou et al., 2021). Fatty acid depletion may therefore also lead to impaired cell function. As can be observed in Table 4A in Annex G), 48h exposure to PFOA caused a repression of the gene set 'electron transport chain oxphos system in mitochondria' in DCs. Since oxidative phosphorylation is the process where oxygen is reduced to generate adenosine triphosphate (ATP), this may indicate that exposure of DCs to PFOA caused a reduction in the generation of the primary energy source important for their biological functions.

Instead of glucose and fatty acids, amino acids can also be used as an energy source. A time of 48h of exposure of DCs to PFOA led to an increase in the expression of several amino acid transporters (Figure 15), which may suggest that amino acids are transported into the cell to serve as an energy source. Similar effects have previously been observed in HepaRG cells exposed to PFOA, PFOS and PFNA, which showed upregulation of genes involved in amino acid transport as well as increased expression of PPARα-target genes (Louisse et al., 2020).

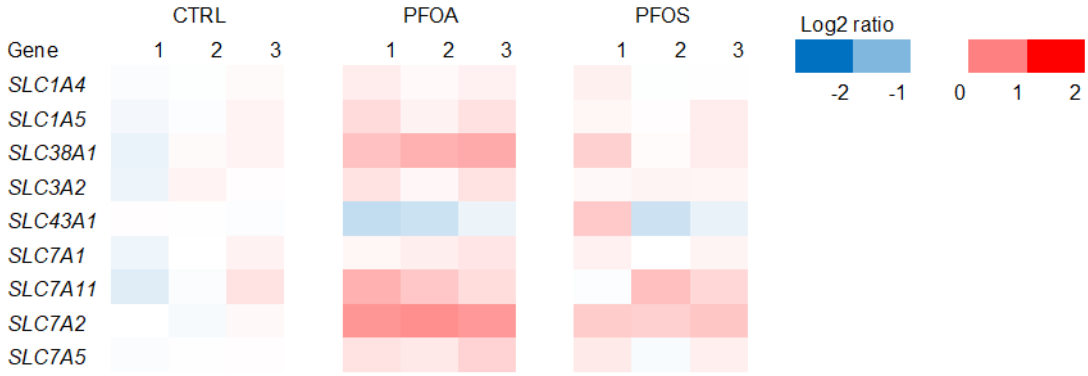

Figure 15: PFAS-induced changes in expression of genes related to amino acid transport across the cell membrane after 48h exposure. All genes were significantly induced upon PFOA exposure ($p<0.05$), except SLC43A1

In summary, a hypothetical mode of action of the effects of PFAS on immune cells, which might partially underly their immunotoxicity, may be that PFAS activate of PPARα leading to a disturbance in energy homeostasis and cell function due to the lack of sufficient fatty acids to be used as an energy source. Since DCs mostly rely on glucose as an energy source (Pearce et al., 2015), these cells may be particularly sensitive to exposure to PFAS. In addition, effects of PFOA and PFOS may also be mediated via glucocorticoid signalling, which will be further elaborated below. It should be noted that there can be an overlap in functions, or co-regulation between PPARα and GR, with the implication that also activation of PPARα could lead to gene expression changes and subsequent immunosuppressive effects similar to GR.

3.5.2 PFAS-mediated effects through GR signalling

In several immune cell systems, including mDCs, T cells and B cells, exposure to PFOA and PFOS caused gene expression changes that appear to involve glucocorticoid signalling. In the top 10 lists of most significantly and most highly upregulated genes, several GR-target genes could be identified, which were primarily modulated by PFOA. Notably, the GR-target gene *FKBP5* was also found to be significantly upregulated in these immune cell systems when exposed to PFOA and PFOS.

FKBP5 (FK506 binding protein) encodes a 51 kDa immunophilin which expression is regulated by the GR (Figure 16). FKBP5 acts as a co-chaperone that changes activity of other proteins. By binding to heat-shock protein 90 (HSP90) of the GR complex, FKBP5 lowers the affinity of glucocorticoids to the GR, thereby delaying nuclear translocation of the GR and thus inhibiting GR signalling (Figure 16) (Zannas et al., 2016). FKBP5 has also been described to bind to the inhibitor of nuclear factor-κB (NF-κB) kinase subunit alpha, which results in the activation of

NF-κB signalling (Zannas et al., 2019). In addition to NF-κB, FKBP5 also interacts with and inhibits calcineurin. Inhibition of calcineurin prevents dephosphorylation of the transcription factor 'nuclear factor of activated T-cells'(NF-AT) and its translocation to the nucleus, resulting in reduced T cell development, activation and differentiation (Figure 17) (Becknell et al., 2012). Taken together, the upregulation of FKBP5 by PFOA in DCs, T cells and B cells may affect immune cell function via various pathways.

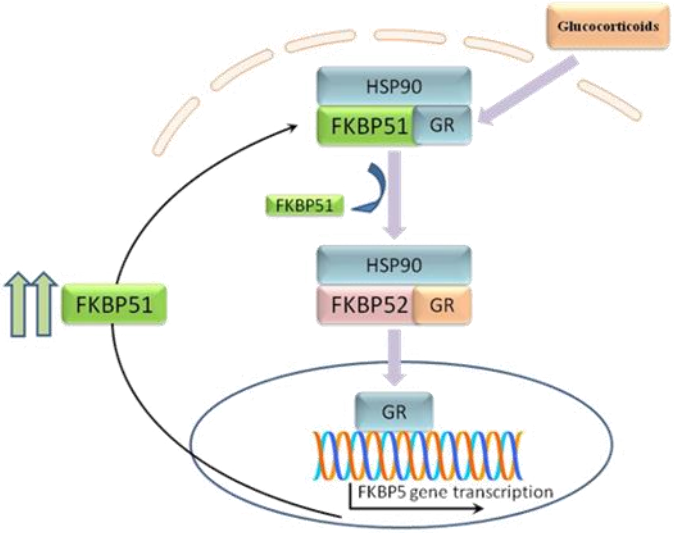

Figure 16: FKBP5 negatively regulates GR signalling. Binding of FKBP5 (FKBP51) to the GR complex via HSP90, lowers affinity of glucocorticoids for the GR. Once glucocorticoids bind to the GR, FKBP5 is dissociated from the complex and replaced by FKBP4 (FKBP52), resulting in GR-mediated transcription, thereby increasing, among others, FKBP5 (https://atlasgeneticsoncology.org)

Interestingly, AOP no. 154 describes a link between the inhibition calcineurin activity leading to an impairment of TD antibody response (Figure 18). It may be possible that this series of events is initiated by the activation of the GR signalling pathway by PFOA and PFOS. In B cells obtained both from male and female donors, it was found that FKBP5 gene expression was also significantly induced upon PFOA and PFOS exposure. It is possible that the series of events, as described in AOP no. 154, also applies for TI antibody responses, i.e. directly targeting B cells. Therefore, a possible explanation for the lower IgM and IgG production in B cells exposed to PFOA and PFOS (see section 2.3.5) might be related to their activation of GR signalling, subsequently leading to induction of FKBP5, inhibition of calcineurin activity and finally suppression of IL-2 and IL-4 production. Further research is needed to explore this possibility, in particularly involvement of GR in the observed results caused by PFAS exposure.

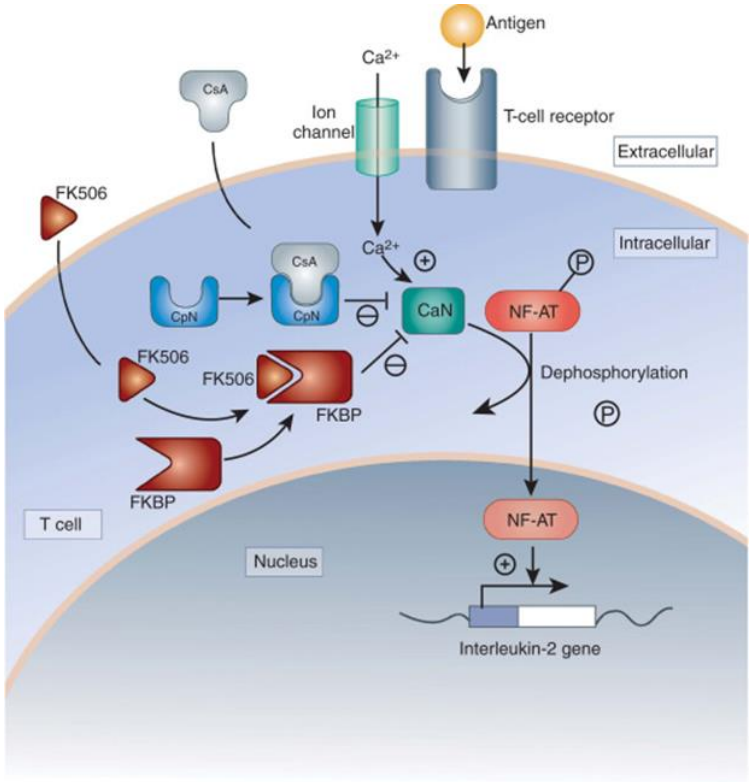

Figure 17: FKBP5 inhibition of Calcineurin. Binding of FKBP5 (FKBP51) to FK506 inhibits calcineurin, thereby preventing dephosphorylation of NF-AT and its translocation to the nucleus. This prevents NF-AT mediated transcription, for example IL-2, necessary for T cell activation (Becknell et al., 2012)

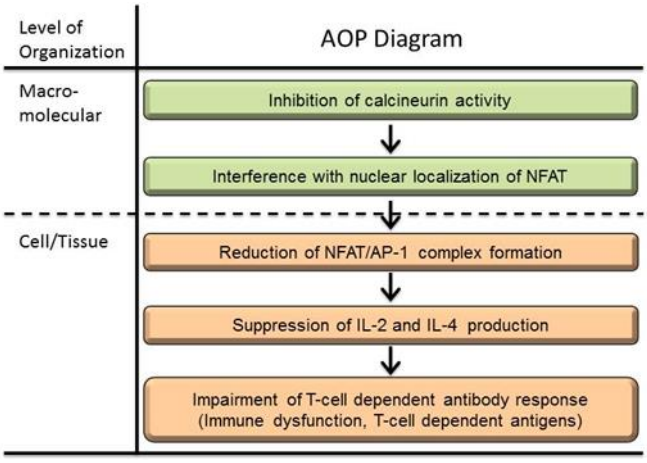

Figure 18: AOP no. 154 on inhibition of calcineurin activity leading to impaired TD antibody response (https://aopwiki.org/)

3.5.3 Concluding remarks

Overall, results clearly demonstrate that PFAS can affect different immune cells and functions, including DC activation, T cell proliferation and differentiation, B cell activation, and antibody production, to varying degrees. In addition to functional tests, RNA sequencing was conducted to enhance comprehension of the mechanisms and processes driving the impacts of the test substances within in vitro test systems. This approach also facilitated the development of hypotheses concerning the substances' mechanisms of action in vivo. RNASeq analysis identified PPARα and GR as the primary affected pathways. It is noteworthy that delineating the distinct activities of these receptors proves challenging, as their functions may overlap or synergize. Further investigation is necessary to understand how these receptors contribute to the observed effects and how their activities interact. The pathways presented here support the observed decrease in antibody responses.

In DC, the potential mechanism of action underlying the effects of PFAS on immune cells, contributing to their immunotoxicity, involves mainly the activation of PPARα. This activation may disrupt energy homeostasis and cellular function due to inadequate availability of fatty acids as an energy source. Given that dendritic cells primarily utilize glucose for energy (Pearce et al., 2015), they may be particularly vulnerable to PFAS exposure. Additionally, the effects of PFOA and PFOS may also involve glucocorticoid signaling. It's worth noting that there may be cross-functionality or co-regulation between PPARα and glucocorticoid receptors, suggesting that PPARα activation could lead to gene expression changes and subsequent immunosuppressive effects akin to glucocorticoid receptors. In lymphocytes, the plausible explanation for the reduced production of IgM and IgG in B cells exposed to PFOA and PFOS (refer to section 2.3.5) could be linked to their activation of GR. This activation may induce FKBP5 expression, inhibit calcineurin activity, and ultimately suppress IL-2 and IL-4 production. Additional investigation is warranted to delve into these potential mechanism,s particularly regarding the involvement of GR in the observed outcomes resulting from PFAS exposure.

We were able to reproduce *in vitro* the decreased antibody production by PFAS observed in epidemiological human studies and *in vivo* animal studies. The proposed approach could be easily expanded to other PFAS.

4 Recommendations

4.1 Introduction

The PFAS family is comprised of thousands of compounds with different and unique physico-chemical, fate and transport properties, many of which are not fully understood. Due to their surfactant nature, PFAS behave differently compared to other contaminants, as they are not biodegradable in the environment.

PFAS are out of the applicability domain of conventional QSARs, fate and exposure models that are driven by octanol-water (LogKow) partitioning, requiring the production of additional test data and partitioning approaches for PFAS (Schülter et al., 2022). The fate and transport properties of PFAS are affected by both the length of the C-F chain and the charge state of

the ions. Anionic (negatively charged) compounds are known to be more mobile and transport further distance from the source compared to cationic (positively charged) and zwitterionic (both positively and negatively charged compounds). The readers are referred to the ITRC PFAS guidance document (ITRC, 2022) to learn more about the chemical properties and classification of more PFAS compounds (i.e., short and long chain compound with various charge state) (Reyenga, 2022). This information should be taken into consideration when selecting the mathematical model.

To analyse the effect of PFAS on the immune system, different *in silico* methods were selected. The fate and distribution model called Armitage was used to estimate the free concentration of the chemical available for cellular exposure. PBK modelling was used to perform QIVIVE to extrapolate *in vitro* effect concentrations to external doses. Moreover, the UISS was used to investigate the effects on vulnerable populations and predict threshold doses the immune adverse outcome.

4.2 Materials and methods

4.2.1 Physiologically Based Kinetic (PBK) models for PFAS

PBK models are sophisticated dosimetry models, simulating the ADME (absorption, distribution, metabolism, excretion) processes in the human body or other organisms. In essence, they comprise of a mathematical representation of a complete organism (human/animal), represented as a series of interconnected compartments linked via the blood flow. PBK modelling allows simulation of concentration-time profile curves in target organs or their surrogates, such as blood. The models are built using ordinary differential equations to describe the ADME processes that govern the fate and transport of a chemical (in vivo) in the body (Rietjens and Louisse, 2011; Kuepfer et al., 2016). In chemical risk assessment, such models can be used to predict the systemic effective doses of substances at a specific target site, but also vice versa, with reverse dosimetry, for the prediction of external dose-responses in vivo starting from the in vitro concentration-response curves (Bois et al., 2010; Clewell et al., 2008).

EFSA PBK models have been developed to estimate the concentration of PFOA and PFOS in the blood after a potential external exposure (Loccinaso et. Al, 2011; EFSA CONTAM Panel, 2018, 2020). In the EFSA 2020 opinion, the PFOA and PFOS human PBK models were used to estimate maternal exposure (daily intake) to PFOA/PFNA and PFOS/PFHxS for women corresponding to a critical serum level in one-year old infants and corresponding milk level at 35 years. Therefore, they were also used to simulate PFAS concentrations in the infant at 1 year after 12 months of breastfeeding. These models were run for 35 years in order to calculate the serum and milk concentrations at 35 years which were used as starting concentrations at the end of pregnancy (at delivery); then, these concentrations were used for estimating the starting serum concentrations for the new-born infant and during the breastfeeding. During this period, human milk replaces the intake via food (EFSA CONTAM Panel, 2020). The model structure represents different life stages from birth, toddlers to adults, depending on which population is modelled. As such the growth follows two curves: one from a French study (Arnich et al., 2012), representing chronic exposure from birth to 50 years old and the other one from the WHO growth curves (WHO) that it is available for girls

and boys up to 5 years old. The French study included 4,078 subjects (3 to 60 years), with 703 subjects of less than 3 years of age; from the reported data (weight, age) from this study, an equation describing the increase in weight according to age was included in the EFSA 2020 model.

The models were built by the EFSA expert panel In the Berkely Madonna software (V. 10.4.3) only for PFOA and PFOS using models first published in 2018 and revised in 2020. The respective PBK models as published from EFSA (EFSA CONTAM Panel, 2020) were also used here with some adaptations, to describe the time-concentration profile curves for the other two PFAS: PFNA and PFHxS. The following paragraphs describe the PBK model which uses the format of the OECD PBK Guidance document (OECD, 2021). In the current study, the PBK models were used to simulate time concentration profiles, from birth to 75 years of age, at different doses to inform the UISS and the UISS-TOX module (Pappalardo et al., 2022, Russo et al., 2022).

The PBK model is extensively described in the 2020 EFSA CONTAM opinion. A brief overview is provided herein. The EFSA CONTAM 2018 model represented a slight modification from the original model code, based on Loccisano et al. (2011), mainly through the integration of a growth equation based on a French dietary survey. The French dietary survey included 4,078 subjects (3 to 60 years), and 703 subjects with an age < 3 years. The reported data (weight, age) from this study allowed building an equation describing the increase in weight according to age. Briefly, PFOA and PFOS are taken up by the gut (oral). From the gut, PFOA and/or PFOS are transported to the liver by the portal blood and only the free fractions of PFOA and/or PFOS in plasma are assumed to be available for partitioning into tissues. Elimination of both PFOA and PFOS is thought to be mainly via urinary excretion, while fecal excretion has not been sufficiently investigated. Although both chemicals were shown to be excreted in the bile, it is believed that the large amounts appearing in the gastrointestinal tract (>97%) are extensively re-absorbed and are subject to enterohepatic recirculation (Harada et al., 2007, Fujii et al., 2015). On the other hand, re-absorption via kidney transporters has been well-studied (Han et al., 2012; Nakagawa et al., 2009; Louisse et al., 2023). Both (intestinal and renal) re-absorption processes are thought to play a key role in the long elimination of half-lives of PFAS in humans. In the applied PBK models, only renal re-absorption is considered, while there is presently no available published PBK model describing the enterohepatic circulation of PFAS. However, research work in this area is ongoing. In the models used here, PFOA or PFOS are eliminated through the filtrate compartment in the kidney. however, beforehand, the two chemicals can be reabsorbed into the plasma through a saturable process with a maximum transporter constant (Tmc) and affinity constant (Kt).

In the EFSA Opinion, the PFOA and PFOS human PBK models were used to estimate daily intake from maternal exposure to PFOA/PFNA and PFOS/PFHxS for one-year-old infants; breastfeeding mothers corresponding milk levels at 35 years. The PBK models were used to simulate PFAS concentrations in the infant at 1 year after 12 months of breastfeeding (EFSA CONTAM Panel, 2020). These models were simulated for 35 years to calculate the serum and milk concentrations at 35 years, which were used as starting concentrations at the end of pregnancy (at delivery). Then, these concentrations were used for estimating the starting serum concentrations for the new-born infant and during breastfeeding. During this period,

human milk replaces food intake. Milk levels are based on published data on milk-to-serum ratios and include the observed decline over time in serum levels during breastfeeding.

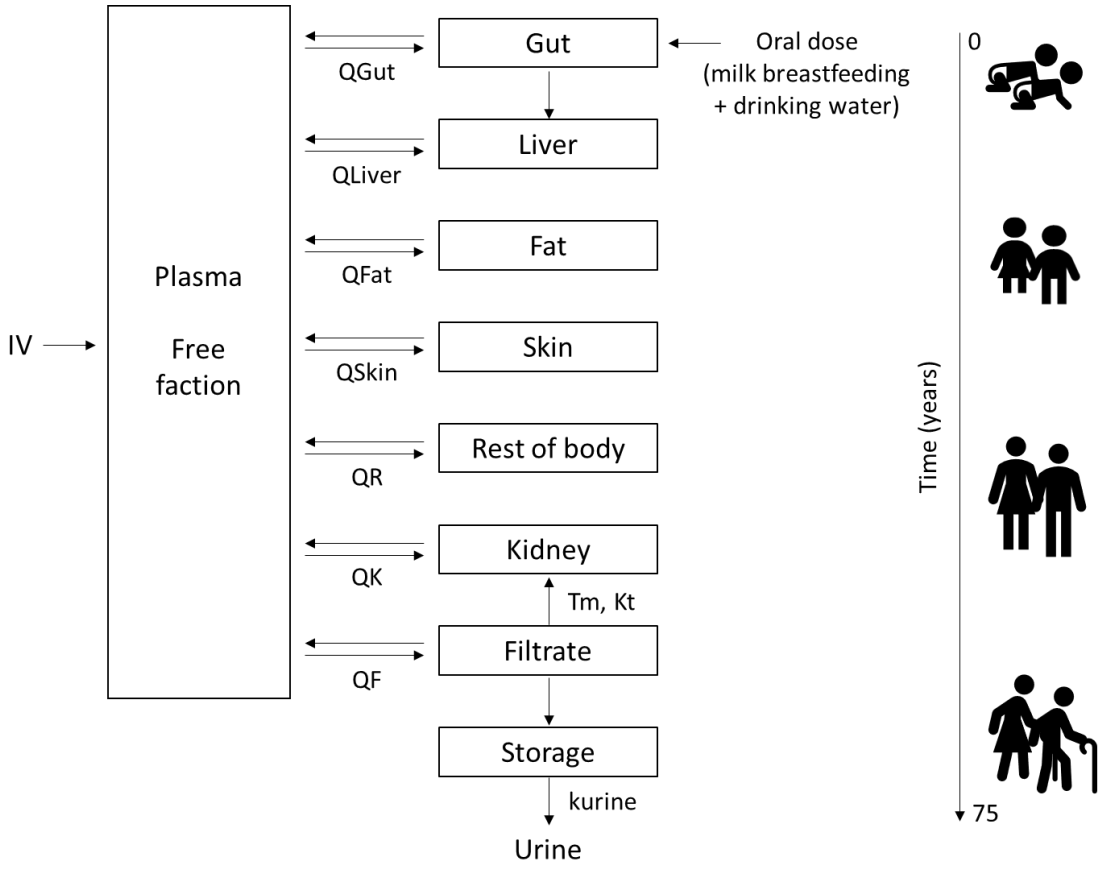

Figure 19: Schematic representation of the PBK model used. The model used a compartmentalised structure where different compartments represent target organs that are interconnected and described mathematically. In the model PFAS enter via the oral route and excrete via the excretion the kidneys. The model was run for simulate a daily intake for 75 years

All model input parameters applied here were based on the EFSA PBK models (EFSA CONTAM, 2018, 2020), as modified (or not) from the original models of Loccisano et al., 2011 (Table 11). In brief, species-related anatomical and physiological parameters relevant for humans were used as available from the literature. Chemical-specific parameters included distribution partition coefficients, plasma protein binding, as well as parameters related to urinary elimination and re-absorption.

Tissue-plasma partition coefficients were derived from animal data (Table 11), and as such there are some uncertainties pertaining to their application. An alternative to these parameters would be the application of tissue-blood partition coefficients, which are based on human data (Pérez et al., 2013, Ericson et al., 2007), as estimated by Fàbrega et al. (2014). Unfortunately, these data also have limitations given that PFOA and PFOS levels in the blood and tissues stem from different studies, and hence, from different subjects, although from the same region in Spain. Partition coefficients as presented by Fàbrega et al. (2014) showed a very high variability in the different PFAS organ levels. Consequently, it was considered

more appropriate to use the animal-based partition coefficients. The same free fractions (unbound) of PFAS in plasma were used as calculated for the developed PBK model for the monkey (Loccisano et al., 2011), based on measured plasma concentrations. This was considered a valid approach, given that differences in PFAS half-lives amongst the species do not seem to specifically depend on protein binding (Han et al., 2003).

PFAS elimination is via urinary excretion and renal re-absorption is determined in the model by two main input parameters, the transporter maximum (Tm; where Tm = Tmc*$BW^{0.75}$) and the affinity constant Kt. The Tmc and Kt values applied here were the same as used earlier by EFSA (EFSA, 2018), in order to reflect a half-life of 2.3 (3 years) and 5.4 (6 years) years, for PFOA (Bartell et al., 2010) and PFOS (Olsen et al., 2007) respectively.

Table 11: Parameters applied to the PBK model for PFOS and PFOA

Input Parameters	**Values**	**Reference**
Integration method	Rosenbrock (Stiff)	EFSA, 2018
DT min	1.00E-06	EFSA, 2018
DT max	10	EFSA, 2018
DT	0.01	EFSA, 2018
Tolerance	0.01	EFSA, 2018
PFOA		
Tmc; (µg/h/$kg^{0.75}$) Maximum resorption rate	6000	EFSA, 2018
Kt; (µg/L) Resorption affinity	55	EFSA, 2018
Free; Free fraction of PFOA in plasma	0.02	fit to plasma concentration in monkey (Loccisano et al. 2011)
PL; Liver/plasma partition coefficient	2.2	Kudo et al., 2007
PF; Fat/plasma partition coefficient	0.04	Kudo et al., 2007
PK; Kidney/plasma partition coefficient	1.05	Kudo et al., 2007
PS k; Skin/plasma partition coefficient	0.1	Kudo et al., 2007
PR; Rest of the body/plasma partition coefficient	0.12	Kudo et al., 2007
PG; Gut/blood plasma coefficient	0.05	Kudo et al., 2007
Kurinec ;urinary elimination rate constant (/h/kg^-0.25)	0.0003	estimated from Harada et al., (2005)
PFOS		
Tmc; (µg/h/$kg^{0.75}$) Maximum resorption rate	3500	EFSA, 2018
Kt; (µg/L) Resorption affinity	23	EFSA, 2018
Free; Free fraction of PFOS in plasma	0.025	fit to plasma concentration in monkey (Loccisano et al., 2011)
PL; Liver/plasma partition coefficient	3.72	de Pierre (Loccisano et al., 2011)
PF; Fat/plasma partition coefficient	0.14	de Pierre (Loccisano et al., 2011)
PK; Kidney/plasma partition coefficient	0.8	de Pierre (Loccisano et al., 2011)

Input Parameters	Values	Reference
PS k; Skin/plasma partition coefficient	0.29	de Pierre (Loccisano et al., 2011)
PR; Rest of the body/plasma partition coefficient	0.2	de Pierre (Loccisano et al., 2011)
PG; Gut/blood plasma coefficient	0.57	de Pierre (Loccisano et al., 2011)
Kurinec ;urinary elimination rate constant (/h/kg^-0.25)	0.001	estimated from Harada et al., (2005)

The same models with slight modifications were applied (in accordance with Fragki et al., 2023) to describe the biokinetics of PFNA and PFHxS, based on information on their reported elimination half-lives. In particular, the PFOA and PFOS PBK models were re-scaled with respect to the PBK transporter maximum capacity for renal tubular reabsorption in order to reach the reported human elimination half-lives of PFNA and PFHxS. Mean elimination half-lives of 3.2 and 8.2 years were applied for PFNA and PFHxS, (Olsen et al., 2007; Zhang et al., 2013). Apart from the renal reabsorption changes, PFNA and PFHxS-specific tissue: blood partition coefficients were used for the liver and kidney (according to Fragki et al., 2023). In the tables below (Table 12 and Table 13), the input parameters for PFNA and PFHxS are reported from Fragki et al. (2023).

Table 12: Models parameters to be considered for the PBK model simulations of PFNA

PFNA	Fragki et al. 2023
Tmc; (µg/h/kg$^{0.75}$) Maximum resorption rate	7900[a]
Kt; (µg/L) Resorption affinity	55
Free; Free fraction of PFNA in plasma, based on value for PFOA	0.02
PL; Liver/plasma partition coefficient	1.46[b]
PF; Fat/plasma partition coefficient	0.04
PK; Kidney/plasma partition coefficient	0.6[b]
PS k; Skin/plasma partition coefficient	0.1
PR; Rest of the body/plasma partition coefficient	0.12
PG; Gut/blood plasma coefficient	0.05
Kurinec ;urinary elimination rate constant (/h/kg^-0.25); based on valued for PFOA	0.0003

[a] estimated in order to result in the desired half-life of 3.2 years; (range 0.34-20; Olsen et al. 2007); [b] NTP 2019a, rat data.

Table 13: Models parameters to be considered for the PBK model simulations of PFHxS

PFHxS	Fragki et al. 2023
Tmc; (µg/h/kg$^{0.75}$) Maximum resorption rate	7000[c]
Kt; (µg/L) Resorption affinity	23
Free; Free fraction of PFHxS in plasma, based on value for PFOS	0.025
PL; Liver/plasma partition coefficient	0.85[e]
PF; Fat/plasma partition coefficient	0.14
PK; Kidney/plasma partition coefficient	0.3[e]
PS k; Skin/plasma partition coefficient	0.29
PR; Rest of the body/plasma partition coefficient	0.2
PG; Gut/blood plasma coefficient	0.57
Kurinec ;urinary elimination rate constant (/h/kg^-0.25); based on value for PFOS	0.001

[c] estimated in order to result in the desired half-life of 3.2 years; (range 0.34-20; Olsen et al. 2007); [d] Fabrega et al. 2014;[e] NTP 2019b, rat data.

The EFSA 2020 code was implemented in Berkeley Madonna, for the EFSA Immuno PFAS project and run in BM V10.4.8. The code was used, as provided by EFSA without any further modification (except for the model parameters reported above for PFNA and PFHxS), and equations and codes are reported in Annex Q (PBK models used).

Simulations were performed for all the four PFAS at different doses to inform the UISS-TOX (see next section 4.2.2). In a second step, the PBK models were also used for further extrapolations of the results regarding the *in vitro* effects to their respective *in vivo* exposure doses, taking into account the correction of *in vitro* concentrations from nominal to free (see next section 4.2.4).

4.2.2 Quantitative modelling through agent-based modelling framework (UISS-TOX)

Modelling and simulation are gradually gaining interest as critical tools for safety and risk assessment of a variety of compounds including drugs, chemicals, consumer products, and food ingredients.

Recently, the agent-based model (ABM) UISS was repurposed to inform chemical risk assessment and in particular it was extended and applied to a case study on allergic contact dermatitis, considering nickel as a skin sensitizer able to induce an immune response that was correctly simulated by UISS implementing UISS-TOX that is specifically tailored for predicting immunotoxicity. The UISS computational framework operates facilitating the simulation of the host immune syste''s reaction to various stimuli. This framework permits the tracking of individual biological entities within a specific adverse health context, along with their immunological interrelations. Furthermore, this approach fosters the emergence of complex behaviours, potentially resulting in the identification of unanticipated dynamics.

4.2.3 Fate and distribution *in vitro* and *in vivo* kinetic models

In vitro mathematical fate and distribution models were used to translate the nominal concentration tested *in vitro* to the free and intracellular concentration. Briefly, these are mathematical models that describes the uptake of a chemical (e.g., a PFAS) at a given concentration in cell cultures, through calculation of chemical partitioning within the well (e.g., migration to the plastic surface of the well, evaporation to the headspace and binding to components of the cell culture medium, proteins and lipids), enabling the prediction of the unbound free concentration in the medium, as well as the intracellular concentration. Thus, these models help to identify the effective exposure concentration of chemicals from which the *in vitro* cell system will be exposed to.

The work was carried out following a step-wise approach. Several mathematical models describing the *in vitro* distribution are available, Proença and her team published a very comprehensive review (Proença et al., 2021) of the available models and their potential application, highlighting limitations and opportunities. From the available models reviewed in Proença et al. (2021), it was decided to use the Armitage model, which was revised, and an update was published in 2021 (Armitage 2014; 2021). The criteria for choosing this model were the interface in mSexcel which was found to be easier to use by any end-user but most importantly the inclusion of new features.

"While the general utility of the Armitage 2014 model was demonstrated in the related publication, this version of the model has several limitations. For example, sorption to plastic was excluded in the mass balance calculations and only neutral forms of organic chemicals could be simulated. Furthermore, parameterization of the model to match the wide range of experimental conditions for many *in vitro* test systems described in the literature was not intuitive. In addition, the original model was not rigorously evaluated due to the lack of suitable experimental data. Several studies quantifying the *in vitro* disposition of organic chemicals have been published since 2014 which now permit model performance to be better assessed" (Armitage et al., 2021). To run the model, it was necessary parameterize the chemicals, the cells and the experiments.

With regards to chemical characterisation, although it is known that PFAS are difficult chemicals as mentioned above, the minimum information requested by the Armitage 2021 model were collected using PUBCHEM (30 September 2022) and are reported in Table 14. Chlorpyrifos at the concentration of 1 µM was used as a positive control.

Table 14: Physico-chemical properties collected from PUBCHEM. eCx in µM is the nominal concentration used in the *in vitro* test system

	MW (g/mol)	MP (°C)	IOC Type	pKa	log $K_{OW,N}$	log $K_{AW,N}$	$C_{SAT,W,N}$ (mg/L)	eC*x* in µM	eCx in µg/mL
PFOA	414,1	55,0	A	2,15	5,30	2,60	4,34E+03	2,41E-03	0,001
PFOA	414,1	55,0	A	2,15	5,30	2,60	4,34E+03	2,41E-02	0,01
PFOA	414,1	55,0	A	2,15	5,30	2,60	4,34E+03	2,41E-01	0,1
PFOA	414,1	55,0	A	2,15	5,30	2,60	4,34E+03	2,41E+00	1
PFOA	414,1	55,0	A	2,15	5,30	2,60	4,34E+03	2,41E+01	10
PFOS	500,1	51,9	A	0,10	6,30	3,30	5,70E+02	2,00E-03	0,001
PFOS	500,1	51,9	A	0,10	6,30	3,30	5,70E+02	2,00E-02	0,01
PFOS	500,1	51,9	A	0,10	6,30	3,30	5,70E+02	2,00E-01	0,1
PFOS	500,1	51,9	A	0,10	6,30	3,30	5,70E+02	2,00E+00	1
PFOS	500,1	51,9	A	0,10	6,30	3,30	5,70E+02	2,00E+01	10
PFNA	464,1	65,0	A	-0,17	5,92	3,10	1,55E+06	2,15E-03	0,001
PFNA	464,1	65,0	A	-0,17	5,92	3,10	1,55E+06	2,15E-02	0,01
PFNA	464,1	65,0	A	-0,17	5,92	3,10	1,55E+06	2,15E-01	0,1
PFNA	464,1	65,0	A	-0,17	5,92	3,10	1,55E+06	2,15E+00	1
PFNA	464,1	65,0	A	-0,17	5,92	3,10	1,55E+06	2,15E+01	10
PFHxS	400,1	190,0	A	0,14	5,17	2,20	2,43E+02	2,50E-03	0,001
PFHxS	400,1	190,0	A	0,14	5,17	2,20	2,44E+02	2,50E-02	0,01
PFHxS	400,1	190,0	A	0,14	5,17	2,20	2,45E+02	2,50E-01	0,1
PFHxS	400,1	190,0	A	0,14	5,17	2,20	2,46E+02	2,50E+00	1
PFHxS	400,1	190,0	A	0,14	5,17	2,20	2,47E+02	2,50E+01	10
Chlorpyrifos	350,6	82,9	N		4,70	-3,92	1,12E+00	1,00E+00	

For the *in vitro* assays, two different type of cells were used: the human promyelocytic cell line THP-1, human PBMC obtained from healthy male and female donors. THP-1 cells are similar to monocytes, while PBMC are composed by different type of cells (i.e. monocytes, lymphocytes, natural killer cells), with the majority of cells present being lymphocytes (about 70-90%). The characterization reported in the Table 15 below was applied, for both type of cells used.

Table 15: Cells characteristics

Characteristics of cells		
Storage lipids	0,005	-
Membrane lipids	0,025	-
Structural protein (NLOM)	0,10	-
Density (cells)	1	kg/L
pH	7,4	-

The mass of the cells depends on the average cell number inside the medium and it is an automated value calculated by the model. This value is reported below in a single scenario.

For all of the treatments with PBMC the medium used was RPMI-1640 without phenol red supplemented with 5% heat inactivated human serum, 2 mM L-glutamine, 100 IU/mL penicillin, 0.1 mg/mL streptomycin, 10 µg/mL gentamycin and 50 µM 2-mercaptoethanol. While for the THP-1 cells was used the same medium with a difference in the serum used that was 5% of FBS delipidated.

Depending on volumes needed and on the treatment conditions, different type of plates were used: for the study of the effect of PFAS on DC maturation, 6-well plates were used; for the study of leukotoxicity and the *in vitro* primary antibody response, 24-well plate were used; finally, 48-well plates were used to study the differentiation and activation of B and T cells.

Model evaluation and model performance were assessed. The analysis was carried out for the four PFAS using available literature data. PFAS were tested *in vitro* in HepG2 by Rosenmai and colleagues (Rosenmai et al., 2017) report the uptake of PFAS with the Armitage models in HepG2 cells expressed as percentage total moles detected in the cells on total moles added to the wells at increasing concentration of PFOA, PFOS, PFNA and PFHxS. The HepG2 cell characterisation was taken from the Paini et al. (2017). The preliminary prediction with the Armitage model using 10µM resulted in a cellular uptake of 1.8% for PFOS and 18.5% for PFOA. With a 2-order magnitude as compared to the *in vitro* data, the model need to be refined.

4.2.4 Quantitative *in vitro* to *in vivo* extrapolation (QIVIVE)

Following the need to developing alternative methods that are rapid and efficient with the aim to replace, reduce or refine the animal use, the *in vitro* to *in vivo* extrapolation (IVIVE) was used as a NAMs to inform PFAS hazard and risk assessment. IVIVE can be considered a NAM because it is a quantitative transposition of *in vitro* experimental data to predict *in vivo* concentrations (Hamon et al., 2015). Traditionally, the term IVIVE is used to refer to estimating *in vivo* whole-organ ADME properties by scaling from readouts measured *in vitro*, which is often used when constructing a bottom-up PBK model (Chang et al., 2022). Furthermore, the term IVIVE has been used to describe the process of converting an *in vitro* concentration associated with bioactivity to an external exposure level (Yoon et al., 2012). It is also referred to as reverse dosimetry which involves using a PBK model to determine a plausible exposure level that leads to a plasma (or tissue) concentration equivalent to the *in vitro* concentration. The predicted exposure level can then be compared with the (estimated) human exposures to estimate potential health risks (Wetmore et al., 2012). To distinguish this definition from the first definition, some used the term quantitative IVIVE (QIVIVE).

QIVIVE typically assumes that chemicals in an *in vitro* system behave in the same way as they do in the bloodstream. However, this assumption may not be appropriate due to several *in vitro* kinetic factors, such as chemical binding to proteins and lipids in the cell culture medium, evaporation, binding to plastic containers, uptake into the cultured cells, and degradation processes (Groothuis et al., 2015). For those reasons, an *in vitro* bioactivity concentration may be adjusted for these kinetic factors or assumed equivalent to an *in vivo*

plasma concentration (as reported in the Section 4.2.3). Then, PBPK models are used to convert the plasma concentration to an external dose (for information regarding PBK models refer to the section 4.2.1.). These models include parameters that describe the ADME processes, and the values of model parameters may be obtained using *in vitro* assays and *in silico* methods (Sipes et al., 2017).

Different QIVIVE examples exist in the literature for the translation of *in vitro* effect concentrations to respective external doses (Yoon et al., 2012; Kasteel et al., 2021; Noorlander et al., 2022; Fragki et al., 2022). For the current work, two different approaches were applied. The first approach (Figure 20), developed by Wetmore et al. (2015), involves the identification of the *in vitro* point of departure (PoD) from concentration-response data and then the translation of the PoD into an equivalent external dose (Wetmore et al., 2015). It is possible to use different *in vitro* PoDs such as half maximum effective concentration (EC_{50}), half maximum activity concentration (AC_{50}), activity concentration at cutoff (ACC), and benchmark concentration (BMC) at a pre-determined benchmark response (BMR). The second approach (Figure 21), developed by Louisse at al. (2010), involves the conversion of the whole *in vitro* concentration-response dataset into an equivalent external dose-response curve, from which an external PoD is derived (Louisse et al., 2010).

Figure 20: Schematic presentation of the QIVIVE approach developed by Wetmore et al. (2015). *In vitro* PoD is translated to an external dose using PBK modelling

Figure 21: Schematic presentation of the QIVIVE approach developed by Louisse et al. (2010). *In vitro* concentration-response data are translated into *in vivo* dose-response data using PBK modelling, from which an external PoD can be derived

Both approaches were applied here, given that they are based on the same underlying principles, that use a PBK model for the implementation of chemical toxicokinetics in a reverse dosimetry way, as reported in the OECD DNT IVB Annex on QIVIVE (OECD, in preparation). As mentioned, above, the main difference lies in the sequence of steps involved in reaching an external dose of interest. Further, the Wetmore et al. (2015) approach requires to determine the PoD based on in vitro concentration-effect data prior to performing QIVIVE to estimate the corresponding external dose that would result in the same internal concentration as the in vitro PoD. On the other hand, using the Louisse et al. (2010) approach dictates that

the QIVIVE is first conducted, and subsequently an external PoD is determined based on the predicted external dose-response curve.

In this report, the two QIVIVE approaches (Wetmore and Louisse) are presented and applied to PFAS *in vitro* concentration-response data on the T-independent antibody release in human PBMC. The analysed readout is in fact the reduction of total IgG and IgM release induced by PFAS. In the *in vitro* condition, the cells were exposed to the different PFAS for 7 days (168h). Considering that all four PFAS have long elimination half-lives (in the range of years) and that the established TWI (EFSA CONTAM, 2020) is based on a continuous 5-year exposure, an Arean Under the Curve (AUC) approach was applied. As such, the *in vitro* starting points for the QIVIVE were converted into 7-day (168h) AUC values. This conversion was performed by multiplying the concentration with the assay duration (168h) (Daston et al., 2010). Thereafter, PBK modelling was applied for the calculation of the corresponding human exposure which (over time) would lead to the same AUC value in the target system, in this case the immune system. The PBK models for each PFAS described earlier (Section 4.2.1) were used for the implementation of the PFAS toxicokinetic in the QIVIVE. As these models do not contain any specific immune organs, the blood was considered here as a suitable surrogate to simulate PFAS exposure of the immune system. 5 years (AUC5y) were used as an exposure scenario, in accordance with the toddler study used as basis for the establishment of the TWI (EFSA CONTAM, 2020). In other words, it was assumed that the AUC (168h) *in vitro* and the AUC (5y) *in vivo* are equipotent in inducing a reduced antibody response.

For the determination of the PoD in both QIVIVE approaches, the online application Bayesian BMD (https://r4eu.efsa.europa.eu/) was used to run Bayesian Benchmark Dose Modelling analyses using the R-package BMABMDR version 0.0.0.9060. With this software, it was possible to estimate the dose that corresponds to the benchmark response (BMR) of interest. The estimated benchmark dose (BMD) was reported along with its lower (BMDL) and upper (BMDU) confidence bounds. The BMDL represents the lower end of the confidence interval for the BMD, i.e., the estimated dose at which the response is significantly higher than the background response but still within an acceptable range of uncertainty. The BMDU represents the upper end of the confidence interval, and it is the estimated dose at which the response is significantly higher than the background response but still within an acceptable range of uncertainty. When fitting a set of models, a weighted average of the model-specific BMD estimates was obtained. The BMD is compared to the background response level. If the BMDL is higher than zero, it indicates that the substance is associated with a significant increase in risk compared to background. If the BMDL overlaps with doses given to the control group, it suggests that observed effects might not be attributed to the substance being tested.

The software offers the possibility to upload the data using different options. There are 2 ways to create a subset of the data: either by filtering on a certain variable or by manually selecting the observations that are to be excluded from the analysis. The authors reported the data using as data separator the Tab, the file in .txt version and used comma as decimal separator. The analyses were performed considering continuous individual response. The BMR used (also called "Value for Critical Effect Size (CES)") was set to 0.25 so that a 25% change in the mean response compared to the controls was considered. This value was chosen considering the nature of the data. Indeed, in most cases for *in vitro* experiments,

there is a statistically significant effect when treated and control differ by at least 25%. The BMD is the dose corresponding with the BMR of interest. A 90% confidence interval around the BMD will be estimated, the lower bound is reported by BMDL and the upper bound by BMDU. Three different scenarios were run in three different contests: 5 male donors, 5 female donors, 10 donors (male and female) all together using sex as a covariate. However, the BMD model used takes into consideration 5 parameters: the background (response at control group), the fold change (the expected maximum increase/decrease the response will experience after applying a very large dose), the BMD, the parameter which governs the shape of the curve and the variance of the response at each dose administered. When fitting covariate (sex) models, it implies that any of this parameter could be depending on the covariates, and when it is assumed that all of them depends on the covariate, this is the same as to fit a separate model for each subgroup. In our model it was possible to see that many models selected as the best candidate model for all four parameters depend on the covariate, and it means that, in this case, it is reasonable to considered instead a model that is fitted to each subgroup separately (so male and female alone), as there is indications that other parameters might depend as well on the covariate at the expense of efficiency loss. In the shared folder attached all the Report generated by the program are reported.

During the analysis, the application internally performs various tests on the data used for analysis. Depending on the outcome of certain tests, additional sensitivity analyses of the variance are performed and shown in the output. The type and number of tests that are performed are related to the type of response that was selected and the indicated clustering of the data. For continuous individual data without the covariate setting, the program performed:

- Shapiro-Wilk normality test;
- Check for dose-response effect;
- Check for constant variance coefficient of variation (using Bartlett test and Levene's test);
- Goodness of fit (with Bayes factor value).

Sensitivity analyses of variance were performed. The program first tested for normality using the Shapiro-Wilk test before applying the Levene's test for homoscedasticity (assumption of equal or similar variances in different groups being compared). Should the Shapiro-Wilk test be rejected on either the normal or lognormal scale, models on the rejected scale are not considered for the extra outputs as their weights are set to 0. Depending then on the outcome of the Levene's test, additional outputs were created with the variance of the data used to fit the models set to the minimum and maximum of the supplied data. When an analysis was run with a covariate, no additional tests are performed.

As mentioned before, both QIVIVE approaches described above (Wetmore and Louisse) were used here for comparison in order to identify differences, commonalities, and limitations (see section 4.3.6.).

4.3 Results and discussion

4.3.1 PBK model results

The EFSA model 2020 was built based on a well-documented peer-review publication by Loccisano et al. (2011) and based on EFSA 2018. The ESFA expert Panel evaluated the model to be robust. We trust that the model, based on its limitations and assumptions, can predict and its performance suits the current project.

The model was set up to include a long-life exposure to PFAS, covering 75 years (0 to 75 years old), and including exposure at birth and during breast feeding. The French dietary study was selected since it allows for modelling throughout lifetime, whereas the WHO study is restricted to toddlers up to 5 years of age. The PBK model was used to make forward predictions based on selected exposure scenarios, but also in reverse dosimetry to reconstruct the exposure based on human biomonitoring data.

Four different scenarios were applied:

- Scenario 1. Set up to mimic the French study used in the EFSA CONTAM 2020 Scientific Opinion on PFAS. In this opinion PFOA, PFNA, PFHxS and PFOS were simulated with the PBK model. The doses used were 0.187 ng/kg day for PFOA and PFNA and 0.444 ng/kg day for PFHxS and PFOS (Figure 22). Exposure duration was set from birth until the age of 75 years.
- Scenario 2. Based on EFSA's recent safety threshold for the main four PFAS (a group TWI of 4.4 ng/kg week). A daily intake was calculated by dividing the TWI (4.4 ng/kg) by 7 days, resulting in 0.628 ng/kg day (Figure 23). Exposure duration was set from birth until the age of 75 years.
- Scenario 3. Based on food diet intake levels that were found in populations that lived in highly polluted areas. The oral exposures used were 4.18 ng/kg/day for PFOA, 3.68 ng/kg/day for PFNA, 3.45 ng/kg/day for PFHxS and 4.47 ng/kg/day for PFOS, respectively (Figure 24) (data taken from table 10, EFSA CONTAM Opinion 2020). Exposure duration was set from birth until the age of 75 years.
- Scenario 4. The PBK models were applied to obtain human biomonitoring (HBM) data (average age 42 years, with plasma concentration of 8.6 ng/mL for PFOA, 140 ng/mL for PFHxS and PFOS 160 ng/mL) (Figure 25).

Simulation results with forward dosimetry

The first simulations mimicked the French study (scenario 1) in the 2020 EFSA CONTAM Scientific Opinion on PFAS. The four PFAS: PFOA, PFNA, PFHxS and PFOS were simulated. The doses used were PFOA and PFNA with an oral exposure of 0.187 ng/kg day and PFHxS and PFOS with an oral exposure of 0.44 ng/kg day. The results are presented in Figure 22.

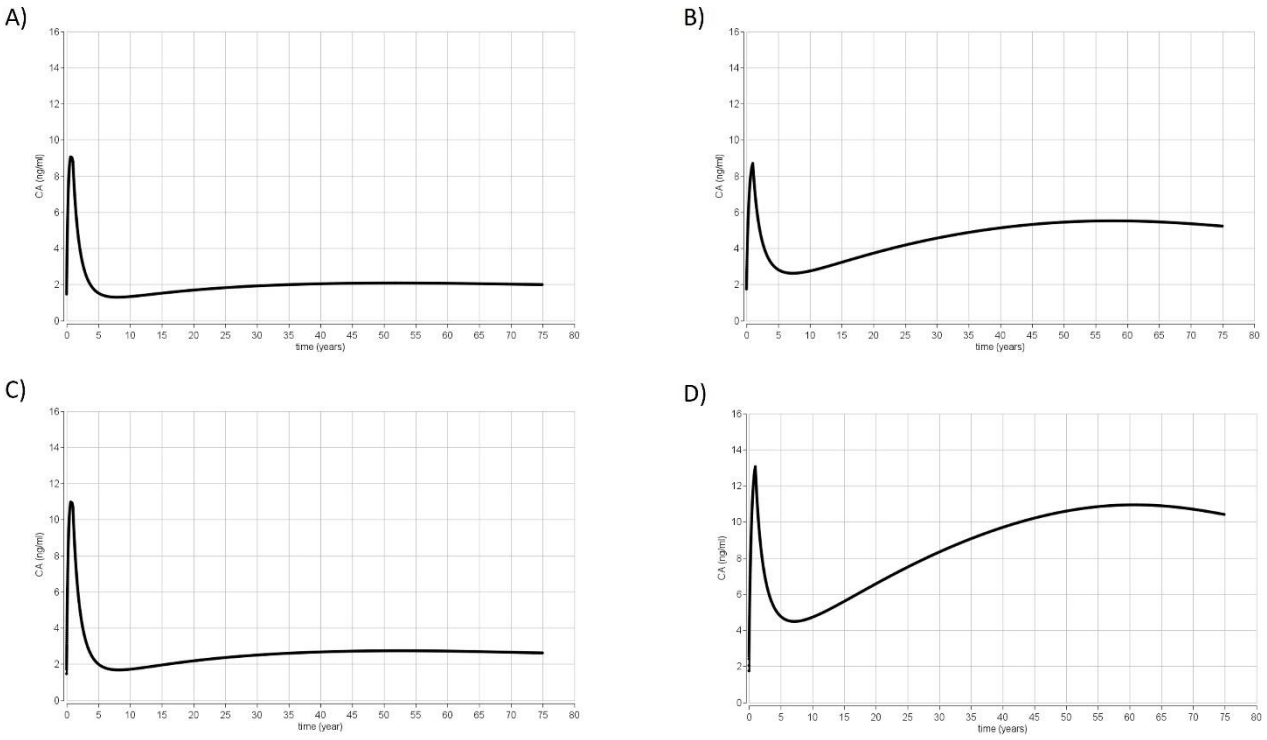

Figure 22: Simulation of the Scenario 1. Results from time concentration simulations using the PBK models for the four PFAS from birth to 75 years old (EFSA CONTAM 2020) for exposure to (A) PFOA and (C) PFNA with an oral exposure of 0.187 ng/kg/day and (B) PFOS and (D) PFHxS with an oral exposure of 0.444 ng/kg/day. The doses are used as in the EFSA 2020 model, which represents a French cohort study. CA represents the total concentration of chemical in blood (ng/mL) (Y axis) and the time is expressed in years (x axis)

The second scenario (scenario 2) was based on the safety threshold for the four PFAS (TWI of 4.4 ng/kg day), as established by the 2020 EFSA CONTAM opinion. A daily intake was calculated by dividing the TWI (4.4 ng/kg day) by 7 days, resulting in 0.628 ng/kg day and the results are represented in Figure 23.

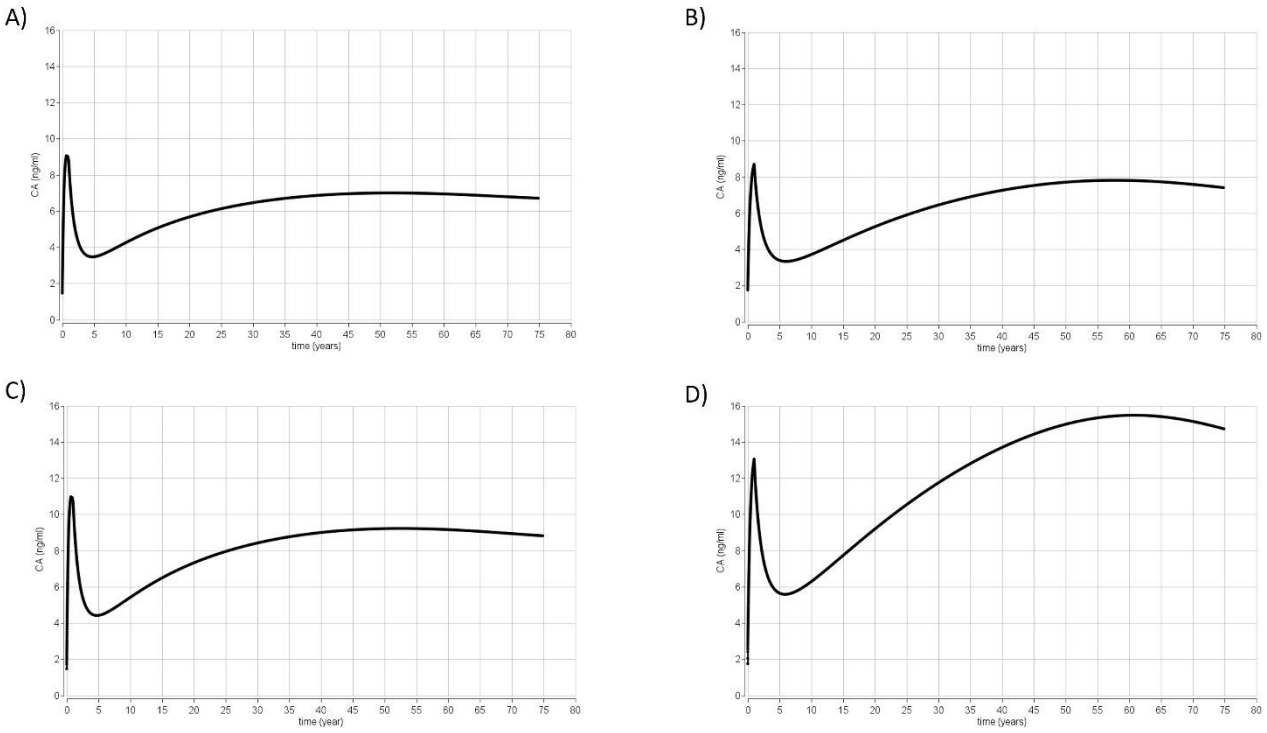

Figure 23: Simulation of the Scenario 2. Results from time concentration simulations using the PBK models for the four PFAS from birth to 75 years old (EFSA 2020 model) for exposure to (A) PFOA, (B) PFOS, (C) PFNA and (D) PFHxS all with an oral exposure of 0.628 ng/kg/day. This dose was selected as the oral exposure estimate from the EFSA 2020 TWI of 4.4 ng/kg. CA represents the total concentration of chemical in blood of the chemicals (ng/mL) (Y axis) and the time is expressed in years (x axis)

The scenario 3 is based on food diet intake level and was selected to represent a worst-case scenario (WSC). The data were taken from Table 10 present in the 2020 EFSA CONTAM Opinion that reported food diet intake that was found in population that lived in highly polluted areas. The table reported for (A) PFOA an oral exposure of 4.18 ng/kg/day, for (B) PFOS an oral exposure of 4.47 ng/kg/day, for (C) PFNA an oral exposure of 3.68 ng/kg day while for (D) PFHxS an oral exposure of 3.45 ng/kg day. The results are represented in Figure 24.

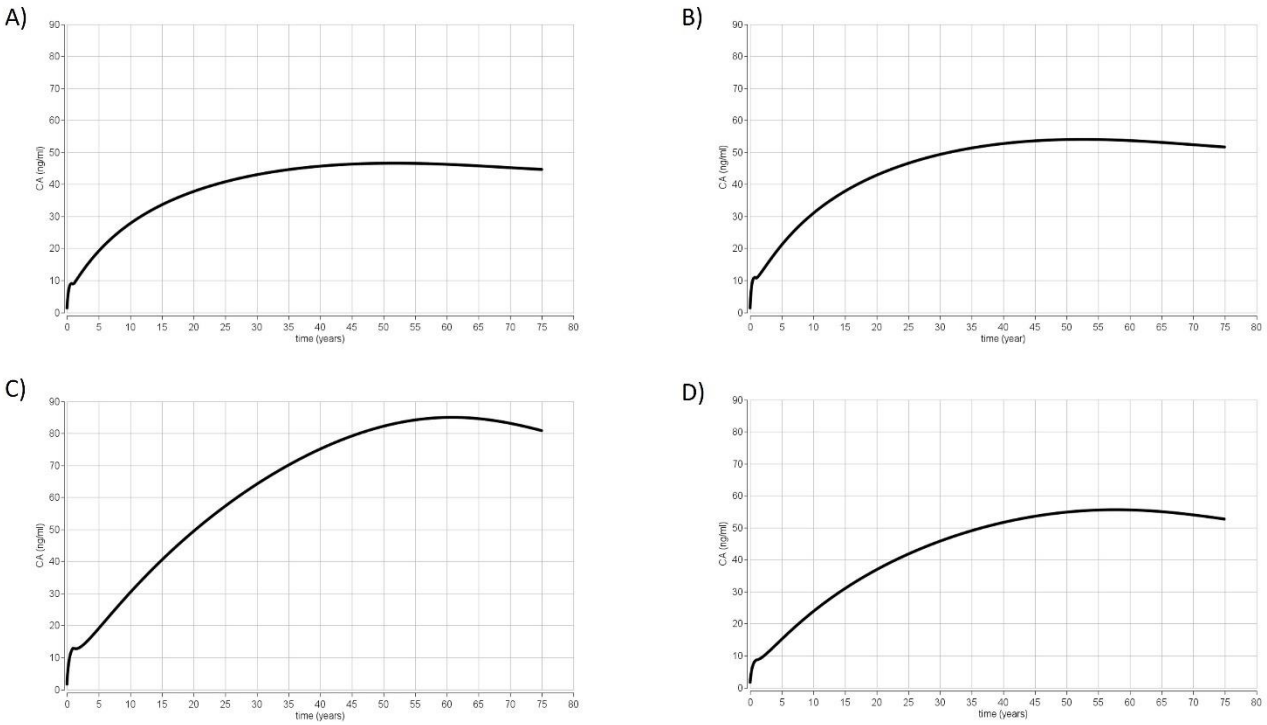

Figure 24: Simulation of the Scenario 3. Results from time concentration simulations using the PBK models for the four PFAS from birth to 75 years old (EFSA CONTAM 2020) for exposure to (A) PFOA with an oral exposure of 4.18 ng/kg/day, (B) PFOS with an oral exposure of 4.47 ng/kg/day, (C) PFNA with an oral exposure of 3.68 ng/kg/day and (D) PFHxS with an oral exposure of 3.45 ng/kg/day. This dose was selected to represent a worst-case scenario (WCS) data were taken table 10 (present in the EFSA CONTAM Panel 2020) in which the mean upper bound was selected. CA represents the total concentration of chemical in blood (ng/mL) (Y axis) and the time is expressed in years (x axis)

Simulations results with reverse dosimetry

Applying HBM data to predict an exposure estimate using the PBK model in reverse-dosimetry fashion constituted the next step. A table published by Li et al. (2020) provided the descriptive statistics from the HBM study group of adults from 20 to 60 years old with a mean age of 42 and the respective PFAS levels in blood: 8.6 ng PFOA/mL, 140 ng PFHxS/mL and 160 ng PFOS/mL. This resulted in the following predictions with regards to continuous oral exposure: (A) 0.8 ng PFOA/kg/day (B) 13.6 ng PFOS/kg/day and (C) 6.3 ng PFHxS/kg/day.

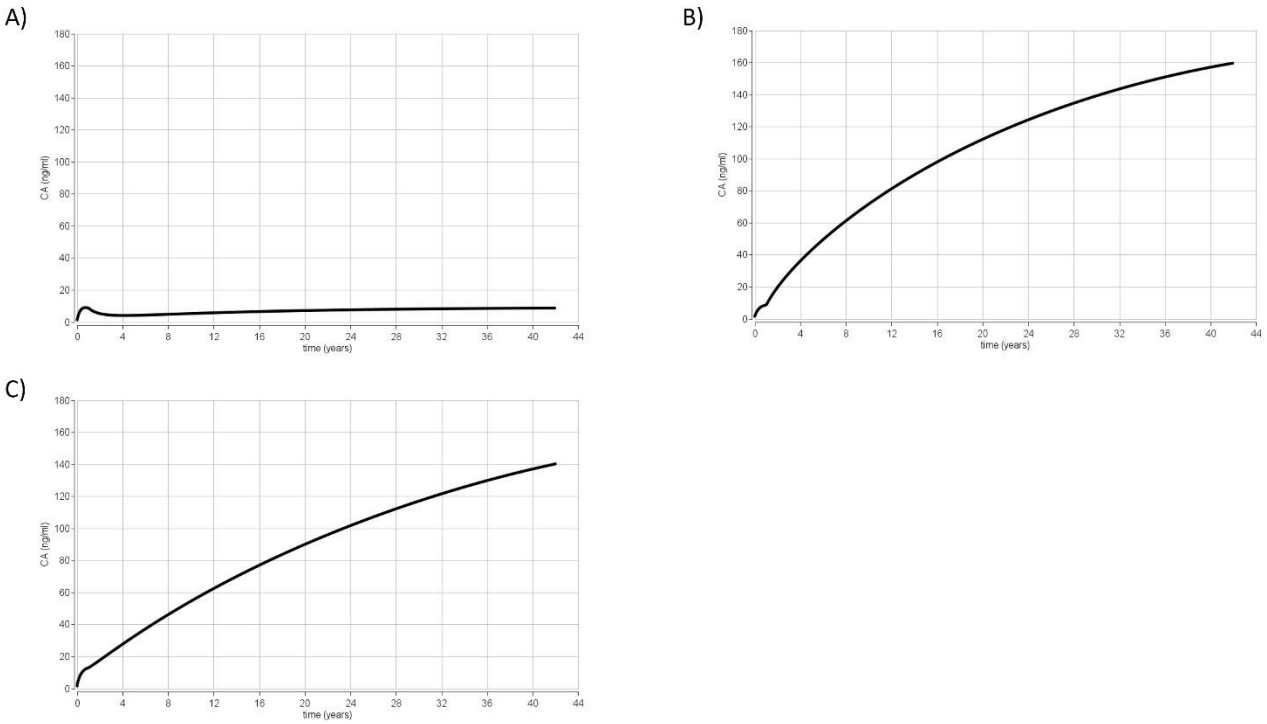

Figure 25: Scenario 4. Results from time concentration simulations using the PBK models for (A) PFOA, (B) PFOS and (C) PFHxS. The PBK models were used to predict the time concentration profile curve with a continuous exposure up to 42 years, based on blood levels of 8.6 PFOA ng/mL, 160 PFOS ng/mL and 140 PFHxS ng/mL, in order to estimate the external exposure. CA represents the total concentration of chemical in blood (ng/mL) (Y axis) and the time is expressed in years (x axis)

4.3.2 UISS-TOX results

Below the results from UISS-TOX for the prediction of the response to vaccination for each scenarios considered (0-4 years (children); 25-26 years (young people); 65-66 years (elderlies).

The perfluoroalkyl substance exposure scenarios were described above (i.e., scenarios 1, 2, and 3) they provided the chemical and immunological inputs that were used to feed the UISS-TOX platform. As a result, the *in silico* model was able to predict, according to three different age ranges and to three different scenarios, the immune system dynamic both from a cellular and humoral response point of view.

The considered three age ranges were:

- 0-4 years (children);
- 25-26 years (young people);
- 65-66 years (elderlies).

A general bacterial challenge was injected to each age group, and we subsequently examined the pro-inflammatory cytokines, antibodies, and B and T cell dynamics in the three different scenarios. Additionally, we modelled and predicted the antibody response following anti-H1N1

and anti-diphtheria vaccine injection in a young cohort of people (25-26 years) and according to the three different exposure scenarios.

Results from UISS-TOX for the prediction of the response to vaccination for children (0-4 years)

We simulated the immune system response after a generic bacterial challenge in young children (0-4 years old) exposed to three different concentrations of PFOA and PFOS coming from the PBK model, evaluating their immune response in terms of cytokine, immunoglobulins, and B- and T-cells dynamics.

Here, we show the cytokines and immunoglobulins dynamics prediction for digital patients in the age range 0-4 years old, unexposed, and exposed to PFAS according to "scenario 3". Regarding the B and T cells immune dynamics and the other scenarios (i.e., scenario 1 and scenario 2), results are presented in Annex R.

Figure 26 and Figure 27 show IL-2, IL-6, TNF- α, and IL-17 dynamics in unexposed children and in exposed children according to "scenario 3", respectively.

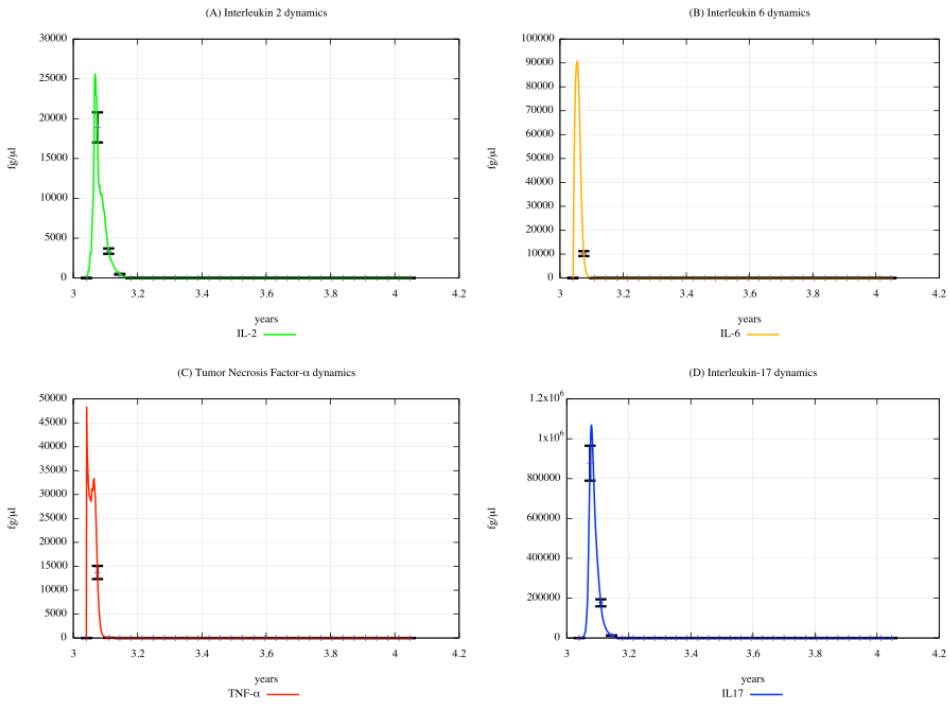

Figure 26: Cytokine dynamics prediction for "not exposed" scenario, age range 0-4 years

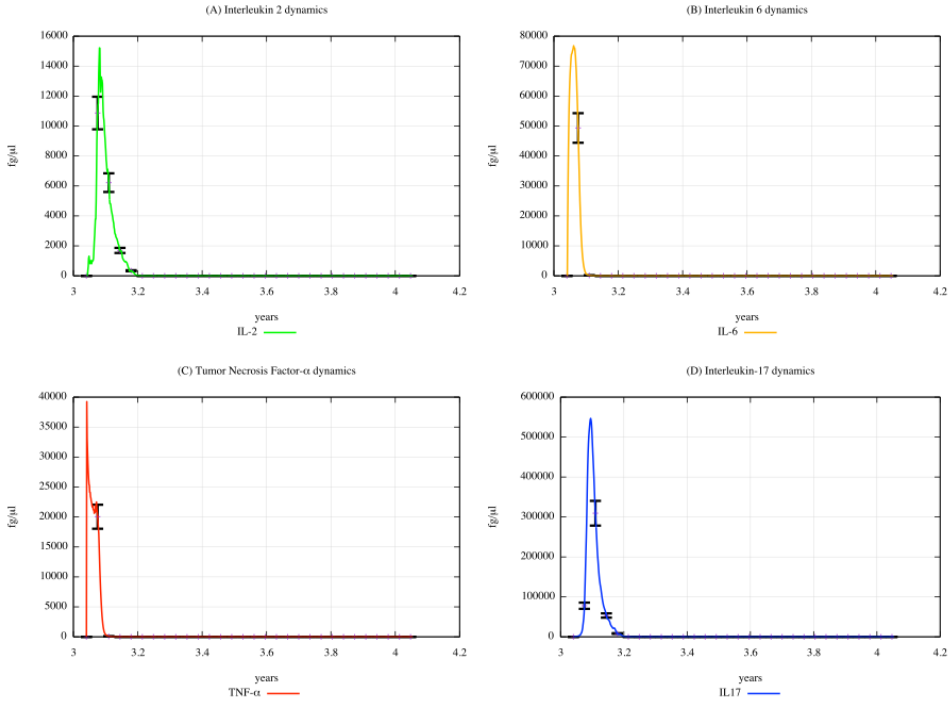

Figure 27: Cytokine dynamics prediction for "scenario 3", age range 0-4 years

From the comparison of Figure 27 (PFAS exposure, scenario 3) with Figure 26 (PFAS unexposed), it can be appreciated that the cytokine concentration levels decrease in the 3rd scenario. This behaviour reflects the data in the literature i.e., PFAS induces a reduction in IL-2, IL-6, TNF-α, and IL-17 (Corsini et al., 2011). It is important to note that IL-6 promotes the differentiation of T lymphocytes into CD4 and CD8; hence, through a reduction of IL-6, PFAS may be responsible for altering T cell populations, particularly CD4 and CD8, as we can see in the plots depicting the dynamics of T and B cells that are shown in Annex R.

Figure 28 and Figure 29 show the immunoglobulin dynamics, particularly the IgM and IgA levels, in young children (0-4 years old) unexposed and exposed to PFAS according to the "scenario 3", respectively.

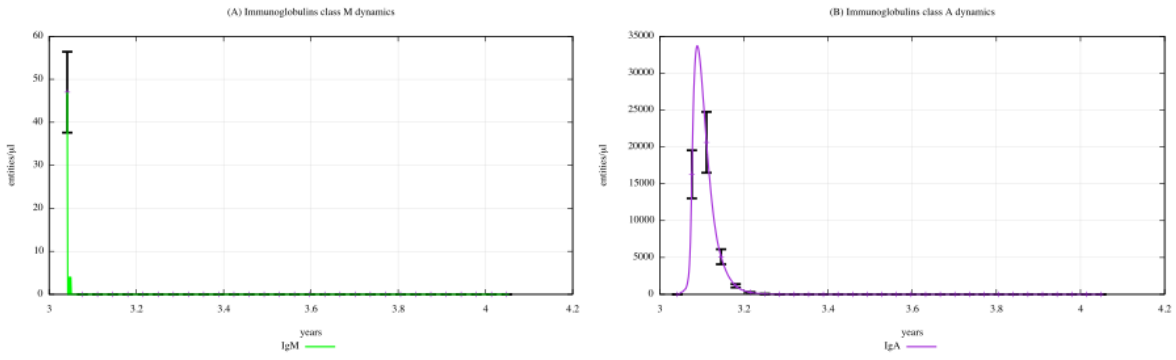

Figure 28: Immunoglobulin dynamics prediction for "not exposed" scenario, age range 0-4 years

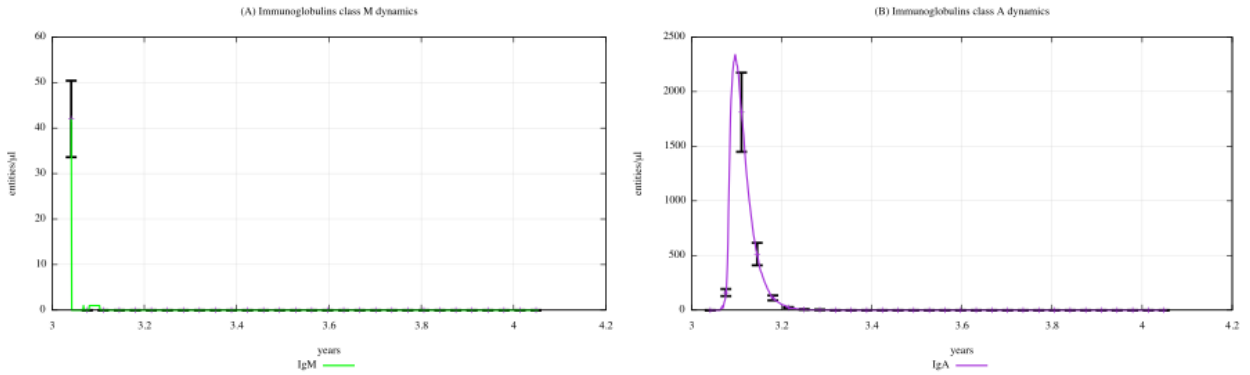

Figure 29: Immunoglobulin dynamics prediction for "scenario 3", age range 0-4 years.

The immunoglobulin concentration gradually decreases along with the three scenarios, as we can also see in the plots representing IgM and IgA dynamics of the scenarios 1 and 2, which are shown in Appendix Q. Comparing Figure 29 (PFAS exposure, "scenario 3") and Figure 28 (PFAS not exposed), we can see that the immunoglobulin concentration levels are much lower in children exposed to PFAS than in unexposed ones. In fact, a reduction in antibody levels is one of PFAS' most significant consequences on humoral response.

Results from UISS-TOX for the prediction of the response to vaccination for young people (25-26 years)

We simulated the immune system response after a generic bacterial challenge in digital patients aged 25-26 (young people) who were previously unexposed and exposed to the different concentrations of PFOA and PFOS coming from the three PBK model scenarios. We evaluated the immune response considering the cytokines, immunoglobulins, and T- and B-cells dynamics. T and B cells dynamics are shown in Annex R.

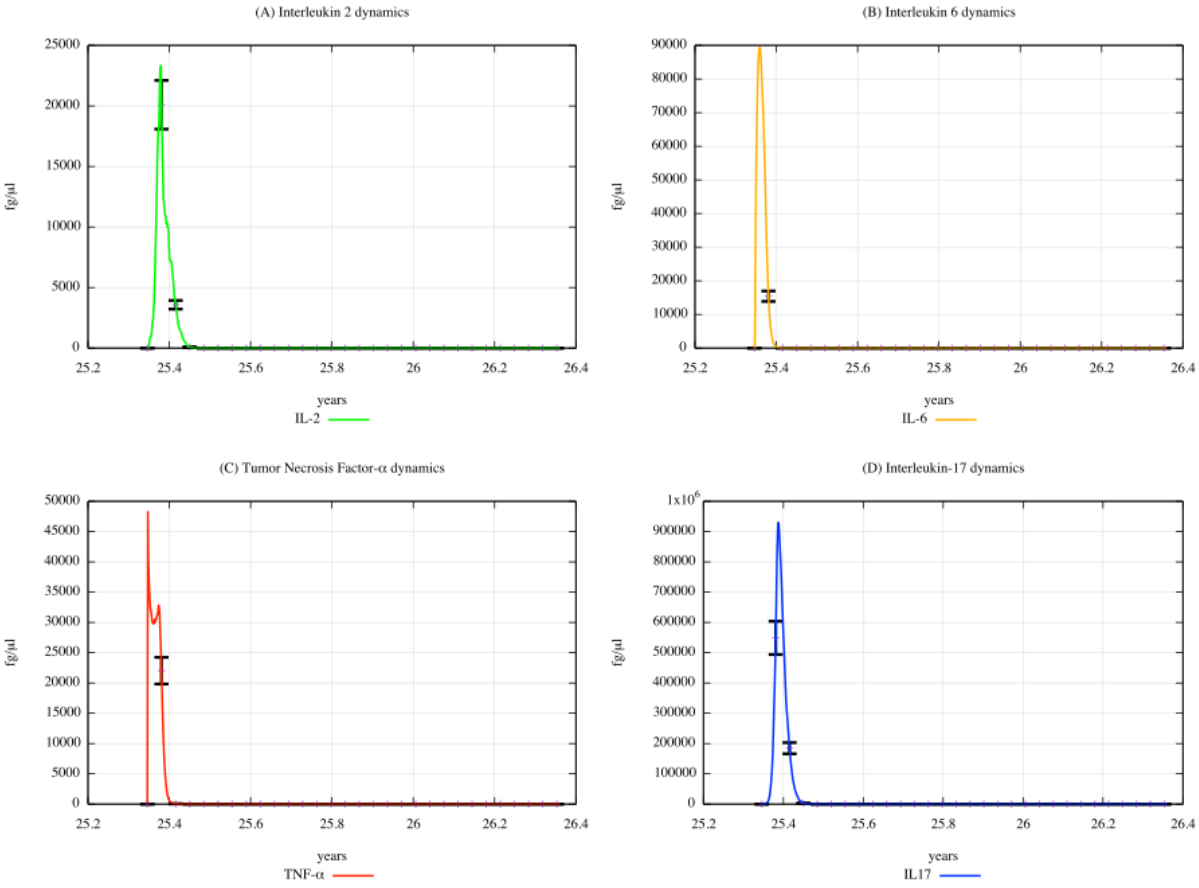

Figure 30: Cytokine dynamics prediction for "not exposed" scenario, age range 25-26 years

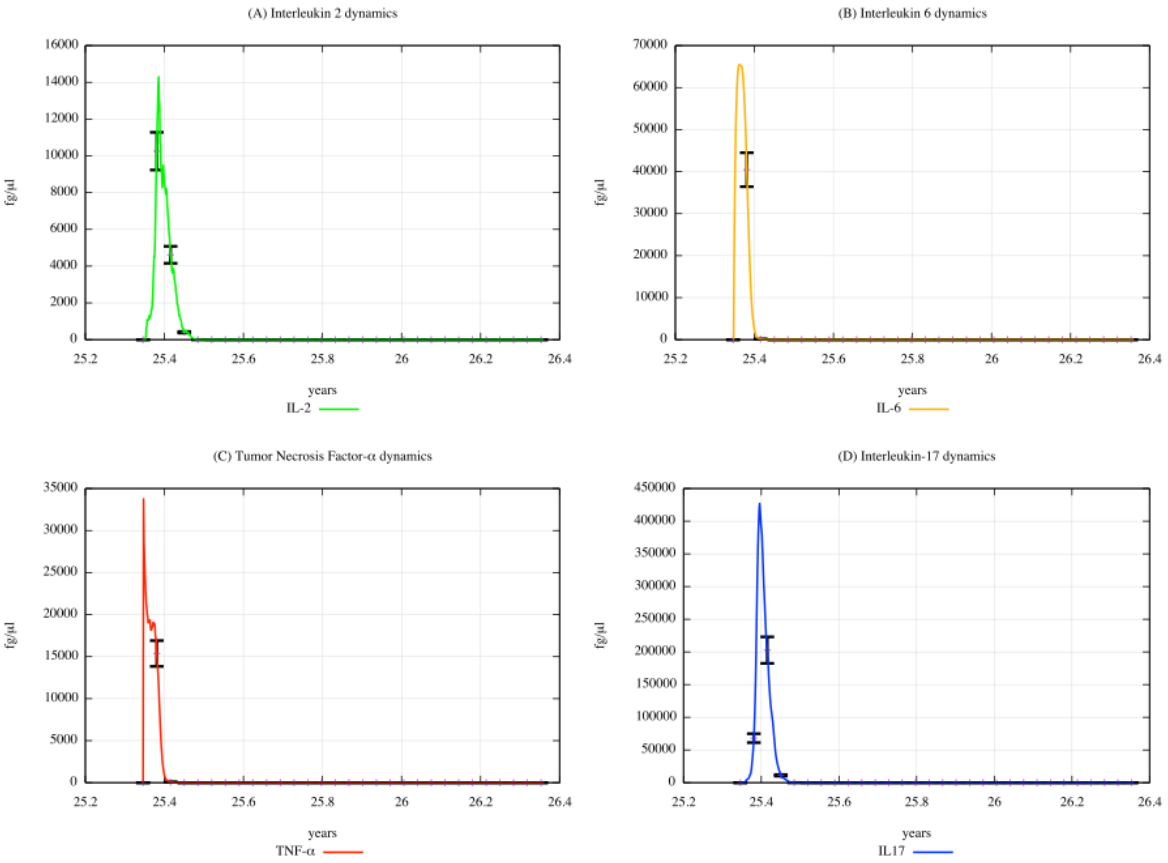

Figure 31: Cytokine dynamics prediction for "scenario 3", age range 25-26 years

Figure 30 and Figure 31 show the cytokine concentration levels in unexposed young people and exposed ones according to the "scenario 3", respectively. From the comparison of the Figures, also considering the ones representing the cytokine dynamics in the scenarios 1 and 2 (shown in Annex R), one can appreciate that the cytokine concentration levels will gradually decrease along with the three scenarios.

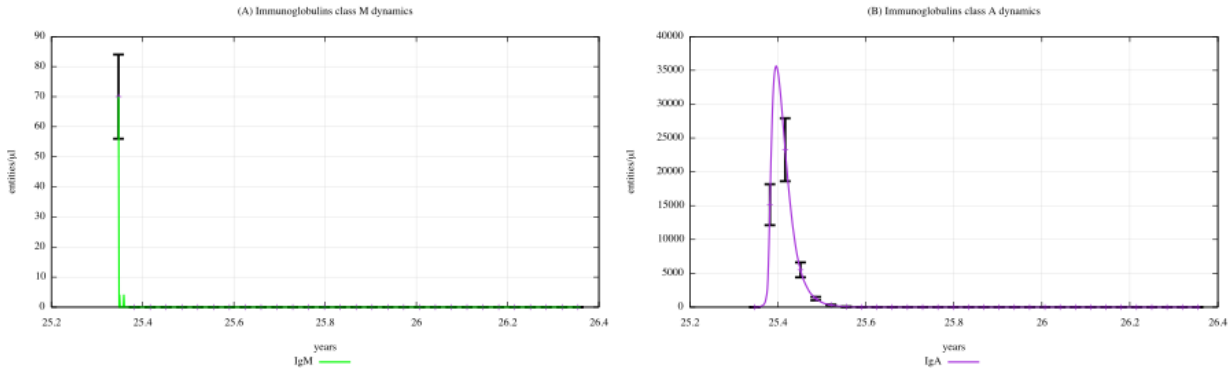

Figure 32: Immunoglobulin dynamics prediction for "not exposed" scenario, age range 25-26 years

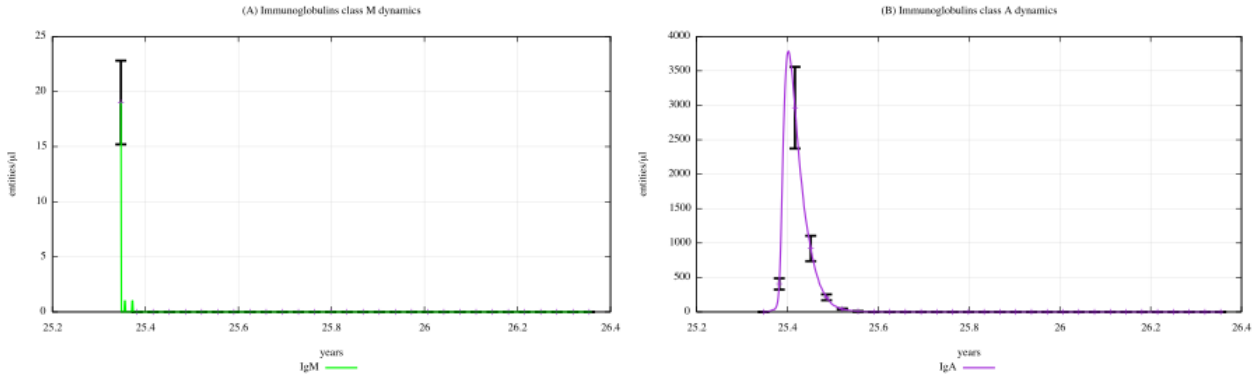

Figure 33: Immunoglobulin dynamics prediction for "scenario 3", age range 25-26 years

Figures 32 and 33 depict the IgM and IgA dynamics in unexposed young people and exposed ones according to "scenario 3", respectively. In Annex R, plots depicting immunoglobulin dynamics in scenarios 1 and 2 are also shown. Comparing Figures 32 and 33, we can notice a substantial reduction in IgM levels when digital patients are exposed to a high dose of PFAS, demonstrating that the perfluoroalkyl substances have a role in reducing the immune system activity in terms of humoral response.

Results from UISS-TOX for the prediction of the response to vaccination for elderlies (65-66 years)

UISS can simulate the immune response also considering the age of digital patients. We simulated the immune response following a bacterial challenge in subjects aged 65 to 66 years, both unexposed and previously exposed to different concentrations of PFAS (i.e., the three scenarios from the PBK model). As outputs, we retrieved several plots depicting cytokines, immunoglobulins, and T and B cells dynamics. We are going to show the cytokines and the IgM and IgA dynamics in unexposed elderlies and in exposed ones according to the

"scenario 3". Results about the scenarios 1 and 2, as well as about the T and B cells dynamics, are presented in Annex R.

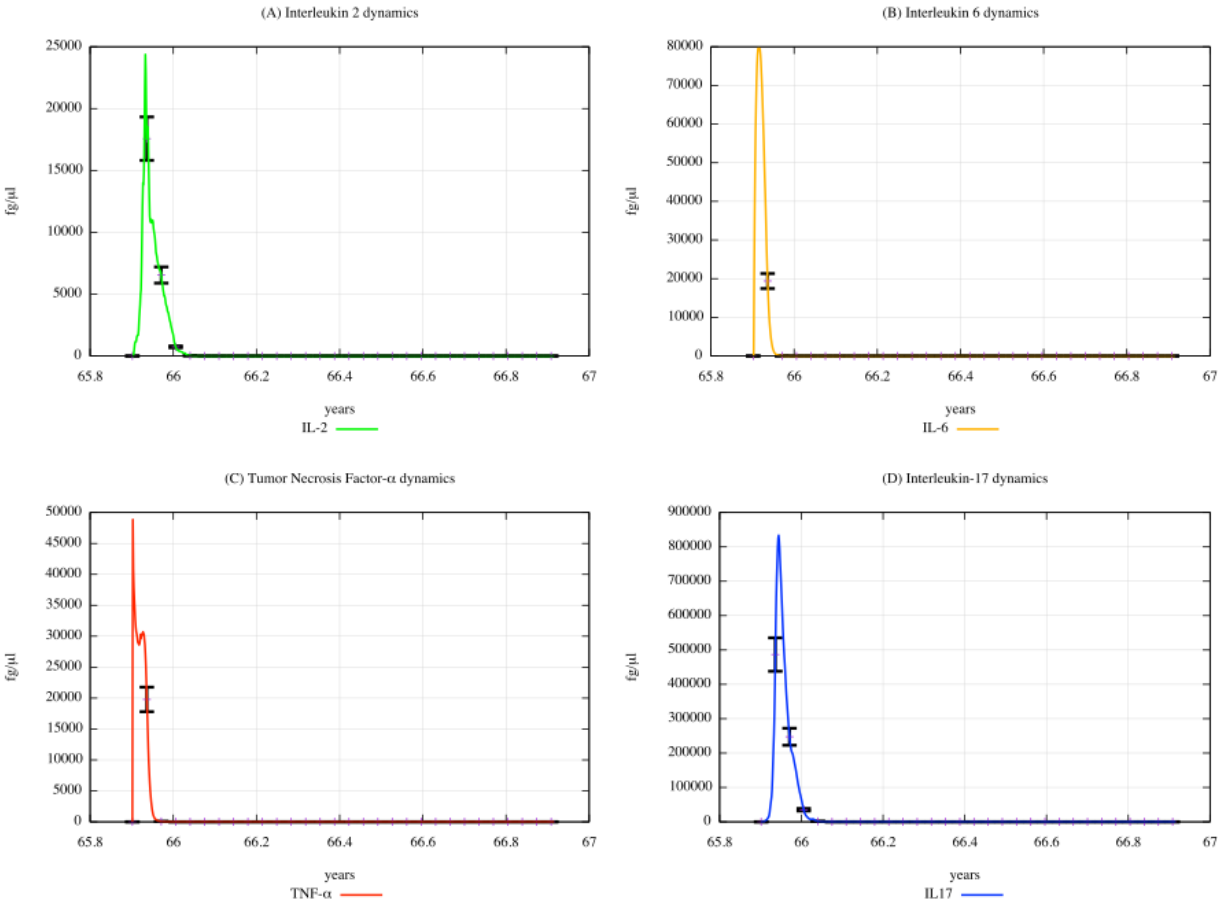

Figure 34: Cytokine dynamics prediction for "not exposed" scenario, age range 65-66 years

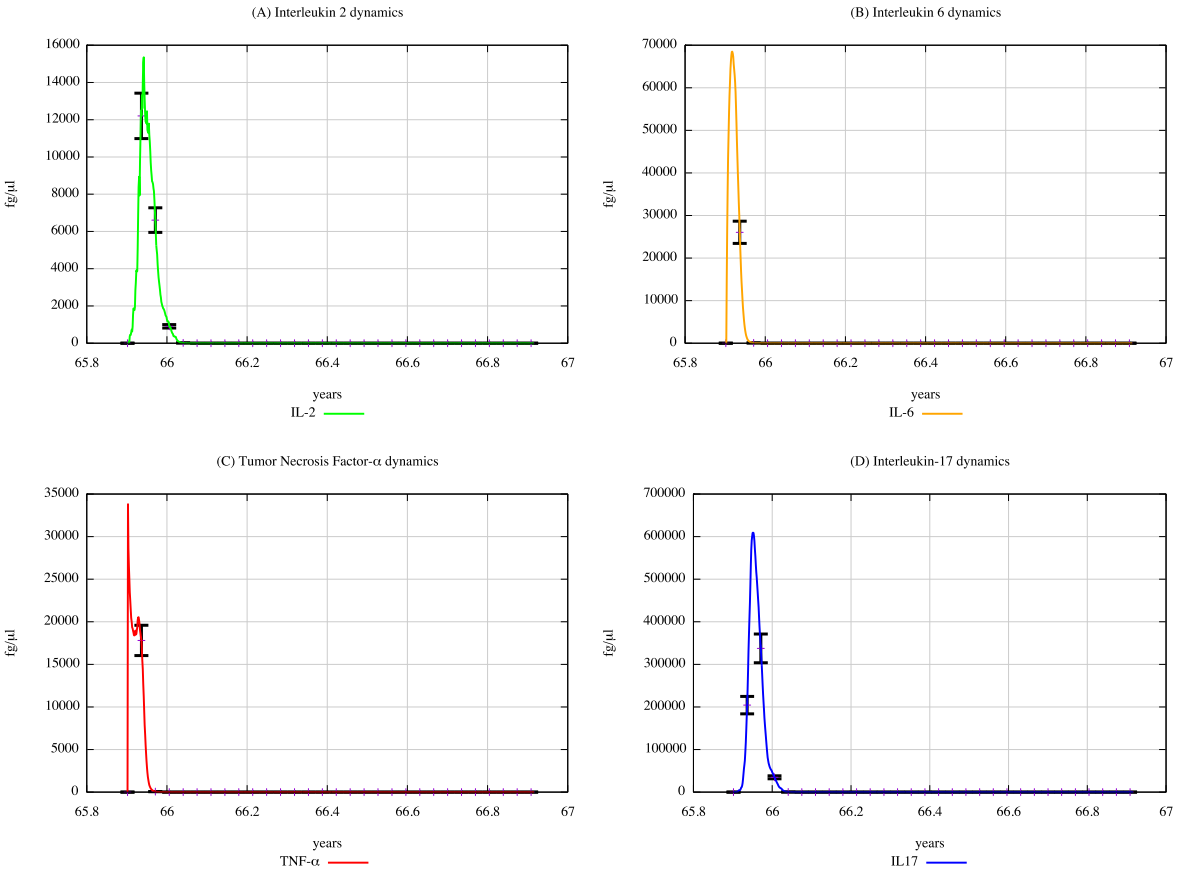

Figure 35: Cytokine dynamics prediction for "scenario 3", age range 65-66 years

From the comparison of Figure 35 (PFAS exposure) with Figure 34 (PFAS not exposure), one can appreciate that the cytokine concentration levels will gradually decrease along with the three scenarios, except for the IL-2 and IL-6 levels observed in scenario 1 (results presented in Annex R).

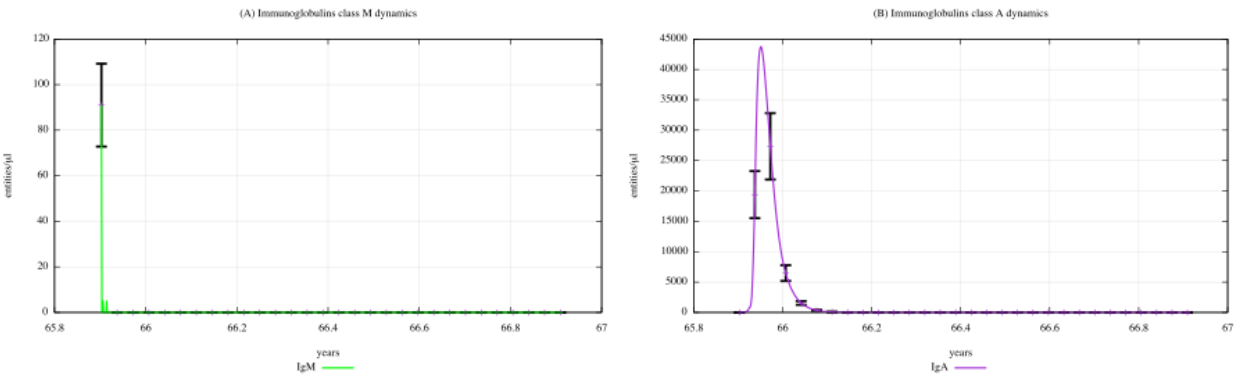

Figure 36: Immunoglobulins dynamics prediction for "not exposed" scenario, age range 65-66 years

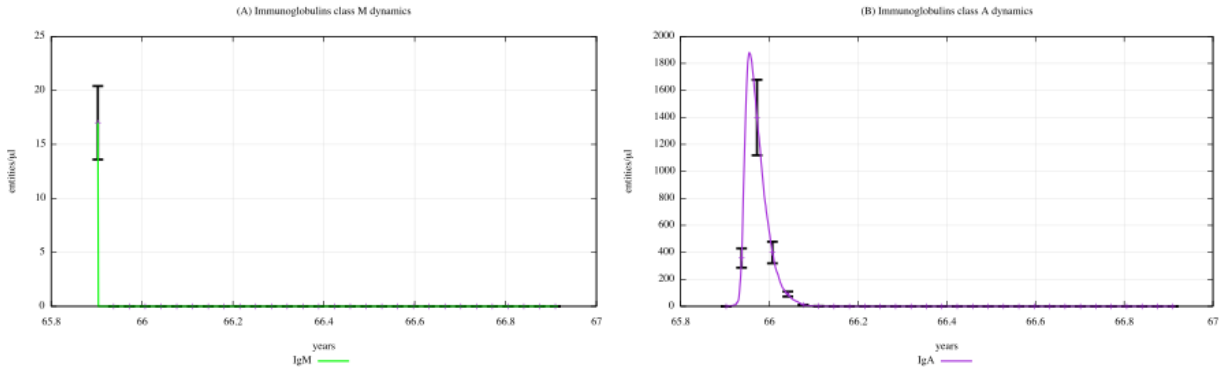

Figure 37: Immunoglobulin dynamics prediction for "scenario 3", age range 65-66 years

Comparing Figure 37 (PFAS exposure) with Figure 36 (PFAS not exposure), one can appreciate that the immunoglobulins concentration levels will gradually decrease along with the three scenarios. In particular, IgM and IgA dynamics are depicted, and we can notice a strong reduction in their concentration when elderly people are previously exposed to PFAS.

To sum up, the young people cohort (25-26 years) seems to be the most affected by perfluoroalkyl substances exposure. Indeed, we can observe a significant reduction in terms of immunological parameters, especially for the cytokine concentration levels (IL-2, IL-6, TNF-α, and IL-17) and B and CD4+ cell dynamics (activated Th17 and Th17 memory cells) for this cohort exposed to PFAS according to scenario 3 (results are shown in Annex R).

In parallel, it is also worth mentioning a relevant reduction in terms of immunoglobulins (particularly, IgM and IgA) both in the elderly cohort (65-66 years) and in the children one (0-4 years) exposed to PFAS according to scenario 3, along with a decrease in B cell dynamics (activated and memory B cells, shown in Annex R).

Immune response after H1N1 and diphtheria vaccines

According to the three different exposure scenarios, we simulated and predicted the antibody response after anti-diphtheria and anti-H1N1 vaccine administration in a cohort of 100 young people (25-26 years) and a cohort of 100 children (0-10 age range), respectively. We evaluated the antibody levels after the vaccine administration in the *in silico* cohorts previously exposed to PFAS according to the three scenarios.

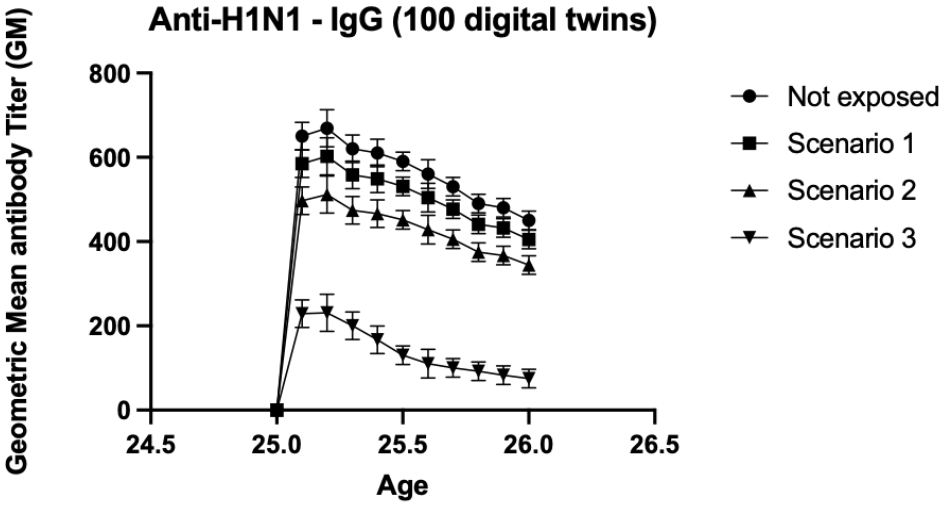

Figure 38: Predicted anti-H1N1 antibodies titers of *in silico* patient cohorts exposed to the two selected PFAS (PFOS and PFOA) according to the three different scenarios after having received influenza vaccination

As we can see in Figure 38, in the *in silico* cohort of 100 young people (25-26 age range) we observed a marked reduction in terms of vaccine response for scenario 3 after an anti-H1N1 challenge.

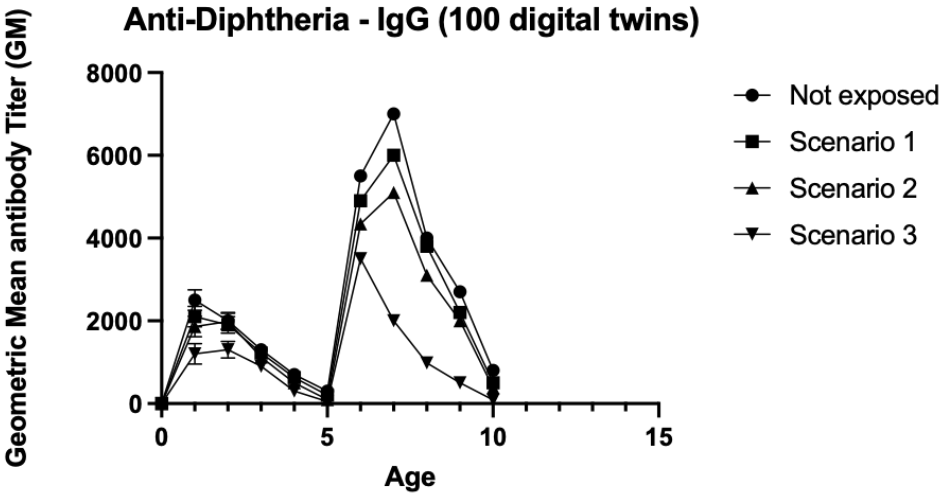

Figure 39: Predicted anti-H1N1 antibodies titers of *in silico* patient cohorts exposed to two different PFAS (PFOA and PFOS) according to the three different scenarios after having received diphtheria vaccination

As Figure 39 shows, in the *in silico* cohort of 100 children (0-10 age range), one can observe a marked reduction in terms of vaccine response in scenario 3 after the second challenge of the anti-diphtheria vaccine, according to the conventional vaccination schedule.

These results demonstrate that exposure to PFAS, in particular considering scenario 3, causes a reduction in the immune response both in the cohort of young people and in the cohort of children, displayed in reduced antibody production following the administration of vaccines.

UISS simulated and predicted the effect of the two considered PFAS on the immune system, considering both the level of exposure and the age range of the *in silico* cohorts. The three *in silico* cohorts consist of children (age range 0-4 years old), young people (age range 25-26 years old), and elderlies (age range 65-66 years old). Specifically, UISS predicted the effect of PFOA and PFOS on the immune system response in terms of cytokines, immunoglobulins (particularly IgM and IgA), and B and T cells dynamics, thus taking into account both cellular and humoral immune response.

UISS showed the higher exposure to PFAS, the lower production of cytokines, immunoglobulins, and B and T cell activity. In particular, the young people cohort (25-26 years) seems to be the most affected by PFAS exposure, according to the significant reduction in immunological parameters, especially for the cytokine concentration levels and B and CD4+ cell dynamics in the exposed people according to scenario 3. Furthermore, evaluating the antibody levels, UISS simulated the effect of PFAS exposure on the immune response to two different vaccine administrations. In an *in silico* cohort of 100 young people (25-26 years old), we observed a marked reduction in vaccine response for scenario 3 after an anti-H1N1 challenge. Similarly, in an *in silico* cohort of 100 children (0-10 age range), we observed a marked reduction in vaccine response in scenario 3 after the second challenge of the anti-diphtheria vaccine. Finally, exposure to PFOA and PFOS induced a reduced antibody response and, therefore, suppressed the immune response to vaccines in both cohorts.

The simulations result for PFNA and PFHxS were performed following the same approach. The results obtained are quite similar to PFOA and PFOS and for that reason not reported.

4.3.3 *In vitro* distribution model results

Starting from the data present in the literature and above reported, the condition for 4 different protocols was simulated and the results are reported below.

Protocol 1 – To simulate the treatment on THP-1 cells differentiated to mDCs, we set up the parameters above reported and changing the following test system parameters to mimic the corresponded *in vitro* protocol (refers to the A.3. "SOP for dendritic cells differentiation and maturation starting from THP-1 cell line" present in the Annex A). Concerning the well plate characteristics, we used 12 well plate with a well volume of 2000 µL, the average cell yield (seeding density) is 2.000.000 cells and a mass per cell of 5 ng. Concerning the input system parameters, the characteristics of cells was set up as follow: storage lipids 0.005%, membrane lipids 0.025% and structural protein 0.10%. The mass of cells was 10 ng. The serum volume was set up at 0.05 L/L because it was 5% inside the medium in the *in vitro* treatment. The characteristic of serum is 24 g/L of albumin and 1.9 g/L lipids. We simulated all the four PFAS (PFOA, PFOS, PFNA and PFHxS) at 5 different concentrations that represent the ones used during the *in vitro* treatment. The ECx were for PFOA 0.002, 0.024, 0.241, 2.41, 24.15 µM; for PFOS 0.002, 0.020, 0.2, 2 and 20 µM; for PFNA 0.002, 0.021, 0.215,

2.15, 21.5 µM; for PFHxS 0.002, 0.024, 0.249, 2,50, 24.99 µM. Chlorpyrifos was used as a positive control. The results are reported in the table 16 and 17 below.

Table 16: Result of the mass fraction (MF) distribution of PFAS in the *in vitro* treatment on THP-1 cells differentiated to mDCs (12 well plate)

Name	EC*x* in µM	MF_{AIR}	$MF_{BULK\ WAT}$	MF_{ALB}	$MF_{S\text{-}LIP}$	MF_{WAT}	MF_{Cells}	$MF_{Plastic}$
PFOA	2.41E-03	2.1%	88.8%	86.1%	0.0%	2.6%	9.2%	0.0%
PFOA	2.41E-02	2.1%	88.8%	86.1%	0.0%	2.6%	9.2%	0.0%
PFOA	2.41E-01	2.1%	88.8%	86.1%	0.0%	2.6%	9.2%	0.0%
PFOA	2.41E+00	2.1%	88.8%	86.1%	0.0%	2.6%	9.2%	0.0%
PFOA	2.41E+01	2.1%	88.8%	86.1%	0.0%		9.2%	0.0%
PFOS	2.00E-03	0.0%	68.6%	67.7%	0.0%	0.9%	31.4%	0.0%
PFOS	2.00E-02	0.0%	68.6%	67.7%	0.0%	0.9%	31.4%	0.0%
PFOS	2.00E-01	0.0%	68.6%	67.7%	0.0%	0.9%	31.4%	0.0%
PFOS	2.00E+00	0.0%	68.6%	67.7%	0.0%	0.9%	31.4%	0.0%
PFOS	2.00E+01	0.0%	68.6%	67.7%	0.0%	0.9%	31.4%	0.0%
PFNA	2.15E-03	0.0%	79.4%	77.9%	0.0%	1.4%	20.6%	0.0%
PFNA	2.15E-02	0.0%	79.4%	77.9%	0.0%	1.4%	20.6%	0.0%
PFNA	2.15E-01	0.0%	79.4%	77.9%	0.0%	1.4%	20.6%	0.0%
PFNA	2.15E+00	0.0%	79.4%	77.9%	0.0%	1.4%	20.6%	0.0%
PFNA	2.15E+01	0.0%	79.4%	77.9%	0.0%	1.4%	20.6%	0.0%
PFHxS	2.50E-03	0.0%	92.2%	89.1%	0.0%	3.0%	7.8%	0.0%
PFHxS	2.50E-02	0.0%	92.2%	89.1%	0.0%	3.0%	7.8%	0.0%
PFHxS	2.50E-01	0.0%	92.2%	89.1%	0.0%	3.0%	7.8%	0.0%
PFHxS	2.50E+00	0.0%	92.2%	89.1%	0.0%	3.0%	7.8%	0.0%
PFHxS	2.50E+01	0.0%	92.2%	89.1%	0.0%	3.0%	7.8%	0.0%
Chlorpyrifos	1.00E+00	0.1%	64.4%	51.5%	10.2%	2.6%	31.6%	3.9%

Table legend: ECx is the chemical concentration
MF is the mass fraction of the chemicals
MF_{AIR} is the mass fraction of the chemicals in air (volatile fraction of the chemicals)
$MF_{WATBULK}$ is the mass fraction of the chemicals in water (bulk mass fraction sum of the single MF_{ALB} $MF_{S\text{-}LIP}$ MF_{WAT})
MF_{ALB} is the mass fraction of the chemicals linked to the albumin
$MF_{S\text{-}LIP}$ is the mass fraction of the chemicals linked to the lipids
MF_{WAT} is the mass fraction of the chemicals in water (free fraction not linked)
MF_{CELLS} is the mass fraction of the chemicals into the cells
$MF_{PLASTIC}$ is the mass fraction of the chemicals linked to the plastic

Table 17: Result of the concentrations of PFAS in the *in vitro* treatment on THP-1 cells differentiated to mDCs (12 well plate)

Name	$C_{NOM,initial}$ (µmol/L medium)	$C_{BULK\ WAT}$ (µmol/L medium)	C_{WAT} (µmol/L water)	C_{AIR} (µmol/L air)	C_{ALB} (µmol/L alb)	$C_{S\text{-}LIP}$ (µmol/L lipid)	C_{cells} (µmol/L cell)	$A_{Plastic}$, µmoles/m2
PFOA	2.4E-03	2.1E-03	6.4E-05	4.1E-13	2.4E+00	3.3E-03	4.4E-02	3.61E-07
PFOA	2.4E-02	2.1E-02	6.4E-04	4.1E-12	2.4E+01	3.3E-02	4.4E-01	3.61E-06
PFOA	2.4E-01	2.1E-01	6.4E-03	4.1E-11	2.4E+02	3.3E-01	4.4E+00	3.61E-05
PFOA	2.4E+00	2.1E+00	6.4E-02	4.1E-10	2.4E+03	3.3E+00	4.4E+01	3.61E-04
PFOA	2.4E+01	2.1E+01	6.4E-01	4.1E-09	2.4E+04	3.3E+01	4.4E+02	3.61E-03
PFOS	2.0E-03	1.4E-03	1.7E-05	5.0E-15	1.5E+00	9.1E-03	1.3E-01	3.58E-07
PFOS	2.0E-02	1.4E-02	1.7E-04	5.0E-14	1.5E+01	9.1E-02	1.3E+00	3.58E-06
PFOS	2.0E-01	1.4E-01	1.7E-03	5.0E-13	1.5E+02	9.1E-01	1.3E+01	3.58E-05
PFOS	2.0E+00	1.4E+00	1.7E-02	5.0E-12	1.5E+03	9.1E+00	1.3E+02	3.58E-04
PFOS	2.0E+01	1.4E+01	1.7E-01	5.0E-11	1.5E+04	9.1E+01	1.3E+03	3.58E-03
PFNA	2.2E-03	1.7E-03	3.0E-05	2.9E-15	1.9E+00	6.5E-03	8.9E-02	3.76E-07
PFNA	2.2E-02	1.7E-02	3.0E-04	2.9E-14	1.9E+01	6.5E-02	8.9E-01	3.76E-06
PFNA	2.2E-01	1.7E-01	3.0E-03	2.9E-13	1.9E+02	6.5E-01	8.9E+00	3.76E-05
PFNA	2.2E+00	1.7E+00	3.0E-02	2.9E-12	1.9E+03	6.5E+00	8.9E+01	3.76E-04
PFNA	2.2E+01	1.7E+01	3.0E-01	2.9E-11	1.9E+04	6.5E+01	8.9E+02	3.76E-03
PFHxS	2.5E-03	2.3E-03	7.6E-05	1.9E-15	2.5E+00	2.9E-03	3.9E-02	3.59E-07
PFHxS	2.5E-02	2.3E-02	7.6E-04	1.9E-14	2.5E+01	2.9E-02	3.9E-01	3.59E-06
PFHxS	2.5E-01	2.3E-01	7.6E-03	1.9E-13	2.5E+02	2.9E-01	3.9E+00	3.59E-05
PFHxS	2.5E+00	2.3E+00	7.6E-02	1.9E-12	2.5E+03	2.9E+00	3.9E+01	3.59E-04
PFHxS	2.5E+01	2.3E+01	7.6E-01	1.9E-11	2.5E+04	2.9E+01	3.9E+02	3.59E-03
Chlorpyrifos	1.0E+00	6.4E-01	2.6E-02	9.0E-12	5.9E+02	1.1E+03	6.3E+01	2.14E-01

Table legend: C_{nom} is the chemical concentration

$C_{WATBULK}$ is the concentration of the chemicals in water (bulk concentration sum of the single MF_{ALB} $MF_{S\text{-}LIP}$ MF_{WAT})

C_{ALB} is the concentration of the chemicals linked to the albumin

$C_{S\text{-}LIP}$ is the concentration of the chemicals linked to the lipids

C_{WAT} is the concentration of the chemicals in water (free fraction not linked)

C_{AIR} is the concentration of the chemicals in air (volatile fraction of the chemicals)

C_{CELLS} is the concentration of the chemicals into the cells

$A_{PLASTIC}$ is the concentration of the chemicals linked to the plastic

Protocol 2 – To simulate the T cells protocols we set up the parameters above reported and changing the following test system parameters to mimic the corresponded *in vitro* protocol (refers to the A.4. "SOP for T helper cells differentiation" present in the Annex A). Concerning the well plate characteristics, we used 48 well plate with a well volume of 1000 µL, the average cell yield (seeding density) is 2.000.000 cells and a mass per cell of 5 ng. The mass of cells was 10 mg. Concerning the input system parameters, the characteristics of cells was set up as follow: storage lipids 0.005%, membrane lipids 0.025% and structural protein 0.10%. The mass of cells was 10 mg. The serum volume was set up at 0.05 L/L because it was 5% inside the medium in the *in vitro* treatment. The characteristic of serum is 42.5 g/L of albumin and 1.9 g/L lipids. We simulated all the four PFAS (PFOA, PFOS, PFNA and PFHxS) at 5 different concentrations that represent the one used during the *in vitro* treatment. The ECx were for PFOA 0.002, 0.024, 0.241, 2.41, 24.15 µM; for PFOS 0.002, 0.020, 0.2, 2 and 20 µM; for PFNA 0.002, 0.021, 0.215, 2.15, 21.5 µM; for PFHxS 0.002, 0.024, 0.249, 2,50, 24.99 µM. Chlorpyrifos was used as a positive control. The results are reported in the table 18 and 19 below.

Table 18: Result of the mass fraction (MF) distribution of PFAS in the *in vitro* T cell protocols (48 well plate – 1000 µL volume into the well)

Name	ECx in µM	MF_{AIR}	$MF_{BULK\ WAT}$	MF_{ALB}	$MF_{S\text{-}LIP}$	MF_{WAT}	MF_{Cells}	$MF_{Plastic}$
PFOA	2.41E-03	0.3%	89.2%	87.7%	0.0%	1.5%	10.5%	0.0%
PFOA	2.41E-02	0.3%	89.2%	87.7%	0.0%	1.5%	10.5%	0.0%
PFOA	2.41E-01	0.3%	89.2%	87.7%	0.0%	1.5%	10.5%	0.0%
PFOA	2.41E+00	0.3%	89.2%	87.7%	0.0%	1.5%	10.5%	0.0%
PFOA	2.41E+01	0.3%	89.2%	87.7%	0.0%	1.5%	10.5%	0.0%
PFOS	2.00E-03	0.0%	65.8%	65.3%	0.0%	0.5%	34.2%	0.0%
PFOS	2.00E-02	0.0%	65.8%	65.3%	0.0%	0.5%	34.2%	0.0%
PFOS	2.00E-01	0.0%	65.8%	65.3%	0.0%	0.5%	34.2%	0.0%
PFOS	2.00E+00	0.0%	65.8%	65.3%	0.0%	0.5%	34.2%	0.0%
PFOS	2.00E+01	0.0%	65.8%	65.3%	0.0%	0.5%	34.2%	0.0%
PFNA	2.15E-03	0.0%	77.2%	76.4%	0.0%	0.8%	22.8%	0.0%
PFNA	2.15E-02	0.0%	77.2%	76.4%	0.0%	0.8%	22.8%	0.0%
PFNA	2.15E-01	0.0%	77.2%	76.4%	0.0%	0.8%	22.8%	0.0%
PFNA	2.15E+00	0.0%	77.2%	76.4%	0.0%	0.8%	22.8%	0.0%
PFNA	2.15E+01	0.0%	77.2%	76.4%	0.0%	0.8%	22.8%	0.0%
PFHxS	2.50E-03	0.0%	91.1%	89.4%	0.0%	1.7%	8.9%	0.0%
PFHxS	2.50E-02	0.0%	91.1%	89.4%	0.0%	1.7%	8.9%	0.0%
PFHxS	2.50E-01	0.0%	91.1%	89.4%	0.0%	1.7%	8.9%	0.0%
PFHxS	2.50E+00	0.0%	91.1%	89.4%	0.0%	1.7%	8.9%	0.0%
PFHxS	2.50E+01	0.0%	91.1%	89.4%	0.0%	1.7%	8.9%	0.0%
Chlorpyrifos	1.00E+00	0.0%	59.4%	52.1%	5.9%	1.5%	36.1%	4.4%

Table legend: ECx is the chemical concentration
MF is the mass fraction of the chemicals
MF_{AIR} is the mass fraction of the chemicals in air (volatile fraction of the chemicals)
$MF_{WATBULK}$ is the mass fraction of the chemicals in water (bulk mass fraction sum of the single MF_{ALB} $MF_{S\text{-}LIP}$ MF_{WAT})
MF_{ALB} is the mass fraction of the chemicals linked to the albumin
$MF_{S\text{-}LIP}$ is the mass fraction of the chemicals linked to the lipids
MF_{WAT} is the mass fraction of the chemicals in water (free fraction not linked)
MF_{CELLS} is the mass fraction of the chemicals into the cells
$MF_{PLASTIC}$ is the mass fraction of the chemicals linked to the plastic

Table 19: Result of the concentrations of PFAS in the *in vitro* T cell protocols (48 well plate – 1000 µL volume into the well)

Name	$C_{NOM,initial}$ (µmol/L medium)	$C_{BULK\ WAT}$ (µmol/L medium)	C_{WAT} (µmol/L water)	C_{AIR} (µmol/L air)	C_{ALB} (µmol/L alb)	$C_{S\text{-}LIP}$ (µmol/L lipid)	C_{cells} (µmol/L cell)	$A_{Plastic}$, µmoles/m2
PFOA	2.4E-03	2.2E-03	3.7E-05	2.3E-13	1.4E+00	1.9E-03	2.5E-02	2.08E-07
PFOA	2.4E-02	2.2E-02	3.7E-04	2.3E-12	1.4E+01	1.9E-02	2.5E-01	2.08E-06
PFOA	2.4E-01	2.2E-01	3.7E-03	2.3E-11	1.4E+02	1.9E-01	2.5E+00	2.08E-05
PFOA	2.4E+00	2.2E+00	3.7E-02	2.3E-10	1.4E+03	1.9E+00	2.5E+01	2.08E-04
PFOA	2.4E+01	2.2E+01	3.7E-01	2.3E-09	1.4E+04	1.9E+01	2.5E+02	2.08E-03
PFOS	2.0E-03	1.3E-03	9.5E-06	2.7E-15	8.4E-01	5.0E-03	6.8E-02	1.95E-07
PFOS	2.0E-02	1.3E-02	9.5E-05	2.7E-14	8.4E+00	5.0E-02	6.8E-01	1.95E-06
PFOS	2.0E-01	1.3E-01	9.5E-04	2.7E-13	8.4E+01	5.0E-01	6.8E+00	1.95E-05
PFOS	2.0E+00	1.3E+00	9.5E-03	2.7E-12	8.4E+02	5.0E+00	6.8E+01	1.95E-04
PFOS	2.0E+01	1.3E+01	9.5E-02	2.7E-11	8.4E+03	5.0E+01	6.8E+02	1.95E-03
PFNA	2.2E-03	1.7E-03	1.7E-05	1.6E-15	1.1E+00	3.6E-03	4.9E-02	2.08E-07
PFNA	2.2E-02	1.7E-02	1.7E-04	1.6E-14	1.1E+01	3.6E-02	4.9E-01	2.08E-06
PFNA	2.2E-01	1.7E-01	1.7E-03	1.6E-13	1.1E+02	3.6E-01	4.9E+00	2.08E-05
PFNA	2.2E+00	1.7E+00	1.7E-02	1.6E-12	1.1E+03	3.6E+00	4.9E+01	2.08E-04
PFNA	2.2E+01	1.7E+01	1.7E-01	1.6E-11	1.1E+04	3.6E+01	4.9E+02	2.08E-03
PFHxS	2.5E-03	2.3E-03	4.3E-05	1.1E-15	1.4E+00	1.7E-03	2.2E-02	2.03E-07
PFHxS	2.5E-02	2.3E-02	4.3E-04	1.1E-14	1.4E+01	1.7E-02	2.2E-01	2.03E-06
PFHxS	2.5E-01	2.3E-01	4.3E-03	1.1E-13	1.4E+02	1.7E-01	2.2E+00	2.03E-05
PFHxS	2.5E+00	2.3E+00	4.3E-02	1.1E-12	1.4E+03	1.7E+00	2.2E+01	2.03E-04
PFHxS	2.5E+01	2.3E+01	4.3E-01	1.1E-11	1.4E+04	1.7E+01	2.2E+02	2.03E-03
Chlorpyrifos	1.0E+00	5.9E-01	1.5E-02	5.1E-12	3.3E+02	6.2E+02	3.6E+01	1.22E-01

Table legend: C_{nom} is the chemical concentration

$C_{WATBULK}$ is the concentration of the chemicals in water (bulk concentration sum of the single MF_{ALB} $MF_{S\text{-}LIP}$ MF_{WAT})

C_{ALB} is the concentration of the chemicals linked to the albumin

$C_{S\text{-}LIP}$ is the concentration of the chemicals linked to the lipids

C_{WAT} is the concentration of the chemicals in water (free fraction not linked)

C_{AIR} is the concentration of the chemicals in air (volatile fraction of the chemicals)

C_{CELLS} is the concentration of the chemicals into the cells

$A_{PLASTIC}$ is the concentration of the chemicals linked to the plastic

Protocol 3 – To simulate the TI antibody response protocol we set up the parameters above reported and changing the following test system parameters to mimic the corresponded *in vitro* protocol (refers to the A.6. "SOP for activation of primary human B cells" present in the Annex A). Concerning the well plate characteristics, we used 48 well plate with a well volume of 500 µL, the average cell yield (seeding density) is 630000 cells and a mass per cell of 5 ng. Concerning the input system parameters, the characteristics of cells was set up as follow: storage lipids 0.005%, membrane lipids 0.025% and structural protein 0.10%. The mass of cells was 3.15 mg. The serum volume was set up at 0.05 L/L because it was 5% inside the medium in the *in vitro* treatment. The characteristic of serum is 42.5 g/L of albumin and 1.9 g/L lipids. We simulated all the four PFAS (PFOA, PFOS, PFNA and PFHxS) at 5 different concentrations that represent the one used during the *in vitro* treatment. The ECx were for PFOA 0.002, 0.024, 0.241, 2.41, 24.15 µM; for PFOS 0.002, 0.020, 0.2, 2 and 20 µM; for PFNA 0.002, 0.021, 0.215, 2.15, 21.5 µM; for PFHxS 0.002, 0.024, 0.249, 2,50, 24.99 µM. Chlorpyrifos was used as a positive control. The results are reported in the table 20 and 21 below.

Table 20: Result of the mass fraction (MF) distribution of PFAS in the *in vitro* TI antibody response protocols (48 well plate – 500 µL volume into the well)

Name	ECx in µM	MF_{AIR}	$MF_{BULK\ WAT}$	MF_{ALB}	$MF_{S\text{-}LIP}$	MF_{WAT}	MF_{Cells}	$MF_{Plastic}$
PFOA	2.41E-03	1.1%	92.1%	90.5%	0.0%	1.6%	6.8%	0.0%
PFOA	2.41E-02	1.1%	92.1%	90.5%	0.0%	1.6%	6.8%	0.0%
PFOA	2.41E-01	1.1%	92.1%	90.5%	0.0%	1.6%	6.8%	0.0%
PFOA	2.41E+00	1.1%	92.1%	90.5%	0.0%	1.6%	6.8%	0.0%
PFOA	2.41E+01	1.1%	92.1%	90.5%	0.0%	1.6%	6.8%	0.0%
PFOS	2.00E-03	0.0%	75.3%	74.8%	0.0%	0.5%	24.6%	0.0%
PFOS	2.00E-02	0.0%	75.3%	74.8%	0.0%	0.5%	24.6%	0.0%
PFOS	2.00E-01	0.0%	75.3%	74.8%	0.0%	0.5%	24.6%	0.0%
PFOS	2.00E+00	0.0%	75.3%	74.8%	0.0%	0.5%	24.6%	0.0%
PFOS	2.00E+01	0.0%	75.3%	74.8%	0.0%	0.5%	24.6%	0.0%
PFNA	2.15E-03	0.0%	84.3%	83.4%	0.0%	0.8%	15.7%	0.0%
PFNA	2.15E-02	0.0%	84.3%	83.4%	0.0%	0.8%	15.7%	0.0%
PFNA	2.15E-01	0.0%	84.3%	83.4%	0.0%	0.8%	15.7%	0.0%
PFNA	2.15E+00	0.0%	84.3%	83.4%	0.0%	0.8%	15.7%	0.0%
PFNA	2.15E+01	0.0%	84.3%	83.4%	0.0%	0.8%	15.7%	0.0%
PFHxS	2.50E-03	0.0%	94.2%	92.4%	0.0%	1.8%	5.8%	0.0%
PFHxS	2.50E-02	0.0%	94.2%	92.4%	0.0%	1.8%	5.8%	0.0%
PFHxS	2.50E-01	0.0%	94.2%	92.4%	0.0%	1.8%	5.8%	0.0%
PFHxS	2.50E+00	0.0%	94.2%	92.4%	0.0%	1.8%	5.8%	0.0%
PFHxS	2.50E+01	0.0%	94.2%	92.4%	0.0%	1.8%	5.8%	0.0%
Chlorpyrifos	1.00E+00	0.1%	68.6%	60.1%	6.8%	1.7%	26.2%	5.1%

Table legend: ECx is the chemical concentration
MF is the mass fraction of the chemicals
MF_{AIR} is the mass fraction of the chemicals in air (volatile fraction of the chemicals)
$MF_{WATBULK}$ is the mass fraction of the chemicals in water (bulk mass fraction sum of the single MF_{ALB} $MF_{S\text{-}LIP}$ MF_{WAT})
MF_{ALB} is the mass fraction of the chemicals linked to the albumin
$MF_{S\text{-}LIP}$ is the mass fraction of the chemicals linked to the lipids
MF_{WAT} is the mass fraction of the chemicals in water (free fraction not linked)
MF_{CELLS} is the mass fraction of the chemicals into the cells
$MF_{PLASTIC}$ is the mass fraction of the chemicals linked to the plastic

Table 21: Result of the concentrations of PFAS in the *in vitro* TIantibody response protocols (48 well plate – 500 µL volume into the well)

Name	$C_{NOM,initial}$ (µmol/L medium)	$C_{BULK\ WAT}$ (µmol/L medium)	C_{WAT} (µmol/L water)	C_{AIR} (µmol/L air)	C_{ALB} (µmol/L alb)	$C_{S\text{-}LIP}$ (µmol/L lipid)	C_{cells} (µmol/L cell)	$A_{Plastic}$, µmoles/m2
PFOA	2.4E-03	2.2E-03	3.8E-05	2.4E-13	1.4E+00	2.0E-03	2.6E-02	2.14E-07
PFOA	2.4E-02	2.2E-02	3.8E-04	2.4E-12	1.4E+01	2.0E-02	2.6E-01	2.14E-06
PFOA	2.4E-01	2.2E-01	3.8E-03	2.4E-11	1.4E+02	2.0E-01	2.6E+00	2.14E-05
PFOA	2.4E+00	2.2E+00	3.8E-02	2.4E-10	1.4E+03	2.0E+00	2.6E+01	2.14E-04
PFOA	2.4E+01	2.2E+01	3.8E-01	2.4E-09	1.4E+04	2.0E+01	2.6E+02	2.14E-03
PFOS	2.0E-03	1.5E-03	1.1E-05	3.1E-15	9.6E-01	5.7E-03	7.8E-02	2.23E-07
PFOS	2.0E-02	1.5E-02	1.1E-04	3.1E-14	9.6E+00	5.7E-02	7.8E-01	2.23E-06
PFOS	2.0E-01	1.5E-01	1.1E-03	3.1E-13	9.6E+01	5.7E-01	7.8E+00	2.23E-05
PFOS	2.0E+00	1.5E+00	1.1E-02	3.1E-12	9.6E+02	5.7E+00	7.8E+01	2.23E-04
PFOS	2.0E+01	1.5E+01	1.1E-01	3.1E-11	9.6E+03	5.7E+01	7.8E+02	2.23E-03
PFNA	2.2E-03	1.8E-03	1.8E-05	1.8E-15	1.2E+00	3.9E-03	5.4E-02	2.27E-07
PFNA	2.2E-02	1.8E-02	1.8E-04	1.8E-14	1.2E+01	3.9E-02	5.4E-01	2.27E-06
PFNA	2.2E-01	1.8E-01	1.8E-03	1.8E-13	1.2E+02	3.9E-01	5.4E+00	2.27E-05
PFNA	2.2E+00	1.8E+00	1.8E-02	1.8E-12	1.2E+03	3.9E+00	5.4E+01	2.27E-04
PFNA	2.2E+01	1.8E+01	1.8E-01	1.8E-11	1.2E+04	3.9E+01	5.4E+02	2.27E-03
PFHxS	2.5E-03	2.4E-03	4.5E-05	1.1E-15	1.5E+00	1.7E-03	2.3E-02	2.10E-07
PFHxS	2.5E-02	2.4E-02	4.5E-04	1.1E-14	1.5E+01	1.7E-02	2.3E-01	2.10E-06
PFHxS	2.5E-01	2.4E-01	4.5E-03	1.1E-13	1.5E+02	1.7E-01	2.3E+00	2.10E-05
PFHxS	2.5E+00	2.4E+00	4.5E-02	1.1E-12	1.5E+03	1.7E+00	2.3E+01	2.10E-04
PFHxS	2.5E+01	2.4E+01	4.5E-01	1.1E-11	1.5E+04	1.7E+01	2.3E+02	2.10E-03
Chlorpyrifos	1.0E+00	6.9E-01	1.7E-02	5.9E-12	3.9E+02	7.1E+02	4.2E+01	1.41E-01

Table legend: C_{nom} is the chemical concentration

$C_{WATBULK}$ is the concentration of the chemicals in water (bulk concentration sum of the single MF_{ALB} $MF_{S\text{-}LIP}$ MF_{WAT})

C_{ALB} is the concentration of the chemicals linked to the albumin

$C_{S\text{-}LIP}$ is the concentration of the chemicals linked to the lipids

C_{WAT} is the concentration of the chemicals in water (free fraction not linked)

C_{AIR} is the concentration of the chemicals in air (volatile fraction of the chemicals)

C_{CELLS} is the concentration of the chemicals into the cells

$A_{PLASTIC}$ is the concentration of the chemicals linked to the plastic

Protocol 4 – To simulate the TD antibody response protocol we set up the parameters above reported and changing the following test system parameters to mimic the corresponded *in vitro* protocol (refers to the A.5. "SOP for *in vitro* primary antibody response" present in the Annex A). Concerning the well plate characteristics, we used 24 well plate with a well volume of 500 µL, the average cell yield (seeding density) is 1.250.000 cells and a mass per cell of 5 ng. Concerning the input system parameters, the characteristics of cells was set up as follow: storage lipids 0.005%, membrane lipids 0.025% and structural protein 0.10%. The mass of cells was 6.25 ng. The serum volume was set up at 0.05 L/L because it was 5% inside the medium in the *in vitro* treatment. The characteristic of serum is 42.5 g/L of albumin and 1.9 g/L lipids. We simulated all the four PFAS (PFOA, PFOS, PFNA and PFHxS) at 5 different concentrations that represent the one used during the *in vitro* treatment. The ECx were for PFOA 0.002, 0.024, 0.241, 2.41, 24.15 µM; for PFOS 0.002, 0.020, 0.2, 2 and 20 µM; for PFNA 0.002, 0.021, 0.215, 2.15, 21.5 µM; for PFHxS 0.002, 0.024, 0.249, 2,50, 24.99 µM. Chlorpyrifos was used as a positive control. The results are reported in the table 22 and 23 below.

Table 22: Result of the mass fraction (MF) distribution of PFAS in the *in vitro* TD antibody response protocols (24 well plate)

Name	ECx in µM	MF_{AIR}	$MF_{BULK\ WAT}$	MF_{ALB}	$MF_{S\text{-}LIP}$	MF_{WAT}	MF_{Cells}	$MF_{Plastic}$
PFOA	2.41E-03	2.7%	84.8%	83.4%	0.0%	1.4%	12.5%	0.0%
PFOA	2.41E-02	2.7%	84.8%	83.4%	0.0%	1.4%	12.5%	0.0%
PFOA	2.41E-01	2.7%	84.8%	83.4%	0.0%	1.4%	12.5%	0.0%
PFOA	2.41E+00	2.7%	84.8%	83.4%	0.0%	1.4%	12.5%	0.0%
PFOA	2.41E+01	2.7%	84.8%	83.4%	0.0%	1.4%	12.5%	0.0%
PFOS	2.00E-03	0.0%	60.6%	60.2%	0.0%	0.4%	39.3%	0.0%
PFOS	2.00E-02	0.0%	60.6%	60.2%	0.0%	0.4%	39.3%	0.0%
PFOS	2.00E-01	0.0%	60.6%	60.2%	0.0%	0.4%	39.3%	0.0%
PFOS	2.00E+00	0.0%	60.6%	60.2%	0.0%	0.4%	39.3%	0.0%
PFOS	2.00E+01	0.0%	60.6%	60.2%	0.0%	0.4%	39.3%	0.0%
PFNA	2.15E-03	0.0%	73.0%	72.2%	0.0%	0.7%	27.0%	0.0%
PFNA	2.15E-02	0.0%	73.0%	72.2%	0.0%	0.7%	27.0%	0.0%
PFNA	2.15E-01	0.0%	73.0%	72.2%	0.0%	0.7%	27.0%	0.0%
PFNA	2.15E+00	0.0%	73.0%	72.2%	0.0%	0.7%	27.0%	0.0%
PFNA	2.15E+01	0.0%	73.0%	72.2%	0.0%	0.7%	27.0%	0.0%
PFHxS	2.50E-03	0.0%	89.1%	87.5%	0.0%	1.7%	10.8%	0.0%
PFHxS	2.50E-02	0.0%	89.1%	87.5%	0.0%	1.7%	10.8%	0.0%
PFHxS	2.50E-01	0.0%	89.1%	87.5%	0.0%	1.7%	10.8%	0.0%
PFHxS	2.50E+00	0.0%	89.1%	87.5%	0.0%	1.7%	10.8%	0.0%
PFHxS	2.50E+01	0.0%	89.1%	87.5%	0.0%	1.7%	10.8%	0.0%
Chlorpyrifos	1.00E+00	0.1%	55.1%	48.3%	5.4%	1.4%	41.9%	2.9%

Table legend: ECx is the chemical concentration
MF is the mass fraction of the chemicals
MF_{AIR} is the mass fraction of the chemicals in air (volatile fraction of the chemicals)
$MF_{WATBULK}$ is the mass fraction of the chemicals in water (bulk mass fraction sum of the single MF_{ALB} $MF_{S\text{-}LIP}$ MF_{WAT})
MF_{ALB} is the mass fraction of the chemicals linked to the albumin
$MF_{S\text{-}LIP}$ is the mass fraction of the chemicals linked to the lipids
MF_{WAT} is the mass fraction of the chemicals in water (free fraction not linked)
MF_{CELLS} is the mass fraction of the chemicals into the cells
$MF_{PLASTIC}$ is the mass fraction of the chemicals linked to the plastic

Table 23: Result of the concentrations of PFAS in the *in vitro* TD antibody response protocols (24 well plate)

Name	$C_{NOM,initial}$ (µmol/L medium)	$C_{BULK\ WAT}$ (µmol/L medium)	C_{WAT} (µmol/L water)	C_{AIR} (µmol/L air)	C_{ALB} (µmol/L alb)	$C_{S\text{-}LIP}$ (µmol/L lipid)	C_{cells} (µmol/L cell)	$A_{Plastic}$, µmoles/m2
PFOA	2.4E-03	2.0E-03	3.5E-05	2.2E-13	1.3E+00	1.8E-03	2.4E-02	1.98E-07
PFOA	2.4E-02	2.0E-02	3.5E-04	2.2E-12	1.3E+01	1.8E-02	2.4E-01	1.98E-06
PFOA	2.4E-01	2.0E-01	3.5E-03	2.2E-11	1.3E+02	1.8E-01	2.4E+00	1.98E-05
PFOA	2.4E+00	2.0E+00	3.5E-02	2.2E-10	1.3E+03	1.8E+00	2.4E+01	1.98E-04
PFOA	2.4E+01	2.0E+01	3.5E-01	2.2E-09	1.3E+04	1.8E+01	2.4E+02	1.98E-03
PFOS	2.0E-03	1.2E-03	8.7E-06	2.5E-15	7.7E-01	4.6E-03	6.3E-02	1.80E-07
PFOS	2.0E-02	1.2E-02	8.7E-05	2.5E-14	7.7E+00	4.6E-02	6.3E-01	1.80E-06
PFOS	2.0E-01	1.2E-01	8.7E-04	2.5E-13	7.7E+01	4.6E-01	6.3E+00	1.80E-05
PFOS	2.0E+00	1.2E+00	8.7E-03	2.5E-12	7.7E+02	4.6E+00	6.3E+01	1.80E-04
PFOS	2.0E+01	1.2E+01	8.7E-02	2.5E-11	7.7E+03	4.6E+01	6.3E+02	1.80E-03
PFNA	2.2E-03	1.6E-03	1.6E-05	1.5E-15	1.0E+00	3.4E-03	4.7E-02	1.97E-07
PFNA	2.2E-02	1.6E-02	1.6E-04	1.5E-14	1.0E+01	3.4E-02	4.7E-01	1.97E-06
PFNA	2.2E-01	1.6E-01	1.6E-03	1.5E-13	1.0E+02	3.4E-01	4.7E+00	1.97E-05
PFNA	2.2E+00	1.6E+00	1.6E-02	1.5E-12	1.0E+03	3.4E+00	4.7E+01	1.97E-04
PFNA	2.2E+01	1.6E+01	1.6E-01	1.5E-11	1.0E+04	3.4E+01	4.7E+02	1.97E-03
PFHxS	2.5E-03	2.2E-03	4.2E-05	1.0E-15	1.4E+00	1.6E-03	2.2E-02	1.99E-07
PFHxS	2.5E-02	2.2E-02	4.2E-04	1.0E-14	1.4E+01	1.6E-02	2.2E-01	1.99E-06
PFHxS	2.5E-01	2.2E-01	4.2E-03	1.0E-13	1.4E+02	1.6E-01	2.2E+00	1.99E-05
PFHxS	2.5E+00	2.2E+00	4.2E-02	1.0E-12	1.4E+03	1.6E+00	2.2E+01	1.99E-04
PFHxS	2.5E+01	2.2E+01	4.2E-01	1.0E-11	1.4E+04	1.6E+01	2.2E+02	1.99E-03
Chlorpyrifos	1.0E+00	5.5E-01	1.4E-02	4.8E-12	3.1E+02	5.7E+02	3.3E+01	1.13E-01

Table legend: C_{nom} is the chemical concentration

$C_{WATBULK}$ is the concentration of the chemicals in water (bulk concentration sum of the single MF_{ALB} $MF_{S\text{-}LIP}$ MF_{WAT})

C_{ALB} is the concentration of the chemicals linked to the albumin

$C_{S\text{-}LIP}$ is the concentration of the chemicals linked to the lipids

C_{WAT} is the concentration of the chemicals in water (free fraction not linked)

C_{AIR} is the concentration of the chemicals in air (volatile fraction of the chemicals)

C_{CELLS} is the concentration of the chemicals into the cells

$A_{PLASTIC}$ is the concentration of the chemicals linked to the plastic

As it is possible to see in all the protocols, only PFOA has a volatile fraction (MF_{AIR}) depended on the volume and area of the well but also on the density of the cells. In all the protocols and for all the four PFAS, the higher fraction of the chemicals linked the albumin (MF_{ALB}) in the medium and no one was able to link the lipid part ($MF_{S\text{-}LIP}$). Furthermore, none of the PFAS tested was able to stick to the plastic ($MF_{PLASTIC}$). Depending on the density of the cells and the area of the well, PFOS is among the four PFAS the chemical most absorbed by the cells, followed in descending order by PFNA, PFOA and PFHxS.

4.3.4 QIVIVE results: Wetmore Approach

As reported in Figure 20, the workflow of the Wetmore QIVIVE approach involves the use of (nominal) concentrations associated with the responses obtained in the *in vitro* protocols. Here, the nominal concentrations were used as applied in the *in vitro* experiments. Concentrations (expressed in µM) and responses (expressed in ng/mL) were analysed with the application Bayesian BMD to obtain a Benchmark concentration (BMC) with the required

Benchmark response (BMR) set at 25%. This concentration was then transformed into µg/L and converted into 7 days (168h) Area Under the Curve (AUC168h) values, considering the 7-day exposure period in the *in vitro* system. Thereafter, PBK modelling was applied to estimate the oral equivalent effect dose which in 5 years would lead to the same AUC value in the target system, in this case the immune system. The PBK models applied here were described in Section 4.2.1.

All the Bayesian BMD report is collected in the Annex R. Here, only the BMC, BMCU and BMCL values obtained are reported. The analysis was performed taking into consideration male and female donors separately as explained above.

Table 24: Data used for the BMD analysis and *in vitro* BMC derivation for male donors

Chemicals	Concentration (µM)	Response (ng/mL)	SD	N	BMC_{25} (µM)	$BMCL_{25}$ (µM)	$BMCU_{25}$ (µM)
PFOA	0.00E+00	310.784	116.377	5	12.884	0.937	23.260
	2.41E-03	276.820	102.049	5			
	2.41E-01	245.402	83.232	5			
	2.41E+01	238.559	100.486	5			
PFNA	0.00E+00	426.505	194.947	5	12.444	1.494	20.759
	2.15E-03	403.720	206.655	5			
	2.15E-01	378.900	175.591	5			
	2.15E+01	290.367	171.730	5			
PFHxS	0.00E+00	432.026	172.470	5	13.734	1.309	24.141
	2.50E-03	422.359	162.337	5			
	2.50E-01	388.910	156.784	5			
	2.50E+01	379.391	144.401	5			
PFOS	0.00E+00	310.784	116.377	5	10.376	0.859	19.08
	2.00E-03	232.544	108.065	5			
	2.00E-01	224.745	97.992	5			
	2.00E+01	173.289	93.523	5			

The estimated BMC at which the specified response (25% change compared to control) occurs is 12.884 µM for PFOA, 12.444 µM for PFNA, 13.734 µM for PFHxS and 10.376 µM for PFOS. The predicted values for the BMCL and the BMCU illustrate a wide confidence interval in which the true BMC is likely to lie with a certain level of confidence (setting to 90%). For PFOA the Shapiro-Wilk normality test reported that there was evidence against normality across dose levels at level 0.05 (p-value 0.0087), however there was no evidence against log-normality across dose levels at level 0.05 (p-value 0.0678). The best fitting model fitted sufficiently well with a Bayes factor of 1.91E+00. For PFNA and PFHxS the Shapiro-Wilk normality test reported that there was evidence against normality across dose levels at level 0.05 (p-value 0.0477 for PFNA and 0.0093 for PFHxS) and there was also evidence against log-normality across dose levels at level 0.05 (p-value 0.0156 for PFNA and 0.0025 for PFHxS). The best fitting model fitted sufficiently well with a Bayes factor of 8.67E-01 for PFNA and 1.71E+00 for PFHxS. In the end, the Shapiro-Wilk normality test for PFOS reported that there was no

evidence against normality across dose levels at level 0.05 (p-value 0.1035) and there was no evidence against log-normality across dose levels at level 0.05 (p-value 0.0928). The best fitting model fitted sufficiently well (Bayes factor was 2.40E+00). Starting from the different BMC_{25} obtained the AUC of 7 days was calculated as shown below:

- PFOA: 12.884 µM x 414.07 g/mol = 5334.88 µg/L x 168h = 896259.48 µg/L (AUC168h).
- PFNA: 12.444 µM x 464.08 g/mol = 5775.01 µg/L x 168h = 970201.94 µg/L (AUC168h).
- PFHxS: 13.734 µM x 438.2 g/mol = 6018.24 µg/L x 168h = 1011064.12 µg/L (AUC168h).
- PFOS: 10.376 µM x 500.13 g/mol = 5189.35 µg/L x 168h = 871810.8 µg/L (AUC168h).

Thereafter, using the PFAS PBK models with reverse dosimetry, the oral equivalent effect doses that correspond to the same AUC in 5 years were predicted. The oral equivalent effect doses obtained were:

- PFOA: 0.0094 ng/kg day (AUC5y = 905632.49 µg/L).
- PFNA: 0.0085 ng/kg day (AUC5y = 970201.94 µg/L).
- PFHxS: 0.011 ng/kg day (AUC5y = 1046916.09 µg/L).
- PFOS: 0.0139 ng/kg/day (AUC5y = 871715.19 µg/L).

In other words, these results suggest that exposure to PFAS above this concentration may interfere with the TI antibody (IgG and IgM) release in humans.

The same analysis was also performed using the results from the female donors (data used for the analysis are present in Table 25).

Table 25: Data used for the BMD analysis and *in vitro* BMC derivation for female donors

Chemicals	Concentration (µM)	Response (ng/mL)	SD	N	BMC_{25} (µM)	$BMCL_{25}$ (µM)	$BMCU_{25}$ (µM)
PFOA	0.00E+00	303.012	157.148	5	12.802	1.038	23.143
	2.41E-03	184.359	118.230	5			
	2.41E-01	221.065	154.746	5			
	2.41E+01	184.876	94.183	5			
PFNA	0.00E+00	518.561	199.768	5	10.318	0.272	20.422
	2.15E-03	404.791	204.506	5			
	2.15E-01	283.558	172.880	5			
	2.15E+01	254.456	168.075	5			
PFHxS	0.00E+00	528.118	178.813	5	12.708	0.977	23.653
	2.50E-03	363.162	209.855	5			
	2.50E-01	335.361	202.378	5			
	2.50E+01	268.967	166.094	5			
PFOS	0.00E+00	253.659	180.298	5	9.864	0.516	18.944
	2.00E-03	151.996	114.097	5			
	2.00E-01	120.059	100.898	5			
	2.00E+01	134.459	129.417	5			

The estimated BMC25 at which the specified response occurs is 12.802 µM for PFOA, 10.318 µM for PFNA, 12.708 µM for PFHxS and 9.864 µM for PFOS. The predicted values for the BMCL and the BMCU illustrate a wide confidence interval in which the true BMC is likely to lie with a certain level of confidence (setting to 95%). For PFOA the Shapiro-Wilk normality test reported that there was no evidence against normality across dose levels at level 0.05 (p-value 0.0585), and also no evidence against log-normality across dose levels at level 0.05 (p-value 0.1771). The best fitting model fitted sufficiently well with a Bayes factor of 3.12E+00. For PFNA and PFHxS the Shapiro-Wilk normality test reported that there was no evidence against normality across dose levels at level 0.05 (p-value 0.2500 for PFNA and 0.1256 for PFHxS) and there was evidence against log-normality across dose levels at level 0.05 (p-value 0.0319 for PFNA and 0.0378 for PFHxS). The best fitting model fitted sufficiently well with a Bayes factor of 5.88E+00 for PFNA and 4.12E+00 for PFHxS. In the end, the Shapiro-Wilk normality test for PFOS reported that there was evidence against normality across dose levels at level 0.05 (p-value 0.0206) and there was no evidence against log-normality across dose levels at level 0.05 (p-value 0.8313). The best fitting model fitted sufficiently well (Bayes factor was 3.09E+00). Starting from the different BMC25 obtained the AUC of 7 days was calculated as shown below:

- PFOA: 12.802 µM x 414.07 g/mol = 5300.92 µg/L x 168h = 890555.26 µg/L (AUC168h).
- PFNA: 10.318 µM x 464.08 g/mol = 4788.38 µg/L x 168h = 804447.41 µg/L (AUC168h).
- PFHxS: 12.708 µM x 438.2 g/mol = 5568.65 µg/L x 168h = 935533.2 µg/L (AUC168h).
- PFOS: 9.864 µM x 500.13 g/mol = 4933.28 µg/L x 168h = 828791.04 µg/L (AUC168h).

Then, using the PFAS PBK models with reverse dosimetry, the oral equivalent effect doses that correspond to the same AUC in 5 years were predicted. The oral equivalent effect doses obtained are:

- PFOA: 0.00925 ng/kg day (AUC5y =891181.02 µg/L).
- PFNA: 0.007 ng/kg day (AUC5y = 804447.41 µg/L).
- PFHxS: 0.0099 ng/kg day (AUC5y = 942214.43 µg/L).
- PFOS: 0.0133 ng/kg/day (AUC5y = 831716.79 µg/L).

4.3.5 QIVIVE results: Louisse approach

The Louisse et al. (2010) approach dictates the QIVIVE translation of the whole concentration-response curve into the equivalent dose-response and subsequently, the determination of the PoD. As such the PBK models were used here for each individual PFAS to translate the (nominal) *in vitro* concentrations used for the *in vitro* protocols to external oral equivalent doses.

Here, an additional stepwise element was added to the QIVIVE with the application of three different tiered scenarios pertaining to the *in vitro* starting points for the extrapolations.

The following three different extrapolation QIVIVE scenarios were applied:

1. QIVIVE scenario 1: *in vitro* Cnominal = *in vivo* PBK CAtotal plasma concentration.

   The nominal PFAS concentration in the medium added to the human PBMC equals the PFAS total concentration in blood (plasma concentration). The QIVIVE scenario 1 used nominal concentrations.

2. QIVIVE scenario 2: *in vitro* Cfree (corrected for albumin binding) = *in vivo* PBK plasma CAfree.

   The unbound PFAS concentration in the medium added to the human PBMC equals to the unbound PFAS concentration in blood (plasma concentration). The QIVIVE scenario 2 considered differences in protein content between the *in vitro* system and the blood (*in vivo*) and assumed that PFAS bind only to protein (albumin). A simple formula was applied to calculate the *in vitro* free concentration C_{free} as $C_{nominal} * F_{up\ in\ vitro}$. $F_{up\ in\ vitro}$ is the fraction of chemical unbound in the *in vitro* assay which was estimated based on the following equation (taken from Kalvass & Maurer, 2002):

$$Fup\ in\ vitro = \frac{1}{\frac{Calbum,\ in\ vitro}{Calbum,\ plasma} \cdot \frac{1 - Fup}{Fup} + 1}$$

   Where:
   F_{up} = unbound fraction of chemical in human plasma taken from the value present in the PBK model from EFSA (2020) (0.025 of PFOS and PFHxS, while 0.02 of PFOA and PFNA),
   $C_{album,in\ vitro}$ = the concentration of albumin used in the *in vitro* assay medium (for d-FBS is 24 g/L, while for human serum was 42.5 g/L that corrected for 5% became respectively 1.2 and 2.13 g/L),
   $C_{album,plasma}$= the concentration of albumin in human plasma 42.5 g/L (Naveen et al., 2016)
   Below in table 26, the $F_{up\ in\ vitro}$ values are reported as used in all the different conditions of serum in the different assays with PFAS. This value was then multiplied with the nominal concentration to obtain the free concentration in the QIVIVE scenario 2.

Table 26: $F_{up\ in\ vitro}$ value for the correction of protein binding in the QIVIVE scenario 2

		PFOA	PFOS	PFNA	PFHxS
d-FBS	**THP-1 differentiated to mDCs**	0.42	0.48	0.42	0.48
Human serum	**TD antibody response**	0.29	0.34	0.29	0.34
	TI antibody response	0.29	0.34	0.29	0.34
	T cells	0.29	0.34	0.29	0.34

3. QIVIVE scenario 3: *in vitro* Cfree water (Armitage model) = *in vivo* PBK plasma CAfree

The nominal PFAS concentration in the medium added to the human PBMC is translated into an *in vitro* PFAS Free water concentration using the Armitage model (see table 16 above). This *in vitro* PFAS Free water concentration value equals the *in vivo* free PFAS concentration in blood.

For all the three scenarios, the *in vitro* concentrations were converted to a dose metric suitable to the time test and life stage for the PBK modelling. Here again the AUC was selected, and as such the *in vitro* AUC (168h) was calculated for the three different scenarios. Thereafter, reverse dosimetry PBK modelling was applied to estimate the oral equivalent effect dose which in 5 years would lead to the same AUC value in the surrogate of the target system, i.e. the blood. The AUC value for the concentration of 20 µM in scenarios 1 and 2 could only be obtained using the original set up of the EFSA PBK model 2020, however lower concentrations are not possible to achieve even at exposure levels of 10^{20} ng/kg day. After several attempts, it was discerned that the issue stemmed from the intake of breast milk in the first year, which had been established through two parameters (below PFOS was used as an example):

- PFOS maternal that represented the maternal serum concentration at delivery, and it was set up to 4.89 µg/L;
- Milk consumption of PFOS set up on 0.8 L/day.

The final value of the AUC is strongly influenced by these values. Consequently, it was considered to bring them to zero (PFOS maternal = 0 µg/L; milk consumption = 0 L/day). However, adopting this approach would have nullified the exposure for the entire first year of the child's life, deviating from mimicking *in vivo* conditions and diverging from the experimental consistency observed in previous PBK models. Consequently, a decision was made to reduce both parameters, ultimately employing the setup with PFOS (as well as PFOA, PFNA, and PFHxS) maternal concentration set at 0.0001 µg/L and a milk consumption of all four PFAS set at 0.0001 L/day. This adjustment enabled the acquisition of all the necessary AUCs.

For the computation of the AUC in scenario 1, the sum of the total concentration of the chemicals in plasma in µg/L (ng/mL), referred to as EFSA PBK model 2020 CA, was utilized. This choice was made under the assumption that the nominal concentration was comparable to the total amount of chemicals. Conversely, in scenarios 2 and 3, the sum of the free concentration of chemicals in plasma in µg/L (ng/mL), denoted in the EFSA PBK model 2020 as CAfree, was employed. In these instances, CAfree was chosen because adjustments were made to the concentration considering protein binding in scenario 2 and considering complete kinetics and binding in scenario 3.

Below Table 27 reports all the AUC and oral equivalent dose for all the four PFAS obtained for the protocol of TI antibody response.

Table 27: AUC and oral equivalent dose for all the four PFAS obtained for the protocol of TI antibody response in the three different scenarios.

	Scenario 1					Scenario 2					Scenario 3				
PFOS	in vitro nominal conc (µM) = CA	µg/L	AUC µg/L*7days	AUC PBK model	Oral equivalent dose (µg/kg/day)	predicted blood conc (µM) Cfree	µg/L	AUC µg/L*7days	AUC PBK model	Oral equivalent dose (µg/kg/day)	predicted Cwat = Cfree (armitage) µM	µg/L	AUC µg/L *7days	AUC PBK model	Oral equivalent dose (µg/kg/day)
	0,00E+00	0	0,00	0,00	0,00E+00	0	0	0,00	0,00	0,00E+00	0	0	0,00	0,00	0,00E+00
	2,00E-03	1	168,04	169,17	2,70E-06	0,00068	0	57,13	57,40	3,67E-05	0,000011	0	0,91	0,92	5,84E-07
	2,00E-01	100	16804,37	16888,69	2,70E-04	0,068	34	5713,49	5738,90	3,67E-03	0,001087	1	91,34	91,33	5,84E-05
	2,00E+01	10.003	1680436,80	1687814,4	2,70E-02	6,8	3.401	571348,51	572251,73	3,67E-01	0,108709	54	9133,90	9133,74	5,84E-03
PFOA	in vitro nominal conc (µM) = CA	µg/L	AUC µg/L*7days	AUC PBK model	Oral equivalent dose (µg/kg/day)	predicted blood conc (µM) Cfree	µg/L	AUC µg/L*7days	AUC PBK model	Oral equivalent dose (µg/kg/day)	predicted intracellular (armitage) µM	µg/L	AUC µg/L *7days	AUC PBK model	Oral equivalent dose (µg/kg/day)
	0,00E+00	0	0,00	0,00	0,00E+00	0	0	0,00	0,00	0,00E+00	0,000	0	0,00	0,00	0,00E+00
	2,41E-03	1	167,99	168,19	1,74E-06	0,00070	0	48,72	48,75	2,53E-05	0,000038	0	2,63	2,63	1,36E-06
	2,41E-01	100	16798,78	16760,40	1,74E-04	0,07003	29	4871,65	4873,83	2,53E-03	0,003777	2	262,72	262,00	1,36E-04
	2,41E+01	9.999	1679878,29	1676035,5	1,74E-02	7,00314	2.900	487164,70	487289,90	2,53E-01	0,377674	156	26272,44	26199,73	1,36E-02
PFNA	in vitro nominal conc (µM) = CA	µg/L	AUC µg/L*7days	AUC PBK model	Oral equivalent dose (µg/kg/day)	predicted blood conc (µM) Cfree	µg/L	AUC µg/L*7days	AUC PBK model	Oral equivalent dose (µg/kg/day)	predicted intracellular (armitage) µM	µg/L	AUC µg/L *7days	AUC PBK model	Oral equivalent dose (µg/kg/day)
	0,00E+00	0	0,00	0,00	0,00E+00	0	0	0,00	0,00	0,00E+00	0,000000	0	0,00	0,00	0,00E+00
	2,15E-03	1	167,99	168,23	1,42E-06	0,00062	0	48,72	48,85	2,07E-05	0,000018	0	1,42	1,42	5,97E-07
	2,15E-01	100	16799,28	16749,80	1,42E-04	0,06249	29	4871,79	4883,19	2,07E-03	0,001816	1	141,60	140,85	5,97E-05
	2,15E+01	10.000	1679927,60	1674944,6	1,42E-02	6,24865	2.900	487179,00	488248,16	2,07E-01	0,181622	84	14160,20	14083,33	5,97E-03
PFHxS	in vitro nominal conc (µM) = CA	µg/L	AUC µg/L*7days	AUC PBK model	Oral equivalent dose (µg/kg/day)	predicted blood conc (µM) Cfree	µg/L	AUC µg/L*7days	AUC PBK model	Oral equivalent dose (µg/kg/day)	predicted intracellular (armitage) µM	µg/L	AUC µg/L *7days	AUC PBK model	Oral equivalent dose (µg/kg/day)
	0,00E+00	0	0,00	0,00	0,00E+00	0	0	0,00	0,00	0,00E+00	0,000000	0	0,00	0,00	0,00E+00
	2,50E-03	1	184,00	184,23	1,93E-06	0,00085	0	62,56	62,57	2,63E-05	0,000045	0	3,29	3,30	1,38E-06
	2,50E-01	110	18399,80	18364,00	1,93E-04	0,08498	37	6255,93	6255,94	2,63E-03	0,004468	2	328,96	328,27	1,38E-04
	2,50E+01	10.952	1839980,00	183634,59	1,93E-02	8,49788	3.724	625593,20	625537,13	2,63E-01	0,446843	196	32895,54	32826,72	1,38E-02

As previously indicated, the decision was made to present the analyses separately for male and female donors in all three scenarios. Consequently, a total of six distinct analyses were conducted for each PFAS.

The QIVIVE scenario 1 assumes that the nominal PFAS concentration in the medium added to the human PBMC equals to the PFAS concentration in blood (plasma concentration). All the Bayesian BMD report are reported below in the Annex. Here we report only the BMD, BMDU and BMDL obtain and eventually statistical results.

The male results (based on the data reported in Table 24) reported a BMD25 of 0.01 ng/kg/day for PFOA, 0.009 ng/kg/day for PFNA, 0.011 ng/kg/day for PFHxS and 0.014 ng/kg/day for PFOS. The fine range between BMDL and BMDU suggests a relatively precise estimate that is essential for making accurate assessments of risk. For PFOA the Shapiro-Wilk normality test reported that there was evidence against normality across dose levels at level 0.05 (p-value 0.0087) but no evidence against log-normality across dose levels at level 0.05 (p-value 0.0678). Best-fitting model fitted sufficiently well (Bayes factor was 1.88E+00). For PFNA and PFHxS there was evidence both against normality and log-normality across dose levels at level 0.05 (p-value 0.0477 for normality and 0.0156 for log-normality for PFNA and p-value 0.0093 for normality and 0.0025 for log-normality for PFNA). Best fitting model fitted sufficiently well (Bayes factor was 9.05E-01 for PFNA and 1.80E+00 for PFHxS). In the end, the Shapiro-Wilk normality test reported that there was no evidence against both normality and log-normality across dose levels at level 0.05 for PFOS (p-value 0.1035 for normality and 0.0928 for log-normality). The best fitting models performed sufficiently well with a Bayes factor of 2.40E+00.

Table 28: Data used for the BMD analysis of QIVIVE scenario 1 for male donors

Chemicals	Oral equivalent dose (µg/kg/day)	Response (ng/mL)	SD	N	BMD_{25}	$BMDL_{25}$	$BMDU_{25}$
PFOA	0.00E+00	310.784	116.377	5	0.01	0.001	0.017
	1.74E-06	276.820	102.049	5			
	1.74E-04	245.402	83.232	5			
	1.74E-02	238.559	100.486	5			
PFNA	0.00E+00	426.505	194.947	5	0.009	0.001	0.014
	1.42E-06	403.720	206.655	5			
	1.42E-04	378.900	175.591	5			
	1.42E-02	290.367	171.730	5			
PFHxS	0.00E+00	432.026	172.470	5	0.011	0.001	0.019
	1.93E-06	422.359	162.337	5			
	1.93E-04	388.910	156.784	5			
	1.93E-02	379.391	144.401	5			
PFOS	0.00E+00	310.784	116.377	5	0.014	0.001	0.026
	2.70E-06	232.544	108.065	5			
	2.70E-04	224.745	97.992	5			
	2.70E-02	173.289	93.523	5			

The female results (based on the data reported in Table 25) reported a BMD_{25} of 0.009 ng/kg/day for PFOA, 0.007 ng/kg/day for PFNA, 0.010 ng/kg/day for PFHxS and 0.013 ng/kg/day for PFOS. These results suggest that continuous exposure to PFAS above this level may interfere with the TI antibody (IgG and IgM) release in humans. The fine range between BMDL and BMDU suggests a relatively precise estimate that is essential for making accurate assessments of risk. For PFOA reported that there was no evidence against both normality and log-normality across dose levels at level 0.05 for PFOA (p-value 0.0585 for normality and 0.1771 for log-normality). The best fitting models fit sufficiently well with a Bayes factor of 3.38E+00. For PFNA and PFHxS the Shapiro-Wilk normality test reported that there was no evidence against normality across dose levels at level 0.05 (p-value 0.2500 for PFNA and 0.1256 for PFHxS) but there was evidence against log-normality across dose levels at level 0.05 (p-value 0.0319 for PFNA and 0.378 for PFHxS). Best fitting model fitted sufficiently well (Bayes factor was 7.12E+00 for PFNA and 4.16E+00 for PFHxS). In the end, the Shapiro-Wilk normality test reported that there was evidence against normality for PFOS with a p-value of 0.0206 and there was no evidence against log-normality across dose levels at level 0.05 (p-value 0.8313). The best fitting models performed sufficiently well with a Bayes factor of 3.09E+00.

Table 29: Data used for the analysis of BMD_{25} analyses of QIVIVE scenario 1 for female donors

Chemicals	Oral equivalent dose (µg/kg/day)	Response (ng/mL)	SD	N	BMD_{25}	$BMDL_{25}$	$BMDU_{25}$
PFOA	0.00E+00	303.012	157.148	5	0.009	0.001	0.017
	1.74E-06	184.359	118.230	5			
	1.74E-04	221.065	154.746	5			
	1.74E-02	184.876	94.183	5			
PFNA	0.00E+00	518.561	199.768	5	0.007	0.000	0.013
	1.42E-06	404.791	204.506	5			
	1.42E-04	283.558	172.880	5			
	1.42E-02	254.456	168.075	5			
PFHxS	0.00E+00	528.118	178.813	5	0.010	0.001	0.018
	1.93E-06	363.162	209.855	5			
	1.93E-04	335.361	202.378	5			
	1.93E-02	268.967	166.094	5			
PFOS	0.00E+00	253.659	180.298	5	0.013	0.001	0.026
	2.70E-06	151.996	114.097	5			
	2.70E-04	120.059	100.898	5			
	2.70E-02	134.459	129.417	5			

The QIVIVE scenario 2 take in consideration that the nominal PFAS concentration in the medium added to the human PBMC equals to the PFAS concentration in blood (plasma concentration) corrected for the respective protein (albumin) binding in the two systems.

The male results (based on the data reported in Table 30) reported a BMD_{25} of 0.144 ng/kg/day for PFOA, 0.134 ng/kg/day for PFNA, 0.152 ng/kg/day for PFHxS and 0.186 ng/kg/day for PFOS. These results suggest that continuous exposure to PFAS above these levels may interfere with the TI antibody (IgG and IgM) release in humans. The fine range between BMDL and BMDU suggests a relatively precise estimate that is essential for making accurate assessments of risk. For PFOA the Shapiro-Wilk normality test reported that there was evidence against normality across dose levels at level 0.05 (p-value 0.0087) but no evidence against log-normality across dose levels at level 0.05 (p-value 0.0678). Best fitting model fitted sufficiently well (Bayes factor was 1.94E+00). For PFNA and PFHxS there was evidence both against normality and log-normality across dose levels at level 0.05 (p-value 0.0477 for normality and 0.0156 for log-normality for PFNA and p-value 0.0093 for normality and 0.0025 for log-normality for PFNA). Best fitting model fitted sufficiently well (Bayes factor was 9.05E-01 for PFNA and 1.72E+00 for PFHxS). In the end, the Shapiro-Wilk normality test reported that there was no evidence against both normality and log-normality across dose levels at level 0.05 for PFOS (p-value 0.1035 for normality and 0.0928 for log-normality). The best fitting models performed sufficiently well with a Bayes factor of 2.43E+00.

Table 30: Data used for the BMD analysis of QIVIVE scenario 2 for male donors

Chemicals	Oral equivalent dose (µg/kg/day)	Response (ng/mL)	SD	N	BMD_{25}	$BMDL_{25}$	$BMDU_{25}$
PFOA	0.00E+00	310.784	116.377	5	0.144	0.013	0.244
	2.53E-05	276.820	102.049	5			
	2.53E-03	245.402	83.232	5			
	2.53E-01	238.559	100.486	5			
PFNA	0.00E+00	426.505	194.947	5	0.134	0.02	0.201
	2.07E-05	403.720	206.655	5			
	2.07E-03	378.900	175.591	5			
	2.07E-01	290.367	171.730	5			
PFHxS	0.00E+00	432.026	172.470	5	0.152	0.015	0.253
	2.63E-05	422.359	162.337	5			
	2.63E-03	388.910	156.784	5			
	2.63E-01	379.391	144.401	5			
PFOS	0.00E+00	310.784	116.377	5	0.186	0.015	0.349
	3.67E-05	232.544	108.065	5			
	3.67E-03	224.745	97.992	5			
	3.67E-01	173.289	93.523	5			

The female results (based on the data reported in Table 31) reported a BMD_{25} of 0.135 ng/kg/day for PFOA, 0.096 ng/kg/day for PFNA, 0.136 ng/kg/day for PFHxS and 0.182 ng/kg/day for PFOS. These results suggest that continuous exposure to PFAS above these levels may interfere with the T cell independent antibody (IgG and IgM) release in humans. The fine range between BMDL and BMDU suggests a relatively precise estimate that is essential for making accurate assessments of risk. For PFOA reported that there was no evidence against both normality and log-normality across dose levels at level 0.05 for PFOA (p-value 0.0585 for normality and 0.1771 for log-normality). The best fitting models fit sufficiently well with a Bayes factor of 3.41E+00. For PFNA and PFHxS the Shapiro-Wilk normality test reported that there was no evidence against normality across dose levels at level 0.05 (p-value 0.2500 for PFNA and 0.1256 for PFHxS) but there was evidence against log-normality across dose levels at level 0.05 (p-value 0.0319 for PFNA and 0.378 for PFHxS). Best fitting model fitted sufficiently well (Bayes factor was 7.12E+00 for PFNA and 4.08E+00 for PFHxS). In the end, the Shapiro-Wilk normality test reported that there was evidence against normality for PFOS with a p-value of 0.0206 and there was no evidence against log-normality across dose levels at level 0.05 (p-value 0.8313). The best fitting models performed sufficiently well with a Bayes factor of 3.18E+00.

Table 31: Data used for the BMD analysis of QIVIVE scenario 2 for female donors

Chemicals	Oral equivalent dose (µg/kg/day)	Response (ng/mL)	SD	N	BMD_{25}	$BMDL_{25}$	$BMDU_{25}$
PFOA	0.00E+00	303.012	157.148	5	0.135	0.013	0.242
	2.53E-05	184.359	118.230	5			
	2.53E-03	221.065	154.746	5			
	2.53E-01	184.876	94.183	5			
PFNA	0.00E+00	518.561	199.768	5	0.096	0.002	0.195
	2.07E-05	404.791	204.506	5			
	2.07E-03	283.558	172.880	5			
	2.07E-01	254.456	168.075	5			
PFHxS	0.00E+00	528.118	178.813	5	0.136	0.010	0.251
	2.63E-05	363.162	209.855	5			
	2.63E-03	335.361	202.378	5			
	2.63E-01	268.967	166.094	5			
PFOS	0.00E+00	253.659	180.298	5	0.182	0.011	0.347
	3.67E-05	151.996	114.097	5			
	3.67E-03	120.059	100.898	5			
	3.67E-01	134.459	129.417	5			

We obtained two different BMD_{25} for male and female donors that are in the same range but not so similar compared to the values obtained from the QIVIVE scenario 1. The results are 0.179 ng/kg/day for female and 0.186 ng/kg/day for male. These results suggest that continuous exposure to PFAS above these levels may interfere with the TI antibody (IgG and IgM) release in humans.

The QIVIVE scenario 3 assumes that the *in vitro* PFAS Free water concentration (i*n vitro* Cfree water), as obtained using the Armitage model, equals the *in vivo* free PFAS concentration in blood (*in vivo* PBK CAfree).

The male results (based on the data reported in Table 32) reported a BMD_{25} of 0.008 ng/kg/day for PFOA, 0.004 ng/kg/day for PFNA, 0.008 ng/kg/day for PFHxS and 0.003 ng/kg/day for PFOS. These results suggest that continuous exposure to PFAS above these levels may interfere with the TI antibody (IgG and IgM) release in humans. The fine range between BMDL and BMDU suggests a relatively precise estimate that is essential for making accurate assessments of risk. For PFOA the Shapiro-Wilk normality test reported that there was evidence against normality across dose levels at level 0.05 (p-value 0.0087) but no evidence against log-normality across dose levels at level 0.05 (p-value 0.0678). Best fitting model fitted sufficiently well (Bayes factor was 1.94E+00). For PFNA and PFHxS there was evidence both against normality and log-normality across dose levels at level 0.05 (p-value 0.0477 for normality and 0.0156 for log-normality for PFNA and p-value 0.0093 for normality and 0.0025 for log-normality for PFNA). Best fitting model fitted sufficiently well (Bayes factor was 8.80E-01 for PFNA and 1.72E+00 for PFHxS). In the end, the Shapiro-Wilk normality test reported that there was no evidence against both normality and log-normality across dose

levels at level 0.05 for PFOS (p-value 0.1035 for normality and 0.0928 for log-normality). The best fitting models performed sufficiently well with a Bayes factor of 2.31E+00.

Table 32: Data used for the BMD analysis of QIVIVE scenario 3 for male donors

Chemicals	Oral equivalent dose (µg/kg/day)	Response (ng/mL)	SD	N	BMD_{25}	$BMDL_{25}$	$BMDU_{25}$
PFOA	0.00E+00	310.784	116.377	5	0.008	0.001	0.013
	1.36E-06	276.820	102.049	5			
	1.36E-04	245.402	83.232	5			
	1.36E-02	238.559	100.486	5			
PFNA	0.00E+00	426.505	194.947	5	0.004	0.001	0.006
	5.97E-07	403.720	206.655	5			
	5.97E-05	378.900	175.591	5			
	5.97E-03	290.367	171.730	5			
PFHxS	0.00E+00	432.026	172.470	5	0.008	0.001	0.013
	1.38E-06	422.359	162.337	5			
	1.38E-04	388.910	156.784	5			
	1.38E-02	379.391	144.401	5			
PFOS	0.00E+00	310.784	116.377	5	0.003	0.000	0.006
	5.84E-07	232.544	108.065	5			
	5.84E-05	224.745	97.992	5			
	5.84E-03	173.289	93.523	5			

The female results (based on the data reported in Table 33) reported a BMD_{25} of 0.007 ng/kg/day for PFOA, 0.003 ng/kg/day for PFNA, 0.007 ng/kg/day for PFHxS and 0.003 ng/kg/day for PFOS. These results suggest that continuous exposure to PFAS above these levels may interfere with the TI antibody (IgG and IgM) release in humans. The fine range between BMDL and BMDU suggests a relatively precise estimate that is essential for making accurate assessments of risk. For PFOA reported that there was no evidence against both normality and log-normality across dose levels at level 0.05 for PFOA (p-value 0.0585 for normality and 0.1771 for log-normality). The best fitting models fit sufficiently well with a Bayes factor of 3.41E+00. For PFNA and PFHxS the Shapiro-Wilk normality test reported that there was no evidence against normality across dose levels at level 0.05 (p-value 0.2500 for PFNA and 0.1256 for PFHxS) but there was evidence against log-normality across dose levels at level 0.05 (p-value 0.0319 for PFNA and 0.378 for PFHxS). Best fitting model fitted sufficiently well (Bayes factor was 6.48E+00 for PFNA and 4.08E+00 for PFHxS). In the end, the Shapiro-Wilk normality test reported that there was evidence against normality for PFOS with a p-value of 0.0206 and there was no evidence against log-normality across dose levels at level 0.05 (p-value 0.8313). The best fitting models performed sufficiently well with a Bayes factor of 3.24E+00.

Table 33: Data used for the BMD analysis of QIVIVE scenario 3 for female donors

Chemicals	Oral equivalent dose (µg/kg/day)	Response (ng/mL)	SD	N	BMD_{25}	$BMDL_{25}$	$BMDU_{25}$
PFOA	0.00E+00	303.012	157.148	5	0.007	0.001	0.013
	1.36E-06	184.359	118.230	5			
	1.36E-04	221.065	154.746	5			
	1.36E-02	184.876	94.183	5			
PFNA	0.00E+00	518.561	199.768	5	0.003	0.000	0.006
	5.97E-07	404.791	204.506	5			
	5.97E-05	283.558	172.880	5			
	5.97E-03	254.456	168.075	5			
PFHxS	0.00E+00	528.118	178.813	5	0.007	0.001	0.013
	1.38E-06	363.162	209.855	5			
	1.38E-04	335.361	202.378	5			
	1.38E-02	268.967	166.094	5			
PFOS	0.00E+00	253.659	180.298	5	0.003	0.000	0.006
	5.84E-07	151.996	114.097	5			
	5.84E-05	120.059	100.898	5			
	5.84E-03	134.459	129.417	5			

Table 34: Oral equivalent effect doses resulting from the two QIVIVE approaches and different scenarios

	Female	Male
Wetmore approach *	PFOA 0.009 ng/kg day PFNA 0.007 ng/kg day PFHxS 0.010 ng/kg day PFOS 0.013 ng/kg day Sum: 0.039 ng/kg day	PFOA 0.009 ng/kg day PFNA 0.009 ng/kg day PFHxS 0.011 ng/kg day PFOS 0.014 ng/kg day Sum: 0.043 ng/kg day
Louisse approach scenario 1 *	PFOA 0.009 ng/kg day PFNA 0.007 ng/kg day PFHxS 0.010 ng/kg day PFOS 0.013 ng/kg day Sum: 0.039 ng/kg day	PFOA 0.010 ng/kg day PFNA 0.009 ng/kg day PFHxS 0.011 ng/kg day PFOS 0.014 ng/kg day Sum: 0.039 ng/kg day
Louisse approach scenario 2 #	PFOA 0.135 ng/kg day PFNA 0.095 ng/kg day PFHxS 0.136 ng/kg day PFOS 0.179 ng/kg day Sum: 0.561 ng/kg day	PFOA 0.144 ng/kg day PFNA 0.134 ng/kg day PFHxS 0.152 ng/kg day PFOS 0.186 ng/kg day Sum: 0.616 ng/kg day
Louisse approach scenario 3 #	PFOA 0.007 ng/kg day PFNA 0.003 ng/kg day PFHxS 0.007 ng/kg day PFOS 0.003 ng/kg day Sum: 0.020 ng/kg day	PFOA 0.008 ng/kg day PFNA 0.004 ng/kg day PFHxS 0.008 ng/kg day PFOS 0.003 ng/kg day Sum: 0.023 ng/kg day

Note: * used CA to obtain the oral equivalent dose, # used CAfree to obtain the oral equivalent dose

4.3.6 Discussion, limitations, and assumptions of PBK modelling and QIVIVE

A number of critical aspects have been identified pertaining to the PBK model and its parameterisation that require further attention. The ongoing research by Husoy and her team aims to incorporate enterohepatic recirculation into the PBK model, leveraging insights from EFSA and Loccisano methodologies and focusing on data gleaned from Human Biomonitoring (HBM). The model currently lacks representation of the lymphatic system, utilizing blood levels as a surrogate for input into the UISS model. While the presence of CA is evident in the model, the absence of CAfree prompts the assumption that CA represents the applied concentration for simulation and downstream analysis. The parameterisation of PFOA and PFOS is well-documented, with comprehensive reports available across multiple outputs. In contrast, the parametrization of PFNA and PFHxS is less extensively reported, though some relevant data are accessible.

The 2018 EFSA CONTAM opinion findings underscore the significance of elimination constants, including transporter maximum and transporter affinity constant, free fraction, and intake as the most influential parameters. For future research, additional considerations should include understanding of temporal dynamics and time-dependent parameters, conducting a sensitivity analysis for key parameters, exploring interactions with co-occurring substances, validating against real-world data, transparently communicating model limitations, and incorporating emerging scientific knowledge for ongoing refinement. Such diligence is integral to enhancing the model's accuracy and applicability in predictive assessments.

With the QIVIVE approaches, the *in vitro* concentration-response data for antibody release changes upon PFAS exposure were converted into a corresponding *in vivo* oral equivalent dose-response relationship. Depending on the QIVIVE approach (Wetmore or Louisse), the extrapolation was performed either for a single point (the *in vitro* BMC) or for the whole dose response curve, which is the main difference between the two approaches. As a starting point for the corresponding PFAS plasma concentration, different scenarios were applied. In each case, toxicity was related to the AUC, considering the chronic low exposure of humans to PFAS and their accumulation in the human body. The summary of these results is reported in Table 34. The predicted oral equivalent effect doses resulted from the *in vitro* data for a 25% benchmark response on antibody release. The sum for the four PFAS from each approach/scenario was, thereafter, compared with the TDI (TWI divided by 7 days= 0.628 ng/kg/day) for the sum of four PFAS as derived by EFSA (EFSA CONTAM Panel, 2020).

In both QIVIVE approaches applied, the *in vitro*-PBK model-based oral equivalent effect doses for the sum of the four chemicals, and for both female and male donors, were (considerably) lower than the TDI derived from the epidemiological data, with the exception of scenario 2 in Louisse approach. This result suggests that the present NAM-based approach for performing PFAS hazard assessment is much more or equally conservative, given the selected effect size (25%). When comparing the two approaches (Wetmore and Louisse scenario 1), where the *in vitro* Cnominal was used as a starting point for the derivation of the PoD, the same outcomes were generated. For the case of PFAS chemicals, the two approaches appear equivalent. Nevertheless, this may not be as such for other type of compounds. The sum oral equivalent effect doses obtained here were more than 10-fold lower than the human-based TDI. Amongst the three different tier scenarios (1, 2 and 3) of the Louisse QIVIVE approach, scenario 3 appears to be the most conservative, with predicted values more than 25-fold lower compared to the human-based TDI, and followed by scenario 1 (15-fold lower). On the other hand, sum values predicted with scenario 2 seem to be in the same range as the TDI, rendering it the least conservative among the three.

One challenge associated in general with QIVIVE and inherent to both approaches applied, pertains to the proper definition of an *in vitro* metric to be the starting point for the extrapolations. Typically, *in vitro* nominal concentrations (here: Wetmore and Louisse scenario 1) are used as the proxy for blood or target tissue concentrations (Algharably et al., 2022; Fisher et al., 2019; Groothuis et al., 2015). This methodology ignores any partitioning or loss processes that may affect the effective concentration of a substance (Henneberger et al., 2021; Proença et al., 2021). Given that it is the free (unbound) fraction of a chemical that is expected to induce a toxic effect (Groothuis et al., 2015); correcting the Cnominal prior to its use for QIVIVE definitely requires some consideration. In the present PFAS QIVIVE,

two additional metrics have been explored next to the Cnominal in one of the two approaches (Louisse): scenario 2 (calculation) incorporates protein binding and scenario 3 considers overall PFAS *in vitro* distribution (calculated using the Armitage model; chapter 4.3.2). Alternatively, PFAS intracellular concentrations can be determined experimentally. The approaches presented here concluded on different results, underscoring the importance of carefully selecting the *in vitro* metric for a chemical's QIVIVE.

The oral equivalent effect doses of the Wetmore approach and the Louisse approach scenario 1 were obtained by analysing an AUC derived from the *in vitro* Cnominal concentration and corresponding to an *in vivo* PBK CA (total plasma concentration). Scenarios 2 and 3 of the Louisse approach used the *in vivo* PBK CAFree instead. CAfree *in vitro* represents the non-protein (albumin) bound fraction in scenario 2, as corrected with a calculation considering differences in albumin content (*in vitro* vs *in vivo*). CA free *in vitro* is the PFAS concentration in water as calculated from the biokinetic model (Armitage). This provides a rationale for the higher oral equivalent effect doses predicted with scenario 2 compared to that from scenario 1. An additional QIVIVE analysis was performed for scenarios 2 and 3, using the *in vivo* PBK CA total plasma concentration and as expected the calculated oral equivalent effect doses were lower compared to scenario 1 (data not shown). Nevertheless, such an analysis does not take into consideration the free PFAS levels in the PBK model and therefore, the former approaches were favoured here.

In the current QIVIVE, the 25% associated with a decrease in antibody release was chosen as an appropriate BMR. These results suggest that continuous exposure to PFAS above the predicted levels may interfere with the TI antibody (IgG and IgM) release in humans. Nevertheless, the degree of change associated with a clear adverse outcome, as observed in the *in vitro* system, is not clearly known at the moment. In addition, in the QIVIVE only a single cell group was used for the extrapolations, while preferably more *in vitro* readouts shall be taken into consideration. It shall be noted here that the results on QIVIVE depend very much on the selected BMR.

From an exposure perspective, the toxicity of a substance can be linked to different internal dose metrics, for example the peak concentration (Cmax), or the AUC. The parameter to use for relating exposure to toxicity depends on various factors, such as the mode of action of the chemical and the toxicological endpoint (Groothuis et al., 2015; Louisse et al., 2017), its toxicokinetic profile, but also the exposure conditions (Groothuis et al., 2015). In the present study, it was assumed that the PFAS-induced toxicity on the immune system is best related to a time-dependent cumulative dose metric (the AUC), considering the nature of the effect, the chronic exposure of humans to PFAS, as well as the rather long elimination half-lives (in the range of years) of these chemicals. This approach for extrapolating from a short 7-day exposure occurring *in vitro* to a long (5 years) *in vivo* exposure, as observed in the toddler study (EFSA CONTAM, 2020), contains uncertainties but it can serve at least as a first tier in human health risk assessment. Studies that assess the impact of time of exposure in the *in vitro* systems would be of interest to understand whether the extrapolation from a 7-day exposure *in vitro* to a 5-year exposure *in vivo* can be justified.

As a general remark, it is highlighted that the PBK models used here (for all PFAS), as well as the reverse dosimetry approach applied for the translation of *in vitro* concentrations to

external doses use a deterministic approach. In other words, all parameters are held fixed at a central value and, as such, they do not accommodate for any variability and uncertainty. Understanding and quantifying the variability and uncertainty embedded in each step of the hazard and risk assessment for a chemical is very important, particularly to increase confidence in the use of NAMs (Loizou et al., 2021; Berggeren et al., 2017; Judson et al., 2011). It is acknowledged that variability and uncertainty in parameter values shall be taken into consideration when using such models for QIVIVE, however, this was considered beyond the scope of the present work.

As an alternative, an uncertainty factor can be introduced to cover the *in vitro* to *in vivo* extrapolation, as currently applied in hazard and risk assessments to address variability, uncertainties, including extrapolations among mammals and experimental durations. However, if we consider the values obtained, they are below or close to the current TDI, indicating that such correction factor is probably not needed. It is foreseen that the increased use of NAM-based methods for next generation risk assessment will provide further rationale to further investigate the impact of parameters values, variability and uncertainty and provide practical solutions for the above mentioned *in vitro in vivo* extrapolation.

4. Conclusions

This study addressed some gaps identified in the EFSA Scientific Opinion 'Risk to human health related to the presence of perfluoroalkyl substances in food' (2020), with regard to the mode of action underlying PFAS immunosuppressive effects such as reduced vaccination efficacy and increased risk of infections. The study also expanded the understanding of immunotoxicity beyond PFOS and PFOA to include PFNA and PFHxS. The approach used in this project offered the possibility to examine the immunotoxic potential of PFAS covering different immune cells, from innate to acquired immune response. Results obtained demonstrate that PFAS can exert varied influences at different levels, with the ability to directly impact DC activation, T cell proliferation and differentiation, as well as B cell activation and antibody production.

In vitro studies encompassed the use of a wide concentration range (0.001-10 µg/mL) to mirror levels observed in the general population and highly exposed individuals. The approach used confirmed PFAS immunosuppressive effects, their relevance to the human exposure, and difference in terms of potency among the four tested PFAS. Considering all parameters investigated and ranking results based on potency at the lowest concentration showing statistical significance, PFOA and PFOS were similarly potent and more potent than PFNA and PFHxS, which exhibited similar potency to each other.

The selected PFAS affected immune cells involved in antibody production to varying extents in both male and female donors. Some effects, such as total Ig release, were evident at very low concentrations (0.001 µg/mL), relevant to general population.

The study successfully explored *in vitro* T cell dependent primary antibody production, a gold standard in animal immunotoxicological investigations. While challenging to reproduce *in vitro*, due to the low frequency of specific naive T and B cells in peripheral blood, the feasibility of the protocol was demonstrated, and promising results were obtained. Despite modest anti-KLH IgM induction, the protocol holds high potential, warranting further efforts for optimization due to its significance. For the hazard identification, additional effort should be put in the optimization of the *in vitro* primary antibody response to KLH. In addition, in the view of abandoning animal products, such as foetal bovine serum, efforts should be made to optimize tests that use a chemically defined medium. Once optimised, additional chemicals need to be tested to demonstrate the predictive capacity the *in vitro* primary antibody response. In conclusion, the project successfully reproduced *in vitro* the decreased antibody production induced by PFAS and provided, using RNASeq, insights into potential mode(s) of action, with the identification of PPARα and GR as the primary affected pathways.

With the combined *in vitro* PBK modelling-facilitated QIVIVE the *in vitro* concentration-response data for antibody release changes upon PFAS exposure were converted into a corresponding *in vivo* oral equivalent dose-response relationship, integrating as such the PFAS toxicokinetics. The predicted oral equivalent effect doses for the sum of the four chemicals, were (considerably) lower than the TDI derived from the epidemiological data, with the exception of scenario 2 in Louisse approach. As such, it appears that the present NAM-based methodology for performing PFAS hazard assessment is much more or at least equally conservative. *In silico* methods, notably, have provided a strategic advantage by enabling the extrapolation of in vitro data to predict in vivo scenarios through PBK models and the UISS-TOX. These models have been crucial for assessing immunotoxic risks across various human populations, including vulnerable groups like children and the elderly. The *in silico* approach not only complements the empirical data but also allows a comprehensive view of the immunotoxic effects of PFAS, predicting outcomes like decreased vaccination responses which are critical for public health assessments.

The synergistic application of these methods allows for a comprehensive risk assessment by covering various aspects of PFAS immunotoxicity from molecular mechanisms to population-level effects. This integration offers a more accurate and human-relevant assessment, reducing uncertainties in health risk evaluation and supporting more informed regulatory decisions. Moving forward, the integration of these approaches should be seen not only as a methodological advancement but as a paradigm shift in toxicological risk assessment, aiming for more predictive and mechanistic models that safeguard human health with fewer ethical concerns than traditional animal testing.

The proposed approach is adaptable to other PFAS, offering a potential shift away from animal experimentation towards human cell-based *in vitro* methods and computer simulations. The proposed approach provides the opportunity to establish new knowledge, and approaches that support the protection of human health from PFAS and other chemicals targeting the immune system. It is important to note, that the same experimental system (PBMC) can also be easily expanded to assess other immune functions, e.g. NK cell activity. Finally, the combination of functional tests within *in silico* methods and *in vitro* to *in vivo* extrapolation demonstrate the enormous potential of what has been done.

References

Abraham K, Mielke H, Fromme H, Völkel W, Menzel J, Peiser M, Zepp F, Willich SN and Weikert C, 2020. Internal exposure to perfluoroalkyl substances (PFASs) and biological markers in 101 healthy 1-year-old children: associations between levels of perfluorooctanoic acid (PFOA) and vaccine response. Arch Toxicol, 94(6), 2131-2147.

Adams NM, Grassmann S and Sun JC, 2020. Clonal expansion of innate and adaptive lymphocytes. Nat Rev Immunol, 20(11):694-707. doi: 10.1038/s41577-020-0307-4.

Alderman G and Stranks MH, 1967. The iodine content of bulk herd milk in summer in relation to estimated dietary iodine intake of cows. Journal of the Science of Food and Agriculture, 18, 151–153.

Algharably EA, Di Consiglio E, Testai E, Pistollato F, Mielke H and Gundert-Remy U, 2022. In Vitro-In Vivo Extrapolation by Physiologically Based Kinetic Modeling: Experience With Three Case Studies and Lessons Learned. Front Toxicol. 18;4:885843. doi: 10.3389/ftox.2022.885843.

Armitage JM, Wania F and Arnot JA, 2014. Application of mass balance models and the chemical activity concept to facilitate the use of in vitro toxicity data for risk assessment. Environ Sci Technol, 48, 9770–9779.

Armitage JM, Sangion A, Parmar R, Looky AB and Arnot JA, 2021. Update and Evaluation of a High-Throughput In vitro Mass Balance Distribution Model: IV-MBM EQP v2.0. Toxics, 9(11), 315.

Arnich N, Sirot V, Rivière G, Jean J, Noël L, Guérin T and Leblanc JC, 2012. Dietary exposure to trace elements and health risk assessment in the 2nd French Total Diet Study. Food and chemical toxicology: an international journal published for the British Industrial Biological Research Association, 50(7), 2432–2449.

Averina M, Brox J, Huber S, Furberg AS and Sørensen M, 2019. Serum perfluoroalkyl substances (PFAS) and risk of asthma and various allergies in adolescents. The Tromsø study Fit Futures in Northern Norway. Environmental research, 169, 114–121.

Bartell SM, Calafat AM, Lyu C, Kato K, Ryan PB and Steenland K, 2010. Rate of decline in serum PFOA concentrations after granular activated carbon filtration at two public water systems in Ohio and West Virginia. Environmental health perspectives, 118(2), 222–228. https://doi.org/10.1289/ehp.0901252.

Becknell B, Greenbaum LA and Smoyer WE, 2012. A new tac for childhood nephrotic syndrome. Kidney International, 82(10), 1049–1051. https://doi.org/10.1038/ki.2012.272.

Behr AC, Lichtenstein D, Braeuning A, Lampen A and Buhrke T, 2018. Perfluoroalkylated substances (PFAS) affect neither estrogen and androgen receptor activity nor steroidogenesis in human cells in vitro. Toxicology Letters, 291(March), 51–60. https://doi.org/10.1016/j.toxlet.2018.03.029.

Behr AC, Plinsch C, Braeuning A and Buhrke T, 2020. Activation of human nuclear receptors by perfluoroalkylated substances (PFAS). Toxicology in Vitro, 62(August 2019), 104700. https://doi.org/10.1016/j.tiv.2019.104700.

Berggren E, White A, Ouedraogo G, Paini A, Richarz AN, Bois FY, Exner T, Leite S, Grunsven LAV, Worth A and Mahony C, 2017. Ab initio chemical safety assessment: A workflow based on exposure considerations and non-animal methods. Comput Toxicol. 4:31-44. doi: 10.1016/j.comtox.2017.10.001.

Berges C, Naujokat C, Tinapp S, Wieczorek H, Höh A, Sadeghi M, Opelz G and Daniel V, 2005. A cell line model for the differentiation of human dendritic cells. Biochem Biophys Res Commun, 5, 896-907.

Bois FY, Jamei M and Clewell HJ. PBPK modelling of inter-individual variability in the pharmacokinetics of environmental chemicals. Toxicology. 2010 Dec 30;278(3):256-67. doi: 10.1016/j.tox.2010.06.007.

Bortnick A, Chernova I, Quinn WJ 3rd, Mugnier M, Cancro MP and Allman D, 2012. Long-lived bone marrow plasma cells are induced early in response to T cell-independent or T cell-dependent antigens. Journal of immunology (Baltimore, Md.: 1950), 188(11), 5389–5396. https://doi.org/10.4049/jimmunol.1102808

Chang X, Tan YM, Allen DG, Bell S, Brown PC, Browning L, Ceger P, Gearhart J, Hakkinen PJ, Kabadi SV, Kleinstreuer NC, Lumen A, Matheson J, Paini A, Pangburn HA, Petersen EJ, Reinke EN, Ribeiro AJS, Sipes N, Sweeney LM and Mumtaz M, 2022. IVIVE: Facilitating the Use of In Vitro Toxicity Data in Risk Assessment and Decision Making. Toxics, 10(5), 232.

Chaplin DD, 2010. Overview of the immune response. J Allergy Clin Immunol, 125(2 Suppl 2):S3-23. doi: 10.1016/j.jaci.2009.12.980. PMID: 20176265; PMCID: PMC2923430.

Clewell RA and Clewell HJ 3rd, 2008. Development and specification of physiologically based pharmacokinetic models for use in risk assessment. Regul Toxicol Pharmacol, 50(1), 129-43. doi: 10.1016/j.yrtph.2007.10.012.

Corsini E, Avogadro A, Galbiati V, dell'Agli M, Marinovich M, Galli CL and Germolec DR, 2011. In vitro evaluation of the immunotoxic potential of perfluorinated compounds (PFCs). Toxicol Appl Pharmacol, 250(2), 108-16. doi: 10.1016/j.taap.2010.11.004. Epub 2010 Nov 12.

Corsini E, Luebke RW, Germolec DR and DeWitt JC, 2014. Perfluorinated compounds: emerging POPs with potential immunotoxicity. Toxicol Lett, 230(2), 263-720.

Dalsager L, Christensen N, Husby S, Kyhl H, Nielsen F, Høst A, Grandjean and Jensen TK, 2016. Association between prenatal exposure to perfluorinated compounds and symptoms of infections at age 1–4 years among 359 children in the Odense Child Cohort. Environment international, 96, 58-64.

Daston GP, Chapin RE, Scialli AR, Piersma AH, Carney EW, Rogers JM and Friedman JM, 2010. A different approach to validating screening assays for developmental toxicity. Birth Defects Res B Dev Reprod Toxicol, 89(6),526-30. doi: 10.1002/bdrb.20276.

DeWitt JC, Blossom SJ and Schaider LA, 2019. Exposure to per-fluoroalkyl and polyfluoroalkyl substances leads to immunotoxicity: epidemiological and toxicological evidence. Journal of exposure science & environmental epidemiology, 29(2), 148–156.

EFSA CONTAM Panel (EFSA Panel on Contaminants in the Food Chain), Knutsen HK, Alexander J, Barregård L, Bignami M, Brüschweiler B, Ceccatelli S, Cottrill B, Dinovi M, Edler L, Grasl-Kraupp B, Hogstrand C, Hoogenboom LR, Nebbia CS, Oswald IP, Petersen A, Rose M, Roudot A-C, Vleminckx C, Vollmer G, Wallace H, Bodin L, Cravedi J-P, Halldorsson TI, Haug LS, Johansson N, van Loveren H, Gergelova P, Mackay K, Levorato S, van Manen M and Schwerdtle T, 2018. Risk to human health related to the presence of perfluorooctane sulfonic acid and perfluorooctanoic acid in food. EFSA Journal 2018;16(12):5194, 284pp. doi:10.2903/j.efsa.2018.05194.

EFSA CONTAM Panel (EFSA Panel on Contaminants in the Food Chain), Schrenk D, Bignami M, Bodin L, Chipman JK, del Mazo J, Grasl-Kraupp B, Hogstrand C, Hoogenboom LR, Leblanc J-C, Nebbia CS, Nielsen E, Ntzani E, Petersen A, Sand S, Vleminckx C, Wallace H, Barregård L, Ceccatelli S, Cravedi J-P, Halldorsson TI, Haug LS, Johansson N, Knutsen HK, Rose M, Roudot A-C, VanLoveren H, Vollmer G, Mackay K, Riolo F and Schwerdtle T, 2020. Scientific Opinion on the risk to human health related to the presence of perfluoroalkyl substances in food. EFSA Journal 2020;18(9):6223, 391pp. https://doi.org/10.2903/j.efsa.2020.6223

Ericson I, Gómez M, Nadal M, Van Bavel B, Lindström G and Domingo JL, 2007. Perfluorinated chemicals in blood of residents in Catalonia (Spain) in relation to age and gender: A pilot study. Environ Int., 33(5), 616–23.

Evans N, Conley JM, Cardon M, Hartig P, Medlock-Kakaley E and Gray LE, 2022. In vitro activity of a panel of per- and polyfluoroalkyl substances (PFAS), fatty acids, and pharmaceuticals in peroxisome proliferator-activated receptor (PPAR) alpha, PPAR gamma, and estrogen receptor assays. Toxicology and Applied Pharmacology, 449. https://doi.org/10.1016/j.taap.2022.116136.

Fàbrega F, Kumar V, Schuhmacher M, Domingo JL and Nadal M, 2014. PBPK modeling for PFOS and PFOA: validation with human experimental data. Toxicology letters, 230(2), 244–251. https://doi.org/10.1016/j.toxlet.2014.01.007.

Fiorentino DF, Bond MW and Mosmann TR, 1989. Two types of mouse T helper cell. IV. Th2 clones secrete a factor that inhibits cytokine production by Th1 clones. J Exp Med., 170, 2081–2095.

Fisher C, Siméon S, Jamei M, Gardner I and Bois YF, 2019. VIVD: Virtual in vitro distribution model for the mechanistic prediction of intracellular concentrations of chemicals in in vitro toxicity assays. Toxicol In Vitro, 58, 42-50. doi: 10.1016/j.tiv.2018.12.017.

Fragki S, Louisse J, Bokkers B, Luijten M, Peijnenburg A, Rijkers D, Piersma AH and Zeilmaker MJ, 2023. New approach methodologies: A quantitative in vitro to in vivo extrapolation case study with PFASs. Food and chemical toxicology: an international journal published for the British Industrial Biological Research Association, 172, 113559.

Fragki S, Hoogenveen R, van Oostrom C, Schwillens P, Piersma AH and Zeilmaker MJ, 2022. Integrating in vitro chemical transplacental passage into a generic PBK model: A QIVIVE approach. Toxicology, 15, 465:153060. doi: 10.1016/j.tox.2021.153060.

Fujii Y, Niisoe T, Harada KH, Uemoto S, Ogura Y, Takenaka K and Koizumi A., 2015 Toxicokinetics of perfluoroalkyl carboxylic acids with different carbon chain lengths in mice and humans. J Occup Health, 57(1), 1–12.

Granum B, Haug LS, Namork E, Stølevik SB, Thomsen C, Aaberge IS, van Loveren H, Løvik M and Nygaard UC, 2013. Pre-natal exposure to perfluoroalkyl substances may be associated with altered vaccine antibody levels and immune-related health outcomes in early childhood. Journal of immunotoxicology, 10(4), 373–379. https://doi.org/10.1016/j.tox.2013.08.012

Groothuis FA, Heringa MB, Nicol B, Hermens JL, Blaauboer BJ and Kramer NI, 2015. Dose metric considerations in in vitro assays to improve quantitative in vitro-in vivo dose extrapolations. Toxicology, 5, 332:30-40. doi: 10.1016/j.tox.2013.08.012.

Hamon J, Renner M, Jamei M, Lukas A, Kopp-Schneider A and Bois FY, 2015. Quantitative in Vitro to in Vivo Extrapolation of Tissues Toxicity. Toxicol. In Vitro, 30, 203–216.

Han X, Snow TA, Kemper RA and Jepson GW. Binding of Perfluorooctanoic Acid to Rat and Human Plasma Proteins, 2003. Chem Res Toxicol, 16(6), 775–81.

Han X, Nabb DL, Russell MH, Kennedy GL and Rickard RW, 2012. Renal elimination of perfluorocarboxylates (PFCAs). Chemical research in toxicology, 25(1), 35–46. https://doi.org/10.1021/tx200363w.

Harada K, Inoue K, Morikawa A, Yoshinaga T, Saito N and Koizumi A. Renal clearance of perfluorooctane sulfonate and perfluorooctanoate in humans and their species-specific excretion, 2005. Environ Res, 99(2), 253–61.

Harada KH, Hashida S, Kaneko T, Takenaka K, Minata M, Inoue K, Saito N and Koizumi A, 2007. Biliary excretion and cerebrospinal fluid partition of perfluorooctanoate and perfluorooctane sulfonate in humans. Environ Toxicol Pharmacol, 24(2), 134–9.

Henneberger L, Huchthausen J, Wojtysiak N and Escher BI, 2021. Quantitative In Vitro-to-In Vivo Extrapolation: Nominal versus Freely Dissolved Concentration. Chem Res Toxicol 19, 34(4), 1175-1182. doi: 10.1021/acs.chemrestox.1c00037.

ITRC (Interstate Technology and Regulatory Council), 2022. PFAS Technical and Regulatory Guidance Document. https://pfas-1.itrcweb.org/.

Judson RS, Kavlock RJ, Setzer RW, Hubal EA, Martin MT, Knudsen TB, Houck KA, Thomas RS, Wetmore BA and Dix DJ, 2011. Estimating toxicity-related biological pathway altering doses for high-throughput chemical risk assessment. Chem Res Toxicol, 18, 24(4), 451-62. doi: 10.1021/tx100428e.

Kaiko GE, Horvat JC, Beagley KW and Hansbro PM, 2008. Immunological decision-making: how does the immune system decide to mount a helper T-cell response? Immunology, 123(3), 326-38.

Kasteel EEJ, Lautz LS, Culot M, Kramer NI and Zwartsen A, 2021. Application of in vitro data in physiologically-based kinetic models for quantitative in vitro-in vivo extrapolation: A case-study for baclofen. Toxicol In Vitro 76:105223. doi: 10.1016/j.tiv.2021.105223.

Kennell AS, Gould KG and Salaman MR, 2014. Proliferation assay amplification by IL-2 in model primary and recall antigen systems. BMC research notes, 7, 662. https://doi.org/10.1186/1756-0500-7-662

Kielsen K, Shamim Z, Ryder LP, Nielsen F, Grandjean P, Budtz-Jørgensen E and Heilmann C, 2016. Antibody response to booster vaccination with tetanus and diphtheria in adults exposed to perfluorinated alkylates. J Immunotoxicol, 13(2), 270-3. doi: 10.3109/1547691X.2015.1067259.

Komatsu H, Shimada S, Terashima M and Osawa T, 1986. Induction of in vitro antigen-specific antibody production against NIP-KLH in nonadherent cells derived from human peripheral blood mononuclear cells. Int Arch Allergy Appl Immunol, 80(4), 431-434.

Komatsu H, Sugimoto J, Goto K, Kushima K, Tsutsui N, Hisada S, Ito S, Kosaka T, Ohishi T, Otsubo Y and Takahashi Y, 2021. Adverse Outcome Pathway on inhibition of calcineurin activity leading to impaired T-cell dependent antibody response. OECD Series on Adverse Outcome Pathways, No. 18, OECD Publishing, Paris, https://doi.org/10.1787/3c988dde-en.

Kudo N, Sakai A, Mitsumoto A, Hibino Y, Tsuda T and Kawashima Y, 2007. Tissue Distribution and Hepatic Subcellular Distribution of Perfluorooctanoic Acid at Low Dose Are Different from Those at High Dose in Rats. Biol Pharm Bull, 30(8), 1535–40.

Kuepfer L, Niederalt C, Wendl T, Schlender JF, Willmann S, Lippert J, Block M, Eissing T and Teutonico D, 2016. Applied Concepts in PBPK Modeling: How to Build a PBPK/PD Model. CPT Pharmacometrics Syst Pharmacol, 5(10), 516-531.

Li Z, Ju X, Silveira PA, Abadir E, Hsu WH, Hart DNJ and Clark GJ, 2019. CD83: Activation Marker for Antigen Presenting Cells and Its Therapeutic Potential. Frontiers in Immunology, 10. doi:10.3389/fimmu.2019.01312

Li Y, Barregard L, Xu Y, Scott K, Pineda D, Lindh CH, Jakobsson K and Fletcher T, 2020. Associations between perfluoroalkyl substances and serum lipids in a Swedish adult population with contaminated drinking water. Environmental Health, 19(1), 33.

Loccisano AE, Campbell JL, Jr Andersen ME and Clewell, HJ, 2011. Evaluation and prediction of pharmacokinetics of PFOA and PFOS in the monkey and human using a PBPK model. Regulatory toxicology and pharmacology: RTP, 59(1), 157–175.

Loizou G, McNally K, Dorne JCM and Hogg A, 2021. Derivation of a Human In Vivo Benchmark Dose for Perfluorooctanoic Acid From ToxCast In Vitro Concentration-Response Data Using a Computational Workflow for Probabilistic Quantitative In Vitro to In Vivo Extrapolation. Front Pharmacol, 11, 12:630457. doi: 10.3389/fphar.2021.630457.

Luster MI, Portier C, Pait DG, White KL Jr, Gennings C, Munson AE and Rosenthal GJ, 1992. Risk assessment in immunotoxicology. I. Sensitivity and predictability of immune tests. Fundam Appl Toxicol, 18(2), 200-10. doi: 10.1016/0272-0590(92)90047-l.

Louisse J, de Jong E and van de Sandt JJ, 2010. The use of in vitro toxicity data and physiologically based kinetic modeling to predict dose-response curves for in vivo developmental toxicity of glycol ethers in rat and man. Toxicol Sci, 118(2), 470-484.

Louisse J, Bosgra S, Blaauboer BJ, Rietjens IM and Verwei M, 2015 Prediction of in vivo developmental toxicity of all-trans-retinoic acid based on in vitro toxicity data and in silico physiologically based kinetic modeling. Arch. Toxicol, 89(7), 1135–1148.

Louisse J, Rijkers D, Stoopen G, Janssen A, Staats M, Hoogenboom R, Kersten S and Peijnenburg A, 2020. Perfluorooctanoic acid (PFOA), perfluorooctane sulfonic acid (PFOS), and perfluorononanoic acid (PFNA) increase triglyceride levels and decrease cholesterogenic gene expression in human HepaRG liver cells. Archives of Toxicology, 94(9), 3137–3155. https://doi.org/10.1007/s00204-020-02808-0.

Louisse J, Dellafiora L, van den Heuvel JJMW, Rijkers D, Leenders L, Dorne JCM, Punt A, Russel FGM and Koenderink JB, 2023. Perfluoroalkyl substances (PFASs) are substrates of the renal human organic anion transporter 4 (OAT4). Archives of toxicology, 97(3), 685–696. https://doi.org/10.1007/s00204-022-03428-6

Louisse J, Dellafiora L, Van Den Heuvel JJMW, Rijkers D, Leenders L, Dorne JLCM, Punt A, Russel FGM and Koenderink JB, 2023. Perfluoroalkyl substances (PFASs) are substrates of the renal human organic anion transporter 4 (OAT4). Archives of Toxicology, 97(3), 685–96.

Nakagawa H, Terada T, Harada KH, Hitomi T, Inoue K, Inui K and Koizumi A, 2009. Human organic anion transporter hOAT4 is a transporter of perfluorooctanoic acid. Basic & clinical pharmacology & toxicology, 105(2), 136–138. https://doi.org/10.1111/j.1742-7843.2009.00409.x

Naveen R, Akshata K, Pimple SS and Chaudhari P, 2016. A Review on Albumin as Drug Carrier in Treating Different Diseases and Disorders. https://www.semanticscholar.org/paper/A-review-on-albumin-as-drug-carrier-in-treating-and-Naveen-Akshata/321e076e1f88e675341aceab91583e56a733eba1

Noorlander A, Zhang M, van Ravenzwaay B and Rietjens IMCM, 2022. Use of Physiologically Based Kinetic Modeling-Facilitated Reverse Dosimetry to Predict In Vivo Acute Toxicity of Tetrodotoxin in Rodents. Toxicol Sci, 187(1), 127-138. doi: 10.1093/toxsci/kfac022.

OECD (Organisation for Economic Co-operation and Development), 2022. Detailed review paper on in vitro test addressing immunotoxicity with a focus on Immunosuppression. Available online: https://www.oecd-ilibrary.org/environment/detailed-review-paper-on-in-vitro-test-addressing-immunotoxicity-with-a-focus-on-immunosuppression_667965bc-en.

Olsen GW, Burris JM, Ehresman DJ, Froehlich JW, Seacat AM, Butenhoff JL and Zobel LR, 2007. Half-life of serum elimination of perfluorooctanesulfonate, perfluorohexanesulfonate, and perfluorooctanoate in retired fluorochemical production workers. Environ Health Perspect, 115(9), 1298-3105.

Paini A, Mennecozzi M, Horvat T, Gerloff K, Palosaari T, Sala Benito JV and Worth A, 2017. Practical use of the Virtual Cell Based Assay: Simulation of repeated exposure experiments in liver cell lines. Toxicology in vitro: an international journal published in association with BIBRA, 45(Pt 2), 233–240.

Pappalardo F, Russo G, Corsini E, Paini A and Worth A, 2022. Translatability and transferability of in silico models: Context of use switching to predict the effects of environmental chemicals on the immune system. Computational and Structural Biotechnology Journal, 20, 1764-1777.

Pearce EJ and Everts B, 2015. Dendritic cell metabolism. Nature Reviews Immunology, 15(1), 18–29. https://doi.org/10.1038/nri3771.

Pérez F, Nadal M, Navarro-Ortega A, Fàbrega F, Domingo JL, Barceló D and Farré M, 2013. Accumulation of perfluoroalkyl substances in human tissues. Environ Int, 59, 354–62.

Pone EJ, Lou Z, Lam T, Greenberg ML, Wang R, Xu Z and Casali P, 2015a. B cell TLR1/2, TLR4, TLR7 and TLR9 interact in induction of class switch DNA recombination: modulation by BCR and CD40, and relevance to T-independent antibody responses. Autoimmunity, 48(1), 1–12. https://doi.org/10.3109/08916934.2014.993027.

Pone EJ, Lam T, Lou Z, Wang R, Chen Y, Liu D, Edinger AL, Xu Z and Casali P, 2015b. B cell Rab7 mediates induction of activation-induced cytidine deaminase expression and class-switching in T-dependent and T-independent antibody responses. Journal of immunology (Baltimore, Md.: 1950), 194(7), 3065–3078. https://doi.org/10.4049/jimmunol.1401896.

Post GB, 2021. Recent US State and Federal Drinking Water Guidelines for Per- and Polyfluoroalkyl Substances. In Environmental Toxicology and Chemistry, 40(3), 550–563. https://doi.org/10.1002/etc.4863

Proença S, Escher BI, Fischer FC, Fisher C, Grégoire S, Hewitt NJ, Nicol B, Paini A and Kramer NI, 2021. Effective exposure of chemicals in in vitro cell systems: A review of chemical distribution models. Toxicol In Vitro, 73:105133. doi: 10.1016/j.tiv.2021.105133.

Reyenga L, 2022. Challenges in Modeling PFAS Fate and Transport at NAPL-impacted Sites. Volume 10, Issue 6 https://oilandgas.geiconsultants.com/ansr-10-6/

Rietjens IM, Louisse J and Punt A, 2011. Tutorial on physiologically based kinetic modeling in molecular nutrition and food research. Mol Nutr Food Res, 55(6), 941-56. doi: 10.1002/mnfr.201000655.

Rosenmai AK, Bengtström L, Taxvig C, Trier X, Petersen JH, Svingen T, Binderup ML, van Vugt-Lussenburg BMA, Dybdahl M, Granby K and Vinggaard AM, 2017. An effect-directed strategy for characterizing emerging chemicals in food contact materials made from paper and board. Food and chemical toxicology: an international journal published for the British Industrial Biological Research Association, 106(Pt A), 250–259.

Russo G, Crispino E, Corsini E, Iulini M, Paini A, Worth A and Pappalardo F, 2022. Computational modelling and simulation for immunotoxicity prediction induced by skin sensitisers. Comput Struct Biotechnol J, 20, 6172–81.

Saxena A, Khosraviani S, Noel S, Mohan D, Donner T and Hamad AR, 2015. Interleukin-10 paradox: A potent immunoregulatory cytokine that has been difficult to harness for immunotherapy. Cytokine, 74(1), 27–34. https://doi.org/10.1016/j.cyto.2014.10.031

Schlüter U, Meyer J, Ahrens A, Borghi F, Clerc F, Delmaar C, Di Guardo A., Dudzina T, Fantke P, Fransman W, Hahn S, Heussen H, Jung C, Koivisto J, Koppisch D, Paini A, Savic N, Spinazzè A, Zare Jeddi M and von Goetz N, 2022. Exposure modelling in Europe: how to pave the road for the future as part of the European Exposure Science Strategy 2020-2030. Journal of exposure science & environmental epidemiology, 32(4), 499–512.

Sipes NS, Wambaugh JF, Pearce R, Auerbach SS, Wetmore BA, Hsieh JH, Shapiro AJ, Svoboda D, DeVito MJ and Ferguson SS, 2017. An Intuitive Approach for Predicting Potential Human Health Risk with the Tox21 10k Library. Environmental science & technology, 51(18), 10786–10796. https://doi.org/10.1021/acs.est.7b00650.

Tuijnenburg P, Aan de Kerk DJ, Jansen MH, Morris B, Lieftink C, Beijersbergen RL, van Leeuwen EMM and Kuijpers TW, 2020. High-throughput compound screen reveals mTOR inhibitors as potential therapeutics to reduce (auto)antibody production by human plasma cells. Eur J Immunol, 50(1), 73-85.

Wculek SK, Khouili SC, Priego E, Heras-Murillo I and Sancho D, 2019. Metabolic Control of Dendritic Cell Functions: Digesting Information. Frontiers in Immunology, 10, 775. https://doi.org/10.3389/fimmu.2019.00775.

Wetmore BA, Wambaugh JF, Ferguson SS, Sochaski MA, Rotroff DM, Freeman K, Clewell HJ 3rd, Dix DJ, Andersen ME, Houck KA, Allen B, Judson RS, Singh R, Kavlock RJ, Richard AM and Thomas RS, 2012. Integration of dosimetry, exposure, and high-throughput screening data in chemical toxicity assessment. Toxicological sciences: an official journal of the Society of Toxicology, 125(1), 157–174. https://doi.org/10.1093/toxsci/kfr254.

Wetmore BA, Wambaugh JF, Allen B, Ferguson SS, Sochaski MA, Setzer RW, Houck KA, Strope CL, Cantwell K, Judson RS, LeCluyse E, Clewell HJ, Thomas RS and Andersen ME, 2015. Incorporating high-throughput exposure predictions with dosimetry-adjusted in vitro bioactivity to inform chemical toxicity testing. Toxicol Sci, 148, 121–136.

Yaqoob P and Calder PC, 2007. Fatty acids and immune function: New insights into mechanisms. British Journal of Nutrition, 98, S41–S45. https://doi.org/10.1017/S0007114507832995

Yoon M, Campbell JL, Andersen ME, Clewell HJ, 2012. Quantitative in vitro to in vivo extrapolation of cell-based toxicity assays results, Crit Rev Toxicol, 42(8), 633-652.

Yoon M, Campbell JL, Andersen ME and Clewell HJ, 2017. Quantitative in Vitro to in Vivo Extrapolation of Cell-Based Toxicity Assay Results. Crit. Rev. Toxicol, 42, 633–652.

Zannas AS, Wiechmann T, Gassen NC and Binder EB, 2016. Gene-Stress-Epigenetic Regulation of FKBP5: Clinical and Translational Implications. Neuropsychopharmacology, 41(1), 261–274. https://doi.org/10.1038/npp.2015.235.

Zannas AS, Jia M, Hafner K, Baumert J, Wiechmann T, Pape JC, Arloth J, Ködel M, Martinelli S, Roitman M, Röh S, Haehle A, Emeny RT, Iurato S, Carrillo-Roa T, Lahti J, Räikkönen K, Eriksson JG, Drake AJ,Waldenberger M, Wahl S, Kunze S, Lucae S, Bradley B, Gieger C, Hausch F, Smith AK, Ressler KJ, Müller-Myhsok B, Ladwig K-H, Rein T, Gassen NC and Binder EB, 2019. Epigenetic upregulation of FKBP5 by aging and stress contributes to NF-κB-driven inflammation and cardiovascular risk. Proceedings of the National Academy of Sciences of the United States of America, 166(23), 11370–11379. https://doi.org/10.1073/pnas.1816847116.

Zhang Y, Beesoon S, Zhu L and Martin JW, 2013. Biomonitoring of perfluoroalkyl acids in human urine and estimates of biological half-life. Environmental science & technology, 47(18), 10619–10627. https://doi.org/10.1021/es401905e.

Zheng L, Dong GH, Zhang YH, Liang ZF, Jin YH and He QC, 2011. Type 1 and Type 2 cytokines imbalance in adult male C57BL/6 mice following a 7-day oral exposure to perfluorooctanesulfonate (PFOS). Journal of immunotoxicology, 8(1), 30–38.

Zhou X, Zhu X and Zeng H, 2021. Fatty acid metabolism in adaptive immunity. FEBS Journal, 290, 584–599. https://doi.org/10.1111/febs.1629

Abbreviations

Ab, Antibody

CD, Cluster of Differentiation

CES, Critical Effect Size

BMC, Benchmark concentration

BMCL, Benchmark concentration lower

BMCU, Benchmark concentration upper

BMD, Benchmark dose

BMDL, Benchmark dose lower

BMDU, Benchmark dose upper

DC, Dentritic cells

GR, Glucocorticoid receptor

IL, Interleukin

IFN, Interferon

IPA, Ingenuity Pathway Analysis

KLH, Keyhole limpet hemocyanin

MF, mass fraction

NAMs, New Approach Methodologies

NES, Normalized Enrichments Score

ODN2006, oligonucleotides 2006

PBMC, Peripheral Blood Mononuclear Cells

PBK, Physiologically Based Kinetic

PFAS, Per- and polyfluoroalkyl substances

PFHxS, perfluorohexane sulfonic acid

PFNA, perfluorononanoic acid

PFOA, perfluorooctanoic acid

PFOS, perfluorooctane sulfonic acid

PoD, Point of departure

QIVIVE, Qantitative In vitro to In vivo Extrapolation

RPFs, Relative Potency Factor

SAC, Staphylococcus aureus Cowan I

SOP, Standard Operating Procedure

Th, T helper

TI, T cell-independent

TD, T cell-dependent

TNF, Tumor Necrosis Factor

TWI, Tolerable Weekly Intake

UISS, Universal Immune System Simulator

WSC, Worst-Case Scenario

Annex A – Standard operation procedures (SOP)

Annex A provides the overview of all SOPs used to produce the data obtained and shown in the report:

A.1 SOP for purification of peripheral blood mononuclear cells (PBMCs) from buffy coat

A.2 SOP for the evaluation of leukotoxicity

A.3 SOP for the differentiation and maturation of dendritic cells starting from the THP-1 cell line

A.4 SOP for the proliferation and differentiation of helper T cells from human PBMCs

A.5 SOP for in vitro primary antibody response

A.6 SOP for Activation of Primary Human B Cells

Annex A is available in the supporting information section of this report.

Annex B – *in vitro* raw data

Annex B shows all the i*n vitro* raw data. Each Excel sheet contains the data of a different protocol (SOP) except for the study of the effects on T cells which, due to data quantity issues, it was preferred to make 4 separate sheets (one for each substance analyzed).

Annex B is available in the Zenodo platform. Doi: 10.5281/zenodo.12527498.

Annex C - RIN values and RNA concentrations

Annex C lists the RNA integrity numbers and RNA concentrations of all samples subjected to RNA sequencing.

Annex C is available in the Zenodo platform. Doi: 10.5281/zenodo.12527498.

Annex D - RNA quality assessment BGI (part 1 and 2)

In Annex D, the results of RNA sample quality and quantity analysis are presented. Library preparation and tendering were for the first part of samples tendered and performed by BGI Genomics Co., Ltd and the second part of the samples by Azenta Life Sciences.

Annex D1 is available in the Zenodo platform. Doi: 10.5281/zenodo.12527498.

Annex D2 is available in the supporting information section of this report.

Annex E - RNAseq Limma iDC 24hrs

Annex E provides the RNAseq output, including differential expression analysis conducted using Limma, of iDCs exposed to PFOA, PFOS, GW7647, and dexamethasone for 24 hours.

Annex E is available in the Zenodo platform. Doi: 10.5281/zenodo.12527498.

Annex F - RNAseq iDCs

Annex F presents the figures and tables of RNAseq analysis of iDCs exposed to PFOA, PFOS, GW7647, and dexamethasone for 24 hours.

Annex F is available in the supporting information section of this report.

Annex G - RNAseq Limma mDC 47hrs and 96hrs

Annex G provides the RNAseq output, including differential expression analysis conducted using Limma, of mDCs exposed to PFOA and PFOS for 48 and 96 hours.

Annex G is available in the Zenodo platform. Doi: 10.5281/zenodo.12527498.

Annex H - RNAseq mDCs

Annex H presents the tables of RNAseq analysis of mDCs exposed to PFOA and PFOS for 48 and 96 hours.

Annex H is available in the supporting information section of this report.

Annex I - RNAseq Limma PBMCs 24hrs

Annex I provides the RNAseq output, including differential expression analysis conducted using Limma, of PBMCs (male and female donors) exposed to PFOA, PFOS, GW7647 and dexamethasone for 24h.

Annex I is available in the Zenodo platform. Doi: 10.5281/zenodo.12527498.

Annex J - RNAseq PBMCs

Annex J presents the figures and tables of RNAseq analysis of PBMCs (male and female donors) exposed to PFOA, PFOS, GW7647 and dexamethasone for 24h.

Annex J is available in the supporting information section of this report.

Annex K - RNAseq (part 1) Limma T cells 5days

Annex K provides the RNAseq output, including differential expression analysis conducted using Limma, of T cells (male and female donors) exposed to PFOA and PFOS for 5 days.

Annex K is available in the Zenodo platform. Doi: 10.5281/zenodo.12527498.

Annex L - RNAseq T cells (part 1)

Annex L presents the tables of RNAseq analysis of T cells (male and female donors) exposed to PFOA and PFOS for 5 days.

Annex L is available in the supporting information section of this report.

Annex M - RNAseq (part 1+2) Limma T cells 5days

Annex M provides the RNAseq output, including differential expression analysis conducted using Limma, of T cells (male and female donors) exposed to PFOA, PFOS, GW7647 and dexamethasone for 5 days.

Annex M is available in the Zenodo platform. Doi: 10.5281/zenodo.12527498.

Annex N - RNAseq T cells (part 1+2)

Annex N presents the figures of RNAseq analysis of T cells (male and female donors) exposed to PFOA, PFOS, GW7647 and dexamethasone for 5 days.

Annex N is available in the supporting information section of this report.

Annex O - RNAseq Limma B cells 7days

Annex O provides the RNAseq output, including differential expression analysis conducted using Limma, of B cells (male and female donors) exposed to PFOA and PFOS for 7 days.

Annex O is available in the Zenodo platform. Doi: 10.5281/zenodo.12527498.

Annex P - RNAseq B cells

Annex P presents the tables of RNAseq analysis of B cells (male and female donors) exposed to PFOA and PFOS for 7 days.

Annex P is available in the supporting information section of this report.

Annex Q - EFSA PBK models

Annex Q presents the EFSA PBK models used.

Q.1 PFNA PBK model

Q.2 PFOA PBK model

Q.3 PFOS PBK model

Q.4 PFHxS PBK model

Annex Q is available in the supporting information section of this report.

Annex R - UISS-TOX

Annex R presents the *in silico* predictions of cellular and molecular dynamics run using UISS-TOX.

R.1 Age range of 0-4 years

R.2 Age range of 25-26 years

R.3 Age range of 65-66 years

Annex R is available in the supporting information section of this report.